UNIVERSIDAD COMPLUTENSE DE MADRID
FACULTAD DE CIENCIAS FÍSICAS

TESIS DOCTORAL

Electronic, heat and ultra cold atoms transport in Quantum dot systems

Transporte electrónico de calor y de átomos ultra fríos en sistemas de puntos cuánticos

MEMORIA PARA OPTAR AL GRADO DE DOCTOR

PRESENTADA POR

Fernando Gallego Marcos

Directores

Gloria Platero Coello
Rafael Sánchez Rodrigo

Madrid, 2018

Electronic, Heat and Ultra Cold Atoms Transport in Quantum Dot Systems

Transporte electrónico, de calor y de átomos ultra fríos en sistemas de puntos cuánticos

presentada por

FERNANDO GALLEGO MARCOS

Facultad de Ciencias Físicas
UNIVERSIDAD COMPLUTENSE DE MADRID

Directores: Gloria Platero Coello & Rafael Sánchez Rodrigo

Tutor: Francisco Dominguez-Adame Acosta

Tesis doctoral presentada a la Universidad Complutense de Madrid de acuerdo con los requerimientos para la obtención del título de DOCTOR EN CIENCIAS FÍSICAS.

MADRID, DICIEMBRE 2016

Table of Contents

Page

Resumen **v**

Abstract **vii**

List of Figures **ix**

1 Introduction **1**

1.1 Quantum dot systems . . . 1

1.1.1 Transport in the weak coupling regime . . . 2

1.1.2 Coherence in quantum dots . . . 4

1.1.3 Quantum dots under electric fields . . . 8

1.1.4 Triple quantum dot . . . 9

1.1.4.1 Long Range transport . . . 11

1.1.5 Fabrication . . . 11

1.2 Theoretical Model . . . 13

1.2.1 Density Matrix . . . 13

1.2.2 Hamiltonian . . . 13

1.2.3 Long Range transition . . . 14

1.2.4 Open System. Master Equation for $\hat{H}(t) = \hat{H}$ . . . 15

1.2.4.1 Example . . . 16

1.2.5 Infinite bias limit . . . 16

1.3 Transport . . . 17

1.3.1 Current directly from ρ . . . 18

1.3.2 Heat Transport . . . 18

1.3.3 Thermodynamics . . . 19

1.4 Driven quantum dots . . . 19

1.4.1 Cotunnel approach in time dependent Hamiltonians . . . 21

1.4.2 Floquet Master Equation Approach . . . 22

1.4.3 Floquet-Secular approximation . . . 23

1.4.3.1 Example . . . 24

1.4.4 Redfield Master Equation 24
1.4.4.1 Example used in the paper: Coherent Long-Range Thermoelectrics in Nonadiabatic Driven Quantum Systems 25

2 Nonequilibrium relaxation transport of ultracold atoms **27**
2.1 Objectives 27
2.2 Model and set up 28
2.3 Spin degree of freedom 30
2.4 Conclusions 30

3 Superexchange blockade in triple quantum dots **45**
3.1 Objectives 45
3.2 Model and set up 47
3.3 Experimental detection of the *dark state* 49
3.4 Conclusions 52

4 Photon assisted long-range tunneling **59**
4.1 Objectives 59
4.2 Model and set up 60
4.3 Resonant Landau-Zener-Stückelberg (LZS) pattern 62
4.4 Conclusions 63

5 Coupled Landau-Zener-Stückelberg quantum dot interferometers **71**
5.1 Objectives 71
5.2 Model and set up 72
5.3 Conclusions 73

6 Coherent Long-Range Thermoelectrics in Nonadiabatic Driven Quantum Systems **81**
6.1 Objectives 81
6.2 Model and set up 82
6.3 Conclusions 83

7 Channel blockade in a two-path triple-quantum-dot system **95**
7.1 Objectives 95
7.2 Model and set up 96
7.3 Conclusions 97

A Master equation **105**
A.1 Redfield Master equation 110
A.1.1 Example for two reservoirs coupled to the left and right quantum dot . . . 111

A.2 Infinite bias limit 112

B Cotunnel approach **113**

B.1 Time dependent 114

C Floquet Theory **117**

List of publications **119**

Acronyms **123**

Bibliography **125**

Resumen

El tema de la presente tesis doctoral es: Transporte a través de sistemas mesoscópicos. Los sistemas mesoscópicos son materiales de un número de partículas pequeño, con un tamaño máximo del orden del micrómetro. Sus propiedades colectivas están regidas por la mecánica cuántica. En estos materiales, se estudia la dinámica de transporte, interacciones y coherencia de sistemas de una y unas pocas partículas.

Los entornos considerados para el desarrollo de esta tesis son las estructuras de puntos cuánticos, donde partículas con un espín definido están confinadas en niveles de energía discretos. Los puntos cuánticos están acoplados por uniones túnel, que superponen las funciones de onda de los niveles de energía superiores. Las partículas en estos estados están deslocalizadas coherentemente por toda la estructura, que se comporta como una molécula artificial. Una fuerte interacción entre partículas está presente en estos sistemas debido a la proximidad entre ellas. Estos sistemas se controlan externamente cambiando voltajes de puerta acoplados capacitivamente a los puntos cuánticos. Por lo tanto, la energía, entropía y la dinámica coherente del sistema cambia de manera controlada. La mayor parte de esta tesis está basada en puntos cuánticos triples, los cuales constituyen un dispositivo perfecto para investigar interferencias entre distintos niveles. Tienen la ventaja de una separación espacial de los estados que permite manipularlos individualmente, y por otro lado el acoplo entre ellos también es controlado externamente. Al estudiar transporte de partículas, el sistema de puntos cuánticos se acopla débilmente a reservorios, con los cuales intercambia carga y energía. En el capítulo 7 se demuestran las interacciones entre distintos caminos entre los reservoiros usando un punto cuántico triple acoplado a tres reservorios. Las interacciones de Coulomb entre los electrones y las correlaciones entre los distintos caminos llevan a un bloqueo de la corriente en uno de los canales cuando el otro tiene una alta conductancia.

Uno de los problemas principales que se tratan en los triples puntos cuánticos son las coherencias entre los estados cuánticos que llevan a las transiciones de largo alcance. Acoplan indirectamente estados distantes que no tienen un túnel directo mediante una transición virtual a través de estados intermedios. Las transiciones de largo alcance generan transferencia de carga y espín entre puntos cuánticos distantes, siendo un primer paso para transferir información cuántica con baja decoherencia entre qubits distantes. En el capítulo 3, se propone un punto cuántico triple con dos electrones para controlar la transición de largo alcance. Debido a esta transición, en el sistema abierto se observa transporte resonante a pesar de que los estados intermedios son inaccesibles energéticamente. Definiendo canales distintos entre los dos extremos del sistema se obtiene un bloqueo de *superexchange* que cancela completamente la corriente a través del dispositivo. Se estudian las correlaciones de carga y espín, mostrando que la interferencia entre dos canales solo ocurre para el subespacio de singletes.

Para manipular los estados del sistema, se tienen que cambiar en el tiempo las puertas acopladas a los puntos cuánticos. Para estudiar las propiedades dependientes del tiempo y

conseguir un mayor control sobre el sistema, algunos de los puntos cuánticos se acoplan a campos oscilantes en el tiempo con una frecuencia, amplitud y diferencia de fase determinada externamente. El campo director renormaliza el acoplo entre los distintos puntos y permite transiciones resonantes entre estados fuera de resonancia mediante la absorción o emisión de n fotones, asegurando un control directo y externo sobre las superposiciones cuánticas. Este efecto es conocido como túnel asistido por fotones. En el capítulo 4 se extiende el estudio de las transiciones asistidas por fotones a transiciones de largo alcance, donde la absorción y emisión de fotones se conserva entre estados distantes. El estudio se realiza con modelos efectivos y aproximaciones de campos rápidamente oscilantes, consiguiendo un Hamiltoniano independiente del tiempo que permite estudiar analíticamente las coherencias y dinámica del sistema. En el capítulo 5 se analizan estructuras lineales de puntos cuánticos donde los extremos están acoplados a campos ac. Todas las transiciones del sistema están dirigidas, generando múltiples transiciones Landau-Zener entre todos los estados. Se investiga la interacción entre transiciones dirigidas de largo alcance y transiciones dirigidas directas. Prediciendo interferencias cuánticas que dependen de una manera no trivial en la diferencia de fase entre los campos. Para campos en oposición de fase, se observan interferencias destructivas entre transiciones directas y de largo alcance, estas interferencias son análogas a las observadas en sistemas de puntos cuánticos no dirigidos con configuración triangular. Si los campos oscilan en fase, los canales mediados por bandas laterales positivas y negativas interfieren. Estas interferencias destructivas pueden ser detectadas experimentalmente ya que son de la misma naturaleza que las transiciones de largo alcance resonantes, las cuales han sido detectadas. En la configuración propuesta todos los parámetros son controlables experimentalmente y los efectos pueden ser observados como cancelaciones de la corriente. Esto es particularmente accesible para cadenas de puntos cuánticos. El transporte de partículas entre el sistema cuántico y los reservorios implica un transporte de energía, el cual es esencial estudiar para entender la termodinámica de los sistemas de puntos cuánticos. En caso de que los reservorios sean suficientemente grandes o estén acoplados a un baño térmico y a un potencial externo, la energía intercambiada no va a cambiar su temperatura o potencial químico. En cambio, para reservorios aislados este intercambio de energía sí hará evolucionar su temperatura y potencial químico hasta llegar al estado estacionario. En el capítulo 2 se estudia la evolución hacia un estado de equilibrio entre dos reservorios aislados de átomos ultra fríos. En el estado inicial, los reservorios tienen distinta temperatura y distinto potencial químico y pueden estar formados tanto por fermiones como por bosones. Los dos reservorios están acoplados a través de un único punto cuántico por el cual se produce el intercambio de partículas y energía. El estudio analítico de este sistema se realiza con una teoría lineal que permite caracterizar las escalas de tiempo y el proceso de relajación de los reservorios. Adicionalmente, este dispositivo es investigado como un transistor o un capacitor de partículas. En sistemas dirigidos, el campo ac es una fuente exclusiva de energía que no intercambia partículas. Su efecto en la termodinámica del sistema se estudia en el capítulo 6. El propósito es extraer la energía del campo ac y transportarla de manera no local a través de una transición de largo alcance a un reservorio distante. En este sistema se implementan máquinas de largo alcance de calor y frio entre dos reservoiros. También se propone un montaje que permite a reservorios distantes obtener energía simétricamente del campo ac.

Abstract

The topic of the present thesis is: *transport through mesoscopic systems*. Mesoscopic systems are materials with a maximum size of the order of the micrometer, whose properties are governed by quantum mechanics. In these materials, the single and few particle transport dynamics, interactions and coherence are studied.

The platforms considered for the development of the present thesis are quantum dots, where particles with a defined spin are confined in discrete energy levels. Different quantum dots are coupled by tunnel junctions, overlapping the wave functions of their higher energy states. The particles in these states are then coherently delocalized along the whole quantum dot structure, which behaves as an artificial molecule. A strong particle-particle interaction is present in these systems due to the short distant between them. These systems can be externally controlled by tunning gate voltages capacitively coupled to the dots; therefore, the energy, entropy, and the coherent dynamics of the systems change in a supervised manner. Most of the thesis is based in triple quantum dots, which constitute a perfect device to investigate multilevel quantum interference. They have the advantage of an spatial separation of the states that, with the recent advances in their tunability, makes it possible to manipulate them individually; on the other hand, the tunnel coupling between them can also be controlled. To study particle transport, the quantum dot systems are weakly coupled to reservoirs, with whom they exchange particles and energy. In Chapter 7 a triple quantum dot with three reservoirs is studied to demonstrate the interactions of the different transport paths between the reservoirs. The Coulomb interaction of the electrons and the correlations between the different paths leads to a current blocking in one of the channels when the other has high conductance.

One of the main problems that is studied in the triple quantum dot are the coherences of the electronic states that lead to the long-range transition. It indirectly couples distant states, which don't have a direct tunnel coupling, by means of a virtual transition through an intermediate and energetically forbidden state. The long-range transition purports charge and spin transfer between distant dots, which is an initial step to the exchange of quantum information between distant qubits with low decoherence. In Chapter 3, a two electron triple quantum dot system is proposed as a controller of the long-range transition. As a consequence of this transition, in the open system resonant transport is observed despite the intermediate states of the triple quantum dot are energetically inaccessible. Different virtual trajectories between the two ends of the system are defined, leading to a superexchange blockade that totally blocks the charge current through the device. The charge and spin correlations are studied, showing that the two path interference only occurs for the singlet subspace.

To manipulate the states of the system one have to change in time the gates coupled to the dots. To study the time dependence properties and get more control over the system, oscillatory fields with a defined frequency, amplitude, and phase are coupled to the dots. The driving field renormalizes the couplings among the different dots and permits resonant transitions between

detuned dots by the absorption or emission of n photons. This effect is known as photon-assisted tunneling, which allows to demonstrate the coherent tunneling in quantum dot systems. The parameters of the field are easily tunable externally, warranting a direct control on the quantum superpositions by changing the renomalization of the couplings. In Chapter 4, the study of photon-assisted transitions with a single field is extended to long-range transitions, where the absorption and emission of photons is conserved between distant quantum states. The study is done with effective models and fast oscillating approximations to get a time independent Hamiltonian to analytically study its coherences and dynamics. In Chapter 5 linear quantum dot structures with multiple fields applied to distant dots are considered. All the transition within the system are driven by an ac field, which generates multiple Landau-Zener passages among them. It is investigated the interaction between long-range and direct photon-assisted transitions in transport experiments. Quantum interferences that depend in a nontrivial way on the phase difference of the locally applied drivings are predicted. For fields in phase opposition, there are destructive interferences between direct and long-range transitions, which are analogous to dark states in closed-loop undriven structures. If the edge dot levels oscillate in phase, quantum paths mediated by positive and negative detuned sidebands interfere, leading to multiple dark states in the Landau-Zener-Stückelberg interference pattern. These destructive interferences can be experimentally detected as they are of the same nature as long-range current resonances, which have been unambiguously observed. In the proposed transport configuration all parameters are experimentally controllable, the features can be measured as cancellations of the current. This is particularly accessible in quantum dot arrays, which are within experimental reach for both electric or magnetic field drivings.

The transport of particles between the quantum system and the reservoirs imply an energy exchange between them, which is essential to understand the thermodynamics of the quantum dot system. When the reservoirs are sufficiently large or coupled to a thermal system and potential contact, the exchange of energy and particles do not make their temperature or chemical potential to change; however, for isolated reservoirs this energy exchange make their temperatures and chemical potential to evolve in time until a steady state is reached. In Chapter 2, it is studied the equilibration process between two isolated reservoirs of ultracold atoms, which have different temperatures and different chemical potentials, and can be either fermions or bosons. The two reservoirs are weakly coupled through a single quantum dot with a determined number of energy levels, through which particles and energy are exchanged. Quantum dots for ultra-cold atoms can be created with laser beams, which define their quantum path. The analytical study of this system is done with a linearized theory which allows one to characterize the time scales and to describe the equilibration process of the reservoirs. Additionally, the proposed device is investigated as a particle transistor or particle capacitor.

In driven systems the ac field is an additional source of energy with whom the quantum system exclusively exchanges energy, not particles. The effect of the ac field on the thermodynamics of triple quantum dot systems is studied in Chapter 6. The purpose is to extract the energy from the ac-field and transport non-locally through a long-range transition to a distant reservoir. The thermodynamics of driven quantum systems detached from reservoirs is analyzed before studying the open system. In this thermodynamic driven system the energy and heat transport between the reservoirs is studied to implement long-range heat and cooling engines. The proposed setup additionally permits a symmetric energy exchange with two distant reservoirs.

List of Figures

Figure **Page**

1.1 The three images are from [2]. (a)- Lateral Double Quantum Dot structure. (b) and (c) Transport in a single and double quantum dot respectively defined with gate potentials. 2

1.2 Left- figure from Ref. [20]. Differential conductance through a single vertical QD vs. the bias voltage and a gate voltage. Coulomb diamonds are seen as white regions, the white color means zero differential conductance, i.e., a constant number of electrons within the QD. The energy levels of the QD are tunned (vertical axis) with an external gate voltage. In the right part of the figure the energy level structure is represented for the points marked in the right figure. The transport between the leads is only possible outside the Coulomb diamonds, green circle at finite source-drain voltage. . . 3

1.3 Image obtained from Ref. [1]. Charge transport vs. the value of the gate voltage coupled to a single QD. Transport peaks are observed when the different energy levels of the QD go through the bias window of the reservoirs. The inset compares the energies to add an additional electron to the dot. 4

1.4 (a)- Theoretical simulation of a stability diagram of a DQD coupled to two reservoirs at zero bias. It plots the charge conductance vs. two gate voltages: U_{G1} and U_{G2}. (N_L,N_R) are the number of particles in each dot. The blue-dashed lines are the resonances between two states with different particle number, and the red-dashed lines are the resonances between two sates with same particle number, i.e., coherently coupled. (b)- Theoretical simulation of the current through a QPC located in the proximity of the DQD. The calculation is done in the same region of the stability diagram as in (a). (c)- Rabi oscillation between the state with one particle in the left dot and the state with one particle in the right dot at the point of the stability diagram where (1,0) and (0,1) are in resonance (marked with a spade in (a)). 5

1.5 SB effect in DQDs. Initially the right dot is occupied with one electron with spin up. The current is blocked as soon as an electron with spin ↑ get into the left QD. (a) The electron has the correct spin to tunnel to the right dot. (b) Due to the Pauli Exclusion principle the electron of the left dot cannot tunnel to the right dot. 7

1.6 The figures are taken from Ref. [54] and [55]. *Left*- (a) Image of a lateral DQD. (b) Driven transport sketch: an electron absorbs one photon to tunnel from the left dot to the right dot, permitting the transport between the reservoirs. (c) Driven current through the device for different values of the driving field. In all the lines there is a central peak that accounts for the resonant transition between the dots. Two additional peaks appear at the energy different between the states equal to the frequency of the driven field. *Right*- Stability diagram of a driven DQD similar to Fig. 1.4, which plots the differential conductance vs. two gate voltages. In Fig. 1.4 only one single conductance peak appears for each TP, but in this system due to the driving, additional resonances appear for the absorption and emission of one (1γ) and two (2γ) photons. . 9

1.7 Images obtained from Ref. [73]. The figures show the three dimensional stability diagram of a TQD. Each of the three planes correspond to a charging event between one of the dots and the reservoirs. The space between the planes are the stability volumes of the different states of the TQD. In the blow up figure, quadruple points are marked, where four different stability volumes coincide. 10

1.8 Schematics pictures obtained from Ref. [2]. (a)- Lateral QD. (b)- Vertical QD. 12

1.9 (a),(b)- Sample produced by Johannes Bayern in the group of Rolf Haug [118]. (a) - General view of the device. (b)- Gates made with electron lithography above the 2DEG. The electrons can be localized in four linearly coupled QDs. (c)- Sample produced by M. C. Rogge in the group of Rolf Haug [85]. Triple Quantum Dot (TQD) sample in triangular shape defined by oxide lines. 12

2.1 Sketch and experimental measurements taken from Ref. [142]. Two identical reservoirs of ultra-cold atoms are coupled through a quasi two dimensional channel. A gate beam blocks the the particle and heat transport between the reservoirs while one of the reservoirs is heated up with a laser heating beam. After the laser beam, the transport between the two reservoirs (now with different temperatures) is permitted again and the relaxation dynamics is studied. In the graphics, the temperature and the particle difference between the reservoirs are measured during the relaxation process. 28

2.2 Time evolution of the particle density $n_{\nu,\sigma} = N_{\nu,\sigma}/\mathcal{N}$ in both reservoirs for each spin. The quantum system that connect the two reservoirs suffers a Zeeman splitting breaking the spin degeneracy in its energy level, the $\uparrow$ particles travels through the lower level at $\omega_\uparrow = 0.9\bar{\omega}$ and the $\downarrow$ particles at $\omega_\downarrow = 2.1\bar{\omega}$. At $t = 0$ the particle number in each reservoir and for each spin are equal $n_{\nu,\sigma} = 0.25$ and there is a temperature gradient between the reservoirs $T_L = 0.45\bar{\omega}$, $T_R = 0.25\bar{\omega}$. 30

3.1 *Left*- Figures from Ref. [101]. In the upper figure, the image of the used TQD sample is shown. The bottom picture shows the transport triangles for finite bias, where resonance transport lines are observed for the LR transition ($L-R_T$ and L_T-R) between the states $(1,1,2)$ and $(2,1,1)$. *Right*- Figures from Ref. [103]. The upper figure shows the TQD sample used in the experiment. A QPC is located in the proximity to detect the charges within the system. At the bottom, the real-time trace of the QPC current exhibits fast steps that appear to correspond to single electron transfer between the states $(1,1,0)$ and $(0,1,1)$. 46
3.2 Two electron states structure within the TQD. 47
3.3 In (a) the level configuration for the different values of U_L is plotted. The blue vertical line is the U_L corresponding to the DS configuration. The dashed lines are the chemical potentials of the leads. In (b) the current through the QPC is plotted vs. U_L for three different values of U_M. A decrease of the QPC current is observed in the DS due to a decrease of the occupation of the state $|0,1,0\rangle$ in the TQD. In (c) we plot the lock-in simulation. The inset shows the structure around the DS condition. 50
3.4 Same simulations as in Fig.3.3, with a level configuration where the DS and LR do not coincide at the same value of U_L and importantly, for the detection of the DS, the DS's energy is far below the chemical potential of the leads. The vertical red lines indicates the value of U_L for the DS. 51

4.1 Transport through a linear TQD weakly coupled to reservoirs on its ends vs. the energy differences between the energy levels of the dots. Each quantum dot has a single energy level and the number of electrons within the TQD is up to one. The simulation is done with the Master equation theory (see Sec. 1.2.4). High current intensity is observed in both figures at $\epsilon_L-\epsilon_R=0$ while the energy difference with the central dot is large. (a)- The couplings between the dots are symmetric. A central peak is observed when all the dots are on resonance. (b)- The couplings are asymmetric. This fact produces a molecular behavior between the dots that are more strongly coupled, showing an anticrossing shape in the resonance of the three dots. 60
4.2 Charge transport between reservoirs in the infinite bias limit through the TQD vs. the amplitude of the ac-field and the energy differences between the outer dots. The left dot of the TQD is coupled to an ac-field. The LZS pattern shows the participation of the three states within the TQD system. *Left:* Central dot in resonance with the left dot for $\epsilon_L-\epsilon_R=3\hbar\omega=\epsilon_C$. *Right:* Full triple quantum dot resonance at $\epsilon_L-\epsilon_R=0=\epsilon_C$. In both cases $\tau=1$, $\hbar\omega=3.3\tau$ and $\epsilon_R=0$. 62

CHAPTER 1

INTRODUCTION

This introduction gives a general idea of the platforms and the theory used in this thesis. It also gives the motivation of the presented works. In the first part, quantum dots are introduced. The electronic transport through a quantum dot system weakly coupled to reservoirs is studied. In this transport regime the Coulomb blockade effect and spin blockade effects are explained. The effect of electric fields in the quantum dot energy levels and consequently in transport is analyzed. Finally, a brief introduction of the fabrication of lateral quantum dots is given. In the second part, the Hamiltonian and the density matrix theory for coherently couple quantum dots is introduced. For the open system, the Master equation is derivated for undriven and driven systems. Then, the equations for particle energy and heat transport are obtained from the results of the Master equation.

1.1 Quantum dot systems

Quantum Dots (QDs) are regions with a size comparable to the electronic wavelength (Fermi wavelength of the host material), where electrons are localized in the three dimensional space [1–3]. The confinement generates a shell structure similar to real atoms, with a discretization of the electronic energies. For this reason, QDs are also named artificial atoms [4, 5]. In a Two Dimensional Electron Gas (2DEG), these regions are generated by gate voltages who deplete the 2DEG (see Fig. 1.1(a)). The number of confined electrons can be controlled [6, 7]. Small changes in the gate voltages are used to manipulate the different parameters of the dots, for instance, the internal energy level structure, the geometry and the tunnel couplings between different dots; making these structures very versatile for manipulating individual electronic states and the spin [8]. Their external control and their larger dimensions in comparison with atoms, makes them suitable for experiments that can not be carried out in atomic physics. These systems allow one

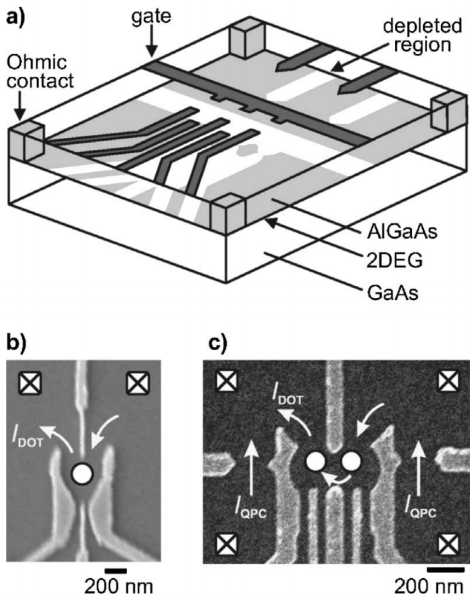

Figure 1.1: The three images are from [2]. (a)- Lateral Double Quantum Dot structure. (b) and (c) Transport in a single and double quantum dot respectively defined with gate potentials.

to study and fabricate nanoscale devices based on quantum transport [9–11], such as the single electron transistor [12–15], and more complex systems as quantum gates for quantum computers [16–18]. The quantum computer is well know to have a computational power much stronger than classical computers . It will solve problems that in classical computers would require an exponential amount of time or memory [19].

1.1.1 Transport in the weak coupling regime

To introduce transport experiments, the single quantum dot weakly coupled to reservoirs is considered [21, 22] (see Fig. 1.1(b)).
In the thesis, the reservoirs are modeled as a free electron gas with a specific temperature (T) and chemical potential (μ) which can be tunned with external potentials. The distribution of the electrons in the reservoirs is given by the Fermi function: $f(\epsilon) = (1 + \mathrm{Exp}[(\epsilon - \mu)/k_B T])^{-1}$. When a reservoir is coupled to the QD, charge fluctuations between them take place, changing the number of electrons in the dot. For strong coupling, charge fluctuations are strong and the number of electrons in the dot is not well defined, i.e., the quantization of the charge in the QD is completely lost. A non-interacting theory is appropriate in this case. In the intermediate regime, the fluctuations are strong but the discreteness of the charge still plays an important role; here, higher order tunneling processes with the reservoirs have to be considered [23–25]. In this dissertation, the weak coupling regime is studied, where the electron number (N) in the dot is always a well defined integer. The interactions and quantization of the charge play a main role and the tunneling with the reservoirs is treated up to first order. To assure weak coupling

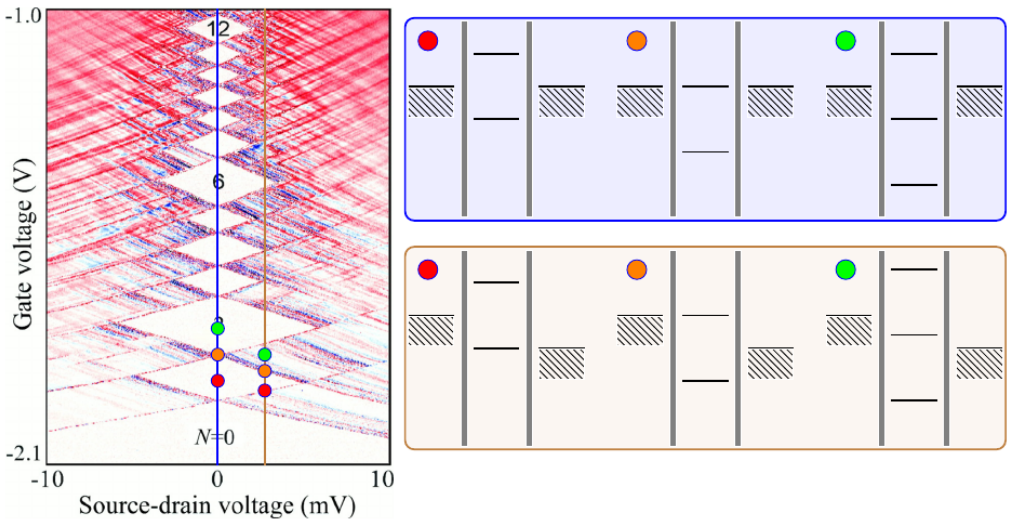

Figure 1.2: Left- figure from Ref. [20]. Differential conductance through a single vertical QD vs. the bias voltage and a gate voltage. Coulomb diamonds are seen as white regions, the white color means zero differential conductance, i.e., a constant number of electrons within the QD. The energy levels of the QD are tunned (vertical axis) with an external gate voltage. In the right part of the figure the energy level structure is represented for the points marked in the right figure. The transport between the leads is only possible outside the Coulomb diamonds, green circle at finite source-drain voltage.

between the quantum dot and the reservoirs, high potential barriers separate them.

In a transport set-up, two o more reservoirs are coupled to the QD. Applying a potential difference between two reservoirs, the charge transport get more probable in one direction. The charge jump from the reservoir to the dot is more probable in the reservoir with higher chemical potential (named *source*) and the opposite in the reservoir with lower chemical potential (named *drain*). This produces a net particle flow between the reservoirs, i.e., particle transport. The asymmetric probability of the particle transport is much greater when the energy level of the QD is between the two Fermi energies; thus, the net electron flow is higher here. This energy region is named *bias window* or just *bias*. When the Fermi energies are equal (zero bias) the transport is equally probable in both directions; hence, there is no transport through the device.

Because of the strong Coulomb interaction between the particles in the QD, transport is a sequence of single electrons tunneling events. The next electron does not tunnel from the source to the dot until the previous one has tunnel to the drain (sequential tunneling), otherwise it would require an extra energy. If reservoirs can not provide the energy to add a single electron to the dot, the current is blocked. The Coulomb interaction is the responsible of this blocking; therefore, this effect is called Coulomb Blockade (CB) [26–28]. Using gate voltages, one can provide externally this energy, and the charge will flow again.

Fig. 1.2 plots the well-known Coulomb diamonds of a single QD, where the diamond-shape white regions are in CB. In the right part of the figure, sketches are plotted for zero bias (blue shadowed

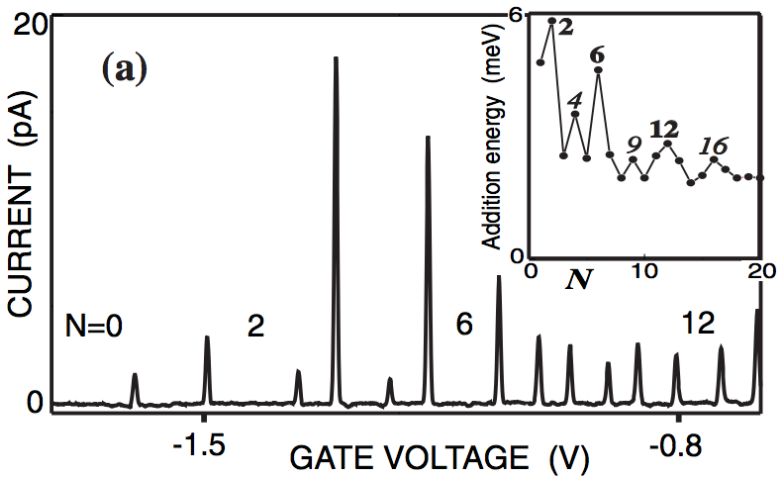

Figure 1.3: Image obtained from Ref. [1]. Charge transport vs. the value of the gate voltage coupled to a single QD. Transport peaks are observed when the different energy levels of the QD go through the bias window of the reservoirs. The inset compares the energies to add an additional electron to the dot.

area) and finite bias (brown shadowed area). At zero bias (vertical blue line), by tuning the gate voltage, the energies are shifted down. The charge occupation of the dot changes when an empty state crosses the Fermi energy (orange dot), changing from one Coulomb diamond (red dot) to another (green dot). At finite bias, the transport is in CB when no energy level is in the bias window (energies between the red and orange dot). Increasing the gate voltages and setting an energy level in the bias window (out of the diamond), there is transport through the device (green circle).

Transport measurements through all the different levels of the QD are a way to obtain information of the energy structure of the QD externally. Tuning the gate voltages coupled to the dot, the energy levels are shifted and transport measurements from all the levels are collected when they are in the bias window of the reservoirs. In Fig 1.3, transport peaks are observed vs. the gate voltage coupled to the QD. The separation between the peaks is the energy difference between the electronic orbitals of the QD, which gives information about the Coulomb interaction between the electrons. The levels where the energy to add an additional electron is higher are the magic numbers of the internal shell structure of the dot.

In this section the current just depends on the charge configuration and can be described with a rate equation [26], where the coherence is not relevant.

1.1.2 Coherence in quantum dots

This thesis treats arrays of quantum dots, where the coherences of the system are very relevant to study the transport properties. The simplest system where the coherences are important is the Double Quantum Dot (DQD) [11, 29, 30].

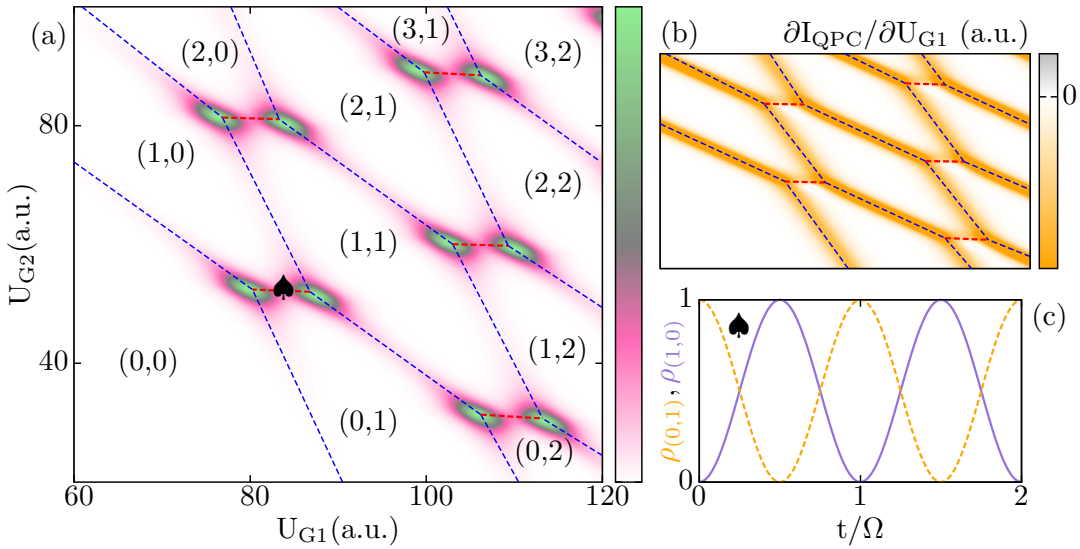

Figure 1.4: (a)- Theoretical simulation of a stability diagram of a DQD coupled to two reservoirs at zero bias. It plots the charge conductance vs. two gate voltages: U_{G1} and U_{G2}. (N_L,N_R) are the number of particles in each dot. The blue-dashed lines are the resonances between two states with different particle number, and the red-dashed lines are the resonances between two sates with same particle number, i.e., coherently coupled. (b)- Theoretical simulation of the current through a QPC located in the proximity of the DQD. The calculation is done in the same region of the stability diagram as in (a). (c)- Rabi oscillation between the state with one particle in the left dot and the state with one particle in the right dot at the point of the stability diagram where (1,0) and (0,1) are in resonance (marked with a spade in (a)).

The DQD is formed by two QDs coupled by a tunnel junction, where the particle can oscillate coherently [6, 31–33]. The tunnel coupling between the dots does not couple states with different spin number, i.e., the spin of the particle is conserved during a tunneling event. The DQD can behave either as a two individual QDs, where the electrons are localized in each QD [34], or as an artificial molecule [33, 35, 36], where the conducting electrons are delocalized over both dots. The behavior is controlled by the relation between the tunnel coupling τ and the energy difference $\Delta\epsilon$ between the localized energy levels of each dot. If $\Delta\epsilon \gg \tau$, the coupling is not strong enough to hybridize states with so large energy differences; hence, the electrons are localized in each dot. In the opposite case, if $\Delta\epsilon \lessapprox \tau$, the states get hybridized and then the DQD behaves as an artificial molecule. Their tunability makes them suitable for quantum information applications [16, 37, 38].

To study it in more detail, the Hamiltonian for a DQD with one level in each side is introduced:

$$\hat{H}_{DQD} = \frac{\Delta\epsilon}{2}\sigma_z + \tau\sigma_x \tag{1.1}$$

where σ_i are the Pauli matrices, τ is the coupling parameter and $\Delta\epsilon$ is the energy difference between the on-site states of the two QDs (see Sec. 1.2 for more information). The eigenenergies

and eigenvalues of $\hat{H}_{DQD}$ are:

$$E_{\pm} = \pm\frac{1}{2}\sqrt{\Delta\epsilon^2 + 4\tau^2}, \quad \begin{cases} |\Psi_+\rangle &= \cos\left[\frac{\theta}{2}\right]|L\rangle + \sin\left[\frac{\theta}{2}\right]|R\rangle \\ |\Psi_-\rangle &= \sin\left[\frac{\theta}{2}\right]|L\rangle - \cos\left[\frac{\theta}{2}\right]|R\rangle \end{cases} \tag{1.2}$$

where $\theta = \arctan[2\tau/\Delta\epsilon]$. Hence:

$$\tau \gg \Delta\epsilon \Rightarrow \theta \approx \frac{\pi}{2} \quad \Rightarrow \quad |\Psi_\pm\rangle = \frac{1}{\sqrt{2}}(|L\rangle \pm |R\rangle) \qquad \Delta E \approx 2\tau \qquad \text{maximally delocalized} \tag{1.3}$$

$$\tau \ll \Delta\epsilon \Rightarrow \theta \approx 0 \quad \Rightarrow \quad |\Psi_+\rangle = |L\rangle\,,\ |\Psi_-\rangle = |R\rangle \qquad \Delta E \approx \Delta\epsilon \qquad \text{localized} \tag{1.4}$$

with $\Delta E = |E_+ - E_-|$. When the particle is maximally delocalized the eigenstates are the molecular *bonding* and *antibonding* states with an energy difference of 2τ; and when the charge is localized the eigenstates are equal to the on-site states of each QD. The gate voltages coupled to the system tune the energies and the tunnel coupling; thus, the behavior from molecular to localized can be changed externally. Coupling one reservoir to the left dot and another to the right dot, the charge flow through the DQD is only possible when the particle oscillates between the two dots, i.e., is delocalized between them. Otherwise, the charge gets localized in one of the dots and the transport is suppressed.

In DQDs and more complex structures, the gate voltages which control the properties of each QD also affect the properties of the other dots. This makes difficult to know how many electrons are confined in each quantum dot, which is an important information in order to perform experiments. In general, to characterize the sample, a one dimensional channel (named Quantum Point Contact (QPC) [39]) is located in the proximity of the device (see Fig. 1.1 (c)). The biased QPC has a current flowing through it (I_{QPC}), which due to the proximity with the QD system, it is very sensitive to the presence of charges in the QDs: $I_{QPC} = I_{QPC}(N_L, N_R)$, where N_i is the number of particles in the i-dot. The current will decrease if a QD gets charged and will increase in the opposite case [28, 40]. The QPC is differently coupled to the QDs; hence, the changes in the intensity of current through the QPC depend on which dot gets an extra electron. Measuring the current through the QPC vs. the gate voltages coupled to the dots, the charging events are detected. In Fig. 1.4 (b) the derivative of I_{QPC} with respect to a gate voltage is plotted vs. two gate voltages. The measured orange lines correspond to charging events from the reservoirs to the dots. In DQDs the charging lines define two dimensional regions (named *stability regions*) in the gate voltage space where the different states of the system are identified. This kind of figures are named *stability diagrams*. In Fig. 1.4(a) the conductance through the DQD is plotted in the same stability diagram. The charging lines obtained in the QPC measurement are marked as blue-dashed lines, and the states corresponding to each region are labeled as (N_L, N_R). The red-dashed lines corresponds to resonances between states that are coupled coherently, i.e., where the particles are delocalized between them. This region is where high conductance is observed. The maximum conductance peaks are when the molecular states are in resonance with the Fermi energy of the reservoirs. These resonances are named Triple Points (TPs) as they involve three

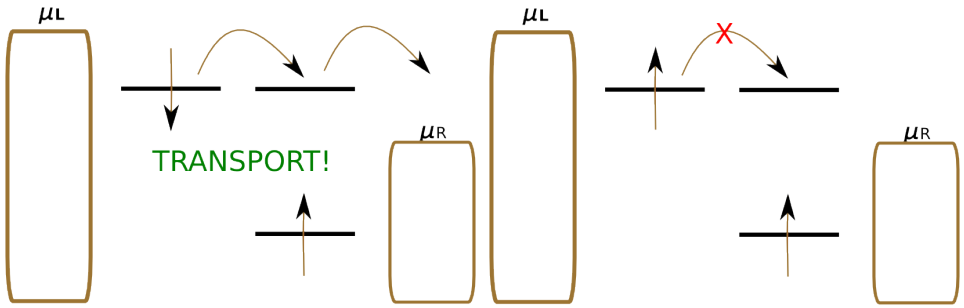

Figure 1.5: SB effect in DQDs. Initially the right dot is occupied with one electron with spin up. The current is blocked as soon as an electron with spin ↑ get into the left QD. (a) The electron has the correct spin to tunnel to the right dot. (b) Due to the Pauli Exclusion principle the electron of the left dot cannot tunnel to the right dot.

different states in resonance. For instance, the TP containing less electrons involve the states $(0,0)-(0,1)-(1,0)$, which generate the transport sequence $(0,0)\rightarrow(0,1)\rightarrow(1,0)\rightarrow(0,0)$. In Fig. 1.4(c) coherent oscillations (named *Rabi oscillations*) of the occupation probability in each i-dot, ρ_i, are plotted. The Rabi frequency is proportional to the coupling between the dots: $\Omega_R = 2\tau$.

Within a QD system one can define the basic block for a quantum computer: the Two Level System (TLS) (qubit)[2, 33, 41]. To build up a single qubit is needed at least either a magnetic field which produces a Zeeman splitting in a QD, or a Double Quantum Dot (DQD) structure which defines a charge qubit with the discrete levels of each dot. The TLS has to be robust against relaxation and decoherence for a sufficient large time in order to maintain the information unchanged before the read-out. The decoherence time scale of the electron spin within the QD is of the order of $T_2 = 1-100\mu s$ for GaAs [2], which is mainly attributed to the interaction with the nuclear field present in most of the devices. If the nuclear field is unknown, the decoherence drops up to the order of $T_2^* = 10ns$. The charge Rabi oscillation in double quantum dots with a tunnel coupling of $\tau = 1$meV have a period of approximately $T_\Omega = 0.01$ns; and weak coupling with the reservoir of $\Gamma = 1\mu$eV has approximately one tunneling event each 10ns. Therefore, the spin in the transport dynamics through a DQD do not have time to suffer relaxation or decoherence with these time scales. Some experiments are exploring new regimes, for instance, hole transport, which has a limited hyperfine interaction with the nuclear spins and hence is expected to reduce decoherence in comparison with electron spins [42–49], and other materials, such as silicon, which for ^{28}Si does not have an atomic spin [50, 51]; however, they have other problems, for example, the indirect band-gap present in silicon which limits the coupling with photons.

One of the most important effects that one can have in DQDs is the Spin Blockade (SB). In quantum mechanics, two fermions cannot have the same quantum numbers. Then, two electrons occupying the same level of a quantum dot can only have opposite spins. This is the origin of the SB effect in transport experiments, where states with two electrons with same spin block the current through the device [2, 30, 32, 52, 53] (see Fig. 1.5). This happens in DQD or bigger

QDs systems: Consider a biased DQD with the left dot coupled to the source, the right dot to the drain, and a tunnel coupling between the two dots. There is one level in each QD and in the right one, double occupancy is accessible. The double occupied state is formed by two electrons with different spins which form a singlet: $|S_{\mathrm{R}}\rangle = |0,\uparrow\downarrow\rangle$. The system is tunned such that this state is the only one that exchanges electrons with the drain; thus, the transport sequence has to contain this state. Initially, an electron with spin up is localized in the right QD, this electron cannot jump to the reservoirs because is below the chemical potential of the drain, i.e, in CB. When an electron comes from the source to the system, depending on the spin number, a singlet or triplet is formed. The different possibilities are:

$$\text{singlets}: \quad |S_{\mathrm{LR}}\rangle = \frac{1}{\sqrt{2}}\Big(|\uparrow,\downarrow\rangle - |\downarrow,\uparrow\rangle\Big) \tag{1.5}$$

$$\text{triplets}: \quad \begin{cases} |T^{+}_{\mathrm{LR}}\rangle = |\uparrow,\uparrow\rangle \\ |T^{0}_{\mathrm{LR}}\rangle = \frac{1}{\sqrt{2}}\Big(|\uparrow,\downarrow\rangle + |\downarrow,\uparrow\rangle\Big) \end{cases} \tag{1.6}$$

If the singlet $|S_{\mathrm{LR}}\rangle$ is formed, it will be able to go through the device to the drain: $|0,\uparrow\rangle \rightarrow |S_{\mathrm{LR}}\rangle \rightarrow |S_{\mathrm{R}}\rangle \rightarrow |0,\uparrow\rangle$ but if a triplet is formed, the current will be blocked [30]: $|0,\uparrow\rangle \rightarrow |T_{\mathrm{LR}}\rangle \not\rightarrow |S_{\mathrm{R}}\rangle$. In Fig. 1.5 there is an intuitive scheme of this effect.

1.1.3 Quantum dots under electric fields

The ac fields are generated by microwaves applied to the gate voltage coupled to the dots [54–58]. They were introduced to characterize with microwave spectroscopy the energy estructure of the quantum dot [11, 54, 55], which also demonstrates the coherent tunnel in DQDs. In quantum information they are used for single qubit manipulations [59–61].

Microwaves induce transitions between the different levels, generating multiple Landau-Zener Transitions (LZT) between the two states of the DQD. The LZT changes the particle occupation of the states with a probability which was first studied by Landau [62] and Zener [63]. For multiple passages it provides a phase difference between different transitions of the states, which leads to a dependence of the observables on it [62, 64]. The periodicity of these passages leads to the Landau-Zener-Stückelberg (LZS) interference. It provides a useful tool that allows for the characterization of the parameters defining the quantum TLS and its interaction with the control fields and the environment [65].

In this thesis the frequencies considered are faster than the rest of the dynamics, i.e, $\omega > \tau \gg \Gamma$, where τ is the coupling parameter between two dots and Γ between the dots and the reservoirs. Additionally in most of the thesis the relation with the amplitude of the driving V is $\omega \mathrm{V} \gg \tau^2$. In this regime, the system is in the fast passage limit [65]. One of the most important processes in fast driven systems is the Photo Assisted Transition (PAT). The microwaves drive the transition between the states of the DQD, in such a way that the transitions are resonant when the energy difference between two states is equal to an integer number of the frequency of the field: $\Delta \mathrm{E} = n\hbar\omega$

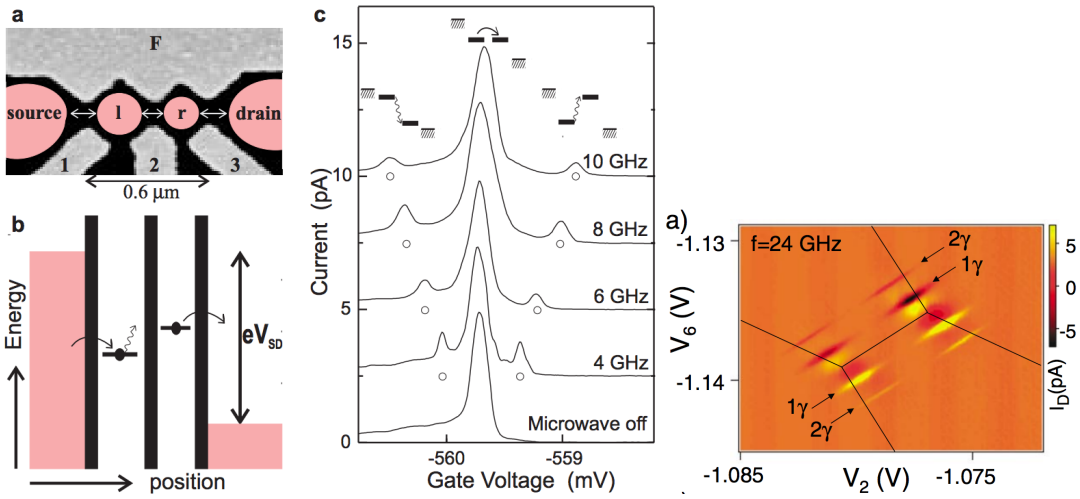

Figure 1.6: The figures are taken from Ref. [54] and [55]. *Left*- (a) Image of a lateral DQD. (b) Driven transport sketch: an electron absorbs one photon to tunnel from the left dot to the right dot, permitting the transport between the reservoirs. (c) Driven current through the device for different values of the driving field. In all the lines there is a central peak that accounts for the resonant transition between the dots. Two additional peaks appear at the energy different between the states equal to the frequency of the driven field. *Right*- Stability diagram of a driven DQD similar to Fig. 1.4, which plots the differential conductance vs. two gate voltages. In Fig. 1.4 only one single conductance peak appears for each TP, but in this system due to the driving, additional resonances appear for the absorption and emission of one (1γ) and two (2γ) photons.

[54, 55]. This is shown as additional resonances in Fig. 1.6, where the particle absorbs the energy of n photons to overcome the transition. For some parameters of the driving, the PAT leads to a strong localization of the particle in resonant transitions, which blocks the current through the device. This effect is known as Coherent Destruction of Tunneling (CDT) [66, 67].

1.1.4 Triple quantum dot

In the recent years, the technical improvements have permitted to build and study experimentally in detail a coherently coupled Triple Quantum Dot (TQD) [68–70]. It is the simplest structure of a qubit array without control of local spin interactions [71] and it represents a step towards the qubit arrays needed for quantum computation. For the case of three confined electrons in the TQD [72–74], exchange interaction between two pairs allows qubit rotation around two axes, hence full control, using only electrostatic gates [75], without using oscillating magnetic fields or Zeeman field gradients. The TQD has a much richer spectrum than DQDs [74, 76, 77], being able to go beyond the physics of it. They can behave as quantum rectifiers and ratchets [78, 79], spin entanglers [80] or coded qubits [37, 81]. They provide as well the implementation of quantum cellular automaton processes [73, 82], a combination of charging and reconfiguration events in the system being a crucial process in quantum information. A TQD is the smallest system that, in principle, allows the implementation of Coherent Transfer by Adiabatic Passage (CTAP) [83, 84].

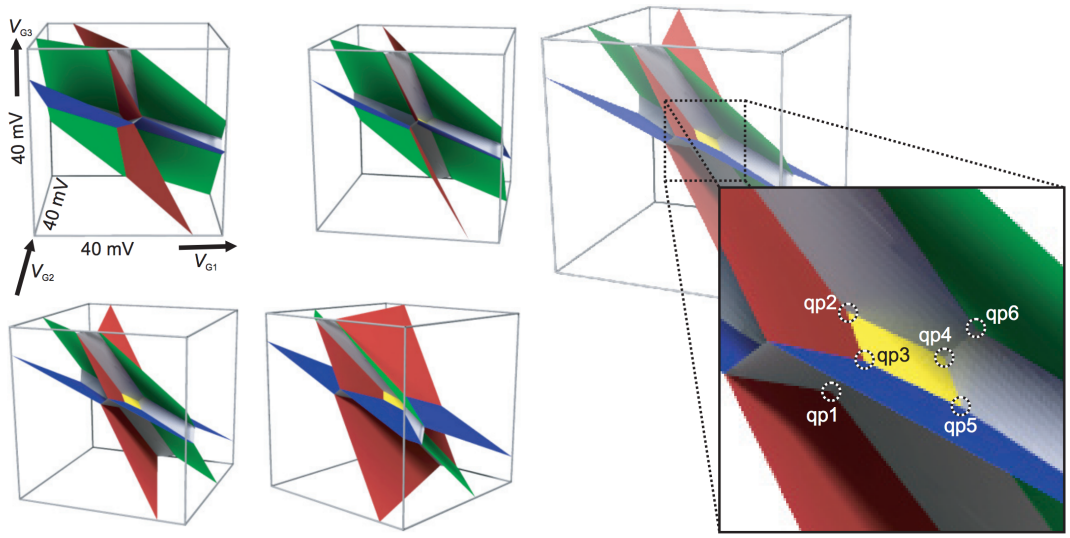

Figure 1.7: Images obtained from Ref. [73]. The figures show the three dimensional stability diagram of a TQD. Each of the three planes correspond to a charging event between one of the dots and the reservoirs. The space between the planes are the stability volumes of the different states of the TQD. In the blow up figure, quadruple points are marked, where four different stability volumes coincide.

CTAP has been proposed as a way to efficiently move electrons along arrays of QDs and entangle quantum mechanical states of distant qubits. The multilevel structure of the TQDs make them very suitable for studying interference phenomena between different transport paths that give rise to charge localization. In transport the charge localization is detected as a current blocking, and it is named Dark State (DS).

The stability diagram of TQDs is defined in the three dimensional gate space. Resonant transport occurs at the coincidence of four states, named Quadruple Point (QP) [68, 70, 73, 85] (see Fig. 1.7) and imply the resonance of the three QDs and the Fermi level of the reservoirs. The TQD can be constructed with two different geometries: the linear, where the two ends are not tunnel coupled, and the triangular or closed loop configuration, where all the dots are coupled coherently (See samples of both structures in Fig. 1.9). Triangular structures are suitable to construct different physical paths through the device and study the interference effects between them [86, 87]. They are also proposed to measure the Aharanov-Bohm effect [88] by applying a magnetic flux to the area of the closed loop structure [89, 90], or to study charge and spin frustration [91].

In this thesis one of the main goals is to study Long Range (LR) interactions between distant states. For that purpose, the linear TQD is the suitable structure since it has two distant dots which are not directly coupled.

1.1.4.1 Long Range transport

The LR coherent transitions mechanism is essential in many fields: Delocalization coming from this transition is essential to understand donor-acceptor reactions through bridge states [92, 93], which is relevant for molecules as complex photosynthetic centers [94] or DNA [95, 96]. LR were also introduced to explain transport and order in magnetic compounds [97, 98], and related ideas leads to the Kondo problem [99, 100] at very low temperatures.

The TQD is a perfect platform to study this transition in detail. The LR coupling has been measured in these systems as current resonances [101, 102] and by real time charge detection [103] (see Fig. 3.1). The transitions go through energetically forbidden intermediate quantum states that are only virtually occupied. The virtual transitions are a consequence of the uncertainty principle, which allows electrons to access energetically forbidden states if they do so on a sufficiently fast timescale [104] (for more information see Chapter 3). In Sec. 1.2.3 an example of an effective Hamiltonian between two distant states is obtained. The states $(1,0,0)$ and $(0,0,1)$ are coupled by a virtual transition through the intermediate state $(0,1,0)$. In Chapters 4 and 5, the control of the LR transition is investigated by introducing a driving.

1.1.5 Fabrication

There are multiple architectures for building QD systems: either vertical or lateral ones [2] are the mainly used for transport experiments. The pros and contras of the two structures are briefly explained in the first part of Ref. [105]. The main contras of vertical QDs are two: first, the properties of the tunnel couplings between the dots are set during the growth of the heterostructure, which limits the experimental tunability, and second, the gate geometry used in the vertical devices makes it difficult to control the dots independently.

This introduction focuses on lateral QDs [33, 36, 68, 106, 107]. They are constructed within a Two Dimensional Electron Gas (2DEG), which is formed at the interface of the AlGaAs/GaAs heterostructure [108–111]. The interest in this heterojunction was first proposed by Esaki and Tsu in an unpublished 1969 report, and was first published and applied to GaAs-based superlattices by Dingle, et al. in 1978 [112]. The main idea of this junction is to separate the carriers from the impurities with a process called MOdulation Doping (MOD); accordingly, the carriers will not suffer Coulomb scattering with the impurities. This process rises the mobility of the electrons within the 2DEG, which increases the switching speed in the MOdulation Doped Field Effect Transistor (MODFET) [113] in comparison with the MOSFET.

The GaAs is a semiconductor with high electron mobility in its lower conduction band [114] and with a small effective mass: $m_{\text{eff}} = 0.067 m_{\text{e}}$ [115], where m_{e} is the electron mass. The goal is to confine electrons in this band coupling undoped GaAs to doped AlGaAs:

The AlGaAs is doped with donor atoms (usually silicon impurities) that populate its conduction band with electrons, the mobility of the electrons in this material is reduced because of their scattering with the impurities. In the interface with the GaAs, the electrons move from AlGaAs to

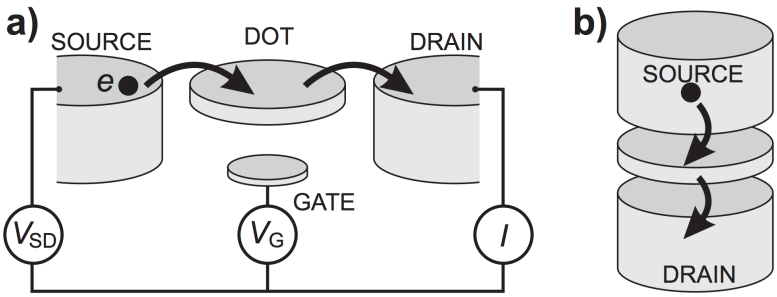

Figure 1.8: Schematics pictures obtained from Ref. [2]. (a)- Lateral QD. (b)- Vertical QD.

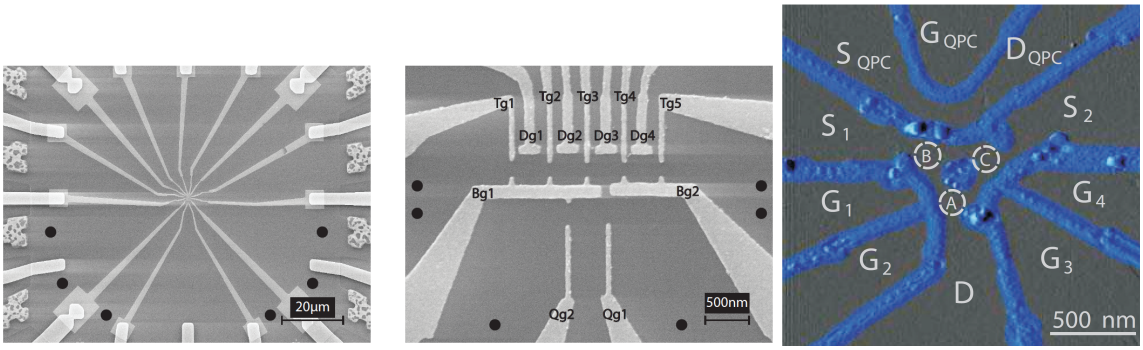

Figure 1.9: (a),(b)- Sample produced by Johannes Bayern in the group of Rolf Haug [118]. (a) - General view of the device. (b)- Gates made with electron lithography above the 2DEG. The electrons can be localized in four linearly coupled QDs. (c)- Sample produced by M. C. Rogge in the group of Rolf Haug [85]. Triple Quantum Dot (TQD) sample in triangular shape defined by oxide lines.

the narrower conduction band of the GaAs, which has lower energy states. The electron transfer generates a strong electric field between the two semiconductors that bend the bands, forming a triangular quantum well at the interface in the GaAs region. Electrons are then confined in the well forming a 2DEG in the direction perpendicular to the interface, quantizing the energy in this direction. The carriers (electrons) confined in the quantum well are then spatially separated from the impurities, obtaining higher mobilities.

The 2DEG has low density of electrons, $n \approx 10^{15} m^{-2}$, with high mobility, $\mu \approx 10 m^2/Vs$, and a mean free path of a few μm. These devices are ideal to fabricate nanostructures, where one can develop and study transport experiments. With different techniques [116, 117] gates are built over the 2DEG. The gates generate electrostatic potentials that deplete the 2DEG, forming small regions where the electrons are confined, i.e., a QDs. In Fig. 1.9 two different QD systems in a 2DEG are shown: one formed by electron lithography (a,b) and another defined by oxide lines (c).

The potential of the QDs changes linearly with the gate voltages; therefore, the electronic energy levels within the dot can be manipulated tunning the gate voltages capacitively coupled to the dots. In lateral QDs the gates voltages affect all the potentials that define the QD; hence, not only the energies are affected, also the tunnel barriers.

1.2 Theoretical Model

1.2.1 Density Matrix

Electrons obey the Schrödinger equation ($\hbar = 1$):

$$\hat{\mathrm{H}}_{\mathrm{S}}(t)\,|\psi_i(t)\rangle = i\frac{\partial}{\partial t}\,|\psi_i(t)\rangle \tag{1.7}$$

which gives the set of solutions $\{|\psi_i(t)\rangle\}_i$. They are pure states defined in the the Hilbert space of the Hamiltonian $\hat{\mathrm{H}}_{\mathrm{S}}(t)$. For a system that is a mix of pure states, there is a probability p_i to be in the pure state $|\psi_i(t)\rangle$, with $\sum_i p_i = 1$. To describe a quantum system in a mixed state, the density matrix $\rho(t)$ is considered. It is defined as:

$$\rho(t) = \sum_i p_i\,|\psi_i(t)\rangle\,\langle\psi_i(t)|\,, \quad \mathrm{Tr}\left\{\rho(t)\right\} = \sum_j \langle\psi_j|\left[\sum_i p_i\,|\psi_i(t)\rangle\,\langle\psi_i(t)|\right]|\psi_j(t)\rangle = \sum_i p_i = 1 \tag{1.8}$$

One can represent the density matrix in any other orthonormal basis of the Hamiltonian $\{|u_n\rangle\}_n$, with whom the eigenstates are decomposed as $|\psi_i(t)\rangle = \sum_n \phi_{i,n}(t)\,|u_n\rangle$, with a normalization condition $\sum_n |\phi_{i,n}(t)|^2 = 1$. The density matrix in the orthonormal basis $\{|u_n\rangle\}_n$ reads:

$$\rho(t) = \sum_{nm}\left[\sum_i p_i\,\langle u_n|\psi_i(t)\rangle\,\langle\psi_i(t)|u_m\rangle\right]|u_n\rangle\,\langle u_m| = \sum_{nm}\rho_{nm}(t)\,|u_n\rangle\,\langle u_m| \tag{1.9}$$

$$\begin{aligned}\mathrm{Tr}\left\{\rho(t)\right\} &= \sum_s \langle u_s|\left[\sum_{nm}\rho_{nm}(t)\,|u_n\rangle\,\langle u_m|\right]|u_s\rangle = \sum_s\sum_i p_i\,\langle u_s|\psi_i(t)\rangle\,\langle\psi_i(t)|u_s\rangle \\ &= \sum_i p_i \sum_s |\phi_{i,s}(t)|^2 = \sum_i p_i = 1\end{aligned} \tag{1.10}$$

The time evolution of the density matrix $\rho(t)$ reads:

$$\begin{aligned}\frac{\partial}{\partial t}\,|\psi_i(t)\rangle\,\langle\psi_i(t)| &= \left(\frac{\partial}{\partial t}\,|\psi_i(t)\rangle\right)\langle\psi_i(t)| + |\psi_i(t)\rangle\left(\frac{\partial}{\partial t}\,\langle\psi_i(t)|\right) \\ &= -i\left(\hat{\mathrm{H}}_{\mathrm{S}}\,|\psi_i(t)\rangle\,\langle\psi_i(t)| - |\psi_i(t)\rangle\,\langle\psi_i(t)|\,\hat{\mathrm{H}}_{\mathrm{S}}\right) \\ &= -i\left[\hat{\mathrm{H}}_{\mathrm{S}}, |\psi_i(t)\rangle\,\langle\psi_i(t)|\right] \\ \frac{\partial}{\partial t}\rho(t) &= -i\left[\hat{\mathrm{H}}_{\mathrm{S}}(t), \rho(t)\right].\end{aligned} \tag{1.11}$$

Eq. 1.11 is the Von-Neumann equation. For the closed system the time evolution of the density matrix totally depends on the initial condition. With this equation one can study the probability time evolution of the system to be in the state $|\alpha\rangle$, i.e. $\langle\alpha|\rho(t)|\alpha\rangle$. For the eigenstates of the Hamiltonian $|\psi_i(t)\rangle$, the probability is always constant in time, $\langle\psi_i(t)|\rho(t)|\psi_i(t)\rangle = p_i$.

1.2.2 Hamiltonian

To model an isolated system of quantum dots coupled by tunneling, the Anderson Hamiltonian is used:

$$\hat{\mathrm{H}}_{\mathrm{S}}(t) = \hat{\mathrm{H}}_{\epsilon}(t) + \hat{\mathrm{H}}_{e-e}(t) + \hat{\mathrm{H}}_{\tau}(t), \tag{1.12}$$

where $\hat{H}_\epsilon = \sum_i \epsilon_i \hat{c}_i^\dagger \hat{c}_i$ is the on-site energy levels of each quantum dot, $\hat{H}_{e-e} = \sum_{ij} V_{ij} \hat{n}_i \hat{n}_j$ is the Coulomb electron-electron interaction for electrons in the same and different dots, and $\hat{H}_\tau = \sum_{ij} \tau_{ij} \hat{c}_i^\dagger \hat{c}_j + \tau_{ij}^* \hat{c}_j^\dagger \hat{c}_i$ is the electron tunneling term between the dots. $\hat{c}_i$ are the fermionic destructive operators that fulfill the fermionic anti-commutation relation $\{\hat{c}_i^\dagger, \hat{c}_j\} = \delta_{ij}$ and $\hat{n}_i = \hat{c}_i^\dagger \hat{c}_i$ is the particle number, $\hat{n}_i = \{0, 1\}$.

1.2.3 Long Range transition

The density matrix contains all the coherences present in the system, i.e., all orders of interaction between the states of the Hamiltonian are considered. In case the energy difference between two levels $\Delta\epsilon$ is much higher than the coupling between them τ: $\Delta\epsilon \gg \tau$, tunneling between neighboring dots is suppressed. The contribution of higher energy processes giving rise to LR transport is then important. The perturbation parameter of this approximation is defined as $\tau/\Delta\epsilon$. In the works presented in this thesis, the approximation is usually named cotunnel approximation or second order approximation. The effective Hamiltonian of the LR approximation is obtained obtained by eliminating the non-contributing states (see Appendix B):

$$\hat{H}_{\text{eff}} = \sum_{n=0}^{\infty} \frac{1}{2n!} \left[\hat{H}_0 + \hat{H}_1, S\right]^{(2n)} + \sum_{m=0}^{\infty} \frac{1}{(2m+1)!} \left[\hat{H}_{AB}, S\right]^{(2m+1)} \tag{1.13}$$

where $[A,B]^0 = A$, $[A,B]^1 = [A,B]$, $[A,B]^2 = [[A,B],B]$, $[A,B]^3 = [[[A,B],B],B]$, ... $\hat{H}_0$ contains the energies of the different states, $\hat{H}_{AB}$ is the coupling between the states where the LR approximation is done, i.e., $\Delta\epsilon \gg \tau$, and $\hat{H}_1$ is the coupling between states where the LR approximation does not apply. The S is a matrix which contains the different orders of the expansion: $S = \sum_{s=1}^{\infty} S^{(s)}$ where $S^{(s)}$ has and order $(\tau/\Delta\epsilon)^s$. S is solved with the equation:

$$0 = \sum_{n=0}^{\infty} \frac{1}{(2n+1)!} \left[\hat{H}_0 + \hat{H}_1, S\right]^{(2n+1)} + \sum_{n=0}^{\infty} \frac{1}{2n!} \left[\hat{H}_{AB}, S\right]^{(2n)} \tag{1.14}$$

where the solution for S up to first order reads:

$$\hat{H}_{AB} + \left[\hat{H}_0, S^{(1)}\right] = 0 \Rightarrow \langle \psi_\alpha^A | S^{(1)} | \psi_\beta^B \rangle = -\frac{\langle \psi_\alpha^A | \hat{H}_{AB} | \psi_\beta^B \rangle}{E_\alpha^A - E_\beta^B}. \tag{1.15}$$

$|\psi_\beta^A\rangle$ and $|\psi_\beta^B\rangle$ are states between which the LR approximation is done.
As a first example, the effective Hamiltonian for a TQD and up to one particle in the system is obtained: $\hat{H}_{3\times3} \rightarrow \hat{H}_{\text{eff},2\times2}$. The Hamiltonian in matrix form reads:

$$\hat{H} = \begin{bmatrix} \epsilon_L & 0 & \tau_{LC} \\ 0 & \epsilon_R & \tau_{CR} \\ \tau_{LC} & \tau_{CR} & \epsilon_C \end{bmatrix} \tag{1.16}$$

where the blue shadowed area is the subset **A**, and the orange one is the subset **B**. Each sub-space is connected by $\hat{H}_{AB}$, where the LR approximation is done. $\hat{H}_1 = 0$ in this example. With Eq. (1.15), $S^{(1)}$ reads:

$$\hat{S}^{(1)} = \begin{bmatrix} 0 & 0 & -\frac{\tau_{LC}}{\epsilon_L - \epsilon_C} \\ 0 & 0 & -\frac{\tau_{CR}}{\epsilon_R - \epsilon_C} \\ \frac{\tau_{LC}}{\epsilon_L - \epsilon_C} & \frac{\tau_{CR}}{\epsilon_R - \epsilon_C} & 0 \end{bmatrix} \tag{1.17}$$

Calculating the effective Hamiltonian with (1.13) and projecting it to the A subspace the solution reads:

$$\mathscr{P}\hat{H}_{eff}\mathscr{P} = \begin{bmatrix} \epsilon_L + \frac{\tau_{LC}^2}{\epsilon_L - \epsilon_C} & \frac{1}{2}\left(\frac{\tau_{LC}\tau_{CR}}{\epsilon_L - \epsilon_C} + \frac{\tau_{LC}\tau_{CR}}{\epsilon_R - \epsilon_C}\right) \\ \frac{1}{2}\left(\frac{\tau_{LC}\tau_{CR}}{\epsilon_L - \epsilon_C} + \frac{\tau_{LC}\tau_{CR}}{\epsilon_R - \epsilon_C}\right) & \epsilon_R + \frac{\tau_{CR}^2}{\epsilon_R - \epsilon_C} \end{bmatrix} \tag{1.18}$$

The effective coupling has been obtained between the two disconnected states of the subset A and their energies have been renormalized. This example introduces the theory of LR transitions used in Chapters 3, 4, 5 and 6.

1.2.4 Open System. Master Equation for $\hat{H}(t) = \hat{H}$

In general the quantum dot systems are coupled to reservoirs with whom they exchange charge and energy. The Hamiltonian for this general system reads,

$$\hat{H} = \hat{H}_S(t) \otimes \mathbb{1}_B + \mathbb{1}_S \otimes \hat{H}_B(t) + \hat{H}_{int}(t), \tag{1.19}$$

where $\hat{H}_B$ is the Hamiltonian for the baths and $\hat{H}_{int}$ is the interaction between the baths and the quantum dot system. The solution for the dynamics of (1.19) is the same as for the closed system:

$$\frac{\partial}{\partial t}\rho(t) = -i\left[\hat{H}(t), \rho(t)\right] \tag{1.20}$$

with the difference that now the Hamiltonian has so many degrees of freedom that in most of the cases is not possible to solve it. Then, some approximations are needed. The thesis is based in the weak coupling regime with the reservoirs, the set of approximations that will be done lead to the Master Equation [119–122]. The Born-Markov-Secular Master equation reads: (see Appendix A for the derivation)

$$\dot{\rho}_S(t) = -i\left[\hat{H}_S, \rho_S(t)\right] + \sum_{a,b}\gamma_{ba}\left[|\psi_b\rangle\langle\psi_a|\rho_S(t)\left(|\psi_b\rangle\langle\psi_a|\right)^\dagger - \frac{1}{2}\left\{\left(|\psi_b\rangle\langle\psi_a|\right)^\dagger|\psi_b\rangle\langle\psi_a|, \rho_S(t)\right\}\right] \tag{1.21}$$

$$= -i\left[\hat{H}_S, \rho_S(t)\right] + \mathscr{L}_\Gamma\rho(t) \tag{1.22}$$

$|\psi_n\rangle$ are the eigenvectors of: $\hat{H}_S|\psi_n\rangle = E_n|\psi_n\rangle$. This is the so called Lindblad Master Equation [123, 124], which is the most general type of Markovian and time-homogeneous master equation

describing non-unitary evolution of the density matrix ρ that is trace-preserving and completely positive for any initial condition. The coupling rate γ_{ba} reads:

$$\gamma_{\mathrm{ba}} = \sum_{\eta\xi} 2\pi\delta_{\mathrm{E_a}-\mathrm{E_b}+\epsilon_\eta-\epsilon_\xi} \left|\langle\psi_\mathrm{b}\xi|\,\hat{\mathrm{H}}_{\mathrm{int}}\,|\psi_\mathrm{a}\eta\rangle\right|^2 \langle\eta|\,\bar{\rho}_\mathrm{B}\,|\eta\rangle \tag{1.23}$$

the delta function $\delta_{\mathrm{E_d}-\mathrm{E_c}+\epsilon_\eta-\epsilon_\xi}$ ensures that the energy is conserved in a transition between the reservoirs and the quantum system.

1.2.4.1 Example

The minimal system of one quantum dot weakly coupled to a single reservoir is considered in this example. The interaction Hamiltonian reads: $\hat{\mathrm{H}}_{\mathrm{int}} = \sum_k \lambda\left(\hat{d}_k^\dagger\hat{c} + \hat{c}^\dagger\hat{d}_k\right)$ where $\hat{d}$ is the annihilation operator of the reservoir, $\hat{c}$ is the annihilation operator of the system, and λ the coupling between them. The derivation of γ_{ba} reads:

$$\begin{aligned}
\gamma_{\mathrm{ba}} =& \sum_{\eta\xi k} 2\pi|\lambda|^2\delta_{\mathrm{E_a}-\mathrm{E_b}+\epsilon_\eta-\epsilon_\xi}\left|\langle\psi_\mathrm{b}\xi|\,\hat{d}_k^\dagger\hat{c} + \hat{c}^\dagger\hat{d}_k\,|\psi_\mathrm{a}\eta\rangle\right|^2\langle\eta|\,\bar{\rho}_\mathrm{B}\,|\eta\rangle \\
=&2\pi|\lambda|^2\sum_{\eta\xi k}\delta_{\mathrm{E_a}-\mathrm{E_b}+\epsilon_\eta-\epsilon_\xi}\left(\left|\langle\psi_\mathrm{b}\xi|\,\hat{d}_k^\dagger\hat{c}\,|\psi_\mathrm{a}\eta\rangle\right|^2 + \left|\langle\psi_\mathrm{b}\xi|\,\hat{c}^\dagger\hat{d}_k\,|\psi_\mathrm{a}\eta\rangle\right|^2\right)\langle\eta|\,\bar{\rho}_\mathrm{B}\,|\eta\rangle \\
=&2\pi|\lambda|^2\sum_{\eta\xi k}\delta_{\mathrm{E_a}-\mathrm{E_b}+\epsilon_\eta-\epsilon_\xi}\left(\left|\langle\psi_\mathrm{b}|\,\hat{c}\,|\psi_\mathrm{a}\rangle\right|^2\left|\langle\xi|\,\hat{d}_k^\dagger\,|\eta\rangle\right|^2 + \left|\langle\psi_\mathrm{b}|\,\hat{c}^\dagger\,|\psi_\mathrm{a}\rangle\right|^2\left|\langle\xi|\,\hat{d}_k\,|\eta\rangle\right|^2\right)\langle\eta|\,\bar{\rho}_\mathrm{B}\,|\eta\rangle \\
=&2\pi|\lambda|^2\left|\langle\psi_\mathrm{b}|\,\hat{c}\,|\psi_\mathrm{a}\rangle\right|^2\sum_{\eta\xi k}\delta_{\mathrm{E_a}-\mathrm{E_b}+\epsilon_\eta-\epsilon_\xi}\langle\eta|\,\hat{d}_k\,|\xi\rangle\langle\xi|\,\hat{d}_k^\dagger\,|\eta\rangle\langle\eta|\,\bar{\rho}_\mathrm{B}\,|\eta\rangle \\
&+2\pi|\lambda|^2\left|\langle\psi_\mathrm{b}|\,\hat{c}^\dagger\,|\psi_\mathrm{a}\rangle\right|^2\sum_{\eta\xi k}\delta_{\mathrm{E_a}-\mathrm{E_b}+\epsilon_\eta-\epsilon_\xi}\langle\eta|\,\hat{d}_k^\dagger\,|\xi\rangle\langle\xi|\,\hat{d}_k\,|\eta\rangle\langle\eta|\,\bar{\rho}_\mathrm{B}\,|\eta\rangle \\
=&2\pi|\lambda|^2\left|\langle\psi_\mathrm{b}|\,\hat{c}\,|\psi_\mathrm{a}\rangle\right|^2\sum_{\eta k}\delta_{\mathrm{E_a}-\mathrm{E_b}+\epsilon_k}\left(1-\langle\eta|\,\hat{d}_k^\dagger\hat{d}_k\,|\eta\rangle\right)\langle\eta|\,\bar{\rho}_\mathrm{B}\,|\eta\rangle \\
&+2\pi|\lambda|^2\left|\langle\psi_\mathrm{b}|\,\hat{c}^\dagger\,|\psi_\mathrm{a}\rangle\right|^2\sum_{\eta k}\delta_{\mathrm{E_a}-\mathrm{E_b}+\epsilon_k}\langle\eta|\,\hat{d}_k^\dagger\hat{d}_k\,|\eta\rangle\langle\eta|\,\bar{\rho}_\mathrm{B}\,|\eta\rangle \\
=&2\pi|\lambda|^2\mathscr{D}(\mathrm{E_a}-\mathrm{E_b})\left\{\left|\langle\psi_\mathrm{b}|\,\hat{c}\,|\psi_\mathrm{a}\rangle\right|^2[1-f(\mathrm{E_a}-\mathrm{E_b})] + \left|\langle\psi_\mathrm{b}|\,\hat{c}^\dagger\,|\psi_\mathrm{a}\rangle\right|^2 f(\mathrm{E_a}-\mathrm{E_b})\right\}
\end{aligned} \tag{1.24}$$

where $\mathscr{D}(\omega)$ is the density of states and $f(\omega) = (1+\mathrm{Exp}[(\omega-\mu)/k_\mathrm{B}T])^{-1}$ the Fermi function. The first term in the keys corresponds to one electron going from the system to the reservoir and the second term from the reservoir to the system.

1.2.5 Infinite bias limit

In the infinite bias limit, the energy difference between the chemical potential of the reservoirs fulfills: $|\mu_\alpha - \mu_{\alpha'}| \gg \{|\mathrm{E_a}-\mathrm{E_b}|, |\tau_{nm}|\}$ $\forall$a,b,m, n and $\mu_\alpha \gg \mathrm{E_a} \gg \mu_{\alpha'}$ $\forall$a. The Fermi distribution function is approximated to a Heavyside. With this approximation the Master equation can be

written in the on-site orthonormal base (see derivation in Appendix A.2):

$$\dot{\rho}_{\mathrm{S}}(t) = -i\left[\hat{\mathrm{H}}_{\mathrm{S}}, \rho_{\mathrm{S}}(t)\right] + \sum_{nm} \tilde{\gamma}_{mn}\left[|m\rangle\langle n|\,\rho_{\mathrm{S}}(t)(|m\rangle\langle n|)^{\dagger} - \frac{1}{2}\left\{(|m\rangle\langle n|)^{\dagger}|m\rangle\langle n|, \rho_{\mathrm{S}}(t)\right\}\right] \tag{1.25}$$

$$\tilde{\gamma}_{mn} = \sum_{\eta\xi} 2\pi\delta_{\epsilon_n-\epsilon_m+\epsilon_\eta-\epsilon_\xi}\,|\langle m\xi|\hat{\mathrm{H}}_{\mathrm{int}}|n\eta\rangle|^2\langle\eta|\bar{\rho}_{\mathrm{B}}|\eta\rangle \tag{1.26}$$

where $|m\rangle, |n\rangle$ are on-site states and ϵ_n the energy of the n state.

1.3 Transport

In general, in the experiments, particle transport $J_{\mathrm{N}}(t)$ is measured through the QD device. TO simulate it, it becomes necessary to calculate the transport from the solution of the Master equation. With the result of the density matrix $\rho(t)$ from the Master equation, the expected value of any operator can be calculated with the equation:

$$\langle\hat{\mathscr{O}}\rangle = \mathrm{Tr}\left[\hat{\mathscr{O}}\rho(t)\right] \tag{1.27}$$

where $\hat{\mathscr{O}}$ is an arbitrary operator. The particle change within each eigenstate $|\psi_\alpha(t)\rangle$ reads:

$$\begin{aligned}\partial_t\langle\mathscr{N}_\alpha\rangle &= \frac{\partial}{\partial t}\mathrm{Tr}\left[\hat{\mathrm{c}}^{\dagger}_\alpha(t)\hat{\mathrm{c}}_\alpha(t)\rho(t)\right] = \partial_t\langle\psi_\alpha(t)|\rho_{\mathrm{S}}(t)|\psi_\alpha(t)\rangle = \langle\psi_\alpha(t)|\,\dot{\rho}_{\mathrm{S}}(t) + i\left[\hat{\mathrm{H}}_{\mathrm{S}}, \rho_{\mathrm{S}}(t)\right]|\psi_\alpha(t)\rangle \\ &= \langle\psi_\alpha(t)|\,\mathscr{L}_\Gamma\rho_{\mathrm{S}}(t)\,|\psi_\alpha(t)\rangle\end{aligned} \tag{1.28}$$

where $\mathscr{N}_\alpha$ is the number of particles in the eigenstate $|\psi_\alpha(t)\rangle$ and $\hat{\mathrm{c}}_\alpha(t) = \sum_n \langle\psi_\alpha(t)|n\rangle\,\hat{\mathrm{c}}_n$. The matrix $\mathscr{L}_\Gamma$ is a sum of elements accounting for the coupling with each reservoir: $\mathscr{L}_\Gamma = \sum_\nu \mathscr{L}^{(\nu)}_\Gamma$. Therefore, with Eq. (1.28) the current, $J^{(\nu)}_{\mathrm{N}}$, from the ν-reservoir to the quantum systems is:

$$J^{(\nu)}_{\mathrm{N}} = \sum_n\sum_\alpha \langle\psi^n_\alpha(t)|\,\mathscr{L}_\Gamma\rho_{\mathrm{S}}(t)\,|\psi^n_\alpha(t)\rangle = \sum_n\sum_\alpha\left[\sum_{\mathrm{a}}\gamma^{(\nu)}_{\alpha\mathrm{a}}\langle\psi^{n-1}_{\mathrm{a}}|\rho_{\mathrm{S}}(t)|\psi^{n-1}_{\mathrm{a}}(t)\rangle - \gamma^{(\nu)}_{\mathrm{a}\alpha}\langle\psi^n_\alpha(t)|\rho_{\mathrm{S}}(t)|\psi^n_\alpha(t)\rangle\right] \tag{1.29}$$

where it has been added for clarity a super-index n referring to the number of particles within each eigenstate. The Master equation neglects the processes with two or more particles, i.e., just one particle per jump is permitted. The current direction is defined positive for incoming particles to the quantum system and negative otherwise. For the Redfield Master equation (See Appendix A.1) the charge current reads

$$\begin{aligned}J^{(\nu),\mathrm{R}}_{\mathrm{N}} = \sum_n\sum_\alpha\Bigg\{&\sum_{\mathrm{ad}}\gamma^{(\nu)}_{\mathrm{a}\alpha,\alpha\mathrm{d}}\langle\psi^{n-1}_{\mathrm{d}}|\rho_{\mathrm{S}}(t)|\psi^{n-1}_{\mathrm{a}}(t)\rangle \\ &-\frac{1}{2}\left[\sum_{\mathrm{bd}}\gamma^{(\nu)}_{\alpha\mathrm{b},\mathrm{bd}}\langle\psi^n_{\mathrm{d}}(t)|\rho_{\mathrm{S}}(t)|\psi^n_\alpha(t)\rangle + \sum_{\mathrm{ab}}\gamma^{(\nu)}_{\mathrm{ab},\mathrm{b}\alpha}\langle\psi^n_\alpha(t)|\rho_{\mathrm{S}}(t)|\psi^n_{\mathrm{a}}(t)\rangle\right]\Bigg\}\end{aligned} \tag{1.30}$$

In the infinite bias limit the transport is obtained with the particle change in the on-site states. The particle change of the on-site state coupled to the ν-reservoir reads:

$$\partial_t\langle\mathscr{N}_\nu\rangle = \frac{\partial}{\partial t}\mathrm{Tr}\left[\hat{\mathrm{c}}^{\dagger}_\nu\hat{\mathrm{c}}_\nu\rho(t)\right] = \langle\nu|\partial_t\rho_{\mathrm{S}}(t)|\nu\rangle \tag{1.31}$$

where $|\nu\rangle$ is the on-site state coupled to the ν-reservoir. $\partial_t \rho_S(t)$ has two terms: $\partial_t \rho_S(t) = -i\left[\hat{H}_S, \rho_S(t)\right] + \mathscr{L}_\Gamma^\infty \rho_S(t)$. The current from the reservoir to the n-QD is the last term. Thus, the solution is:

$$J_N^{(\nu),\infty}(t) = \langle \nu | \mathscr{L}_\Gamma^\infty \rho_S(t) | \nu \rangle = \sum_a \tilde{\gamma}_{\nu a} \langle a | \rho(t) | a \rangle - \tilde{\gamma}_{a\nu} \langle \nu | \rho(t) | \nu \rangle . \tag{1.32}$$

1.3.1 Current directly from ρ

Eq. (1.31) gives the particle change within the n-QD, i.e, the particle transport to the n-QD. This expression contains the particle transport to the n-QD from the reservoirs, $J_N^{(n)}(t)$, and the particle current from other QDs present in the QD system, $\mathscr{I}_N^n(t)$. In order to obtain the transport from the reservoirs to the QD, $\mathscr{I}_N^n(t)$ has to be subtracted from Eq. (1.31). The expression for $\mathscr{I}_N^n(t)$ is

$$\mathscr{I}_N^n(t) = -i\left[\hat{H}_S, \hat{c}_n^\dagger \hat{c}_n\right] = i \sum_{\{n,j\}} \tau_{nj} \hat{c}_n^\dagger \hat{c}_j - \tau_{nj}^* \hat{c}_j^\dagger \hat{c}_n \tag{1.33}$$

$$\begin{aligned} \langle \mathscr{I}_N^n(t) \rangle &= i \sum_{\{n,j\}} \mathrm{Tr}\left[(\tau_{nj} \hat{c}_n^\dagger \hat{c}_j - \tau_{nj}^* \hat{c}_j^\dagger \hat{c}_n) \rho(t) \right] \\ &= i \sum_{\alpha\beta} \sum_{\{n,j\}} \left(\tau_{nj} \langle \psi_\alpha | n \rangle \langle j | \psi_\beta \rangle - \tau_{nj}^* \langle \psi_\alpha | j \rangle \langle n | \psi_\beta \rangle \right) \langle \psi_\beta | \rho_S(t) | \psi_\alpha \rangle \end{aligned} \tag{1.34}$$

where $\{n, j\}$ represents the set of QDs tunnel coupled to the n-QD. Finally the transport from the n-QD to the bath connected to it reads:

$$J_N^{(n)}(t) = \partial_t \langle \mathscr{N}_n \rangle - \langle \mathscr{I}_N^n(t) \rangle . \tag{1.35}$$

The expression (1.35) is equivalent to Eq. (1.29), (1.30), (1.32).

1.3.2 Heat Transport

There are two quantities which are of interest in transport experiments: the heat and energy transport through quantum systems, named $J_H(t)$ and $J_E(t)$ respectively. In the experiments the energy flow is usually inferred from the measures of the charge transport. In the theory it is defined from the energy of electrons going from the different quantum paths within the quantum dot structure. The energy evolution is calculated similarly to Eq. (1.28), the energy change in the eigenstate $|\psi_\alpha(t)\rangle$ reads:

$$\partial_t \langle \mathscr{E}_\alpha \rangle = \frac{\partial}{\partial t} \mathrm{Tr}\left[E_\alpha \hat{c}_\alpha^\dagger(t) \hat{c}_\alpha(t) \rho(t) \right] = E_\alpha \langle \psi_\alpha(t) | \mathscr{L}_\Gamma \rho_S(t) | \psi_\alpha(t) \rangle + \dot{E}_\alpha \langle \psi_\alpha(t) | \rho_S(t) | \psi_\alpha(t) \rangle \tag{1.36}$$

where $\mathscr{E} = \sum_\alpha \mathscr{E}_\alpha$ is the total energy of the quantum system. The energy current has the following expression:

$$J_E^{(\nu)} = \sum_n \sum_\alpha E_\alpha \left[\sum_a \gamma_{\alpha a}^{(\nu)} \langle \psi_a^{n-1} | \rho_S(t) | \psi_a^{n-1}(t) \rangle - \gamma_{a\alpha}^{(\nu)} \langle \psi_\alpha^n(t) | \rho_S(t) | \psi_\alpha^n(t) \rangle \right] \tag{1.37}$$

The term $\dot{\mathrm{E}}_\alpha$ present in driven systems will not be included in the definition of the energy current with the reservoirs since it comes from some external field which drives the internal energy dynamics of the TQD. It will be defined as a new energy transport term:

$$J_{\mathrm{ac}}(t) = \sum_\alpha \dot{\mathrm{E}}_\alpha \langle \psi_\alpha(t)|\rho_{\mathrm{S}}(t)|\psi_\alpha(t)\rangle \,. \tag{1.38}$$

Heat is defined as the energy with respect to the Fermi energy. The heat current is then defined by:

$$J_{\mathrm{H}}^{(\nu)} = J_{\mathrm{E}}^{(\nu)} - \mu_\nu J_{\mathrm{N}}^{(\nu)}, \tag{1.39}$$

where μ_ν is the chemical potential of the ν reservoir.
The energy transport for the Redfield Master equation can be straightforward derived. Notice that the infinite bias approximation to the on-site basis does not couple the quantum system to the reservoirs with the exact values of the energy, and the heat can not be defined with the chemical potential in $\pm\infty$; therefore, it is not valid for calculating the energy and heat transport. In the next sections an oscillatory field is introduced; thus, the energy of the eigenstates is time dependent.

1.3.3 Thermodynamics

The particle and energy exchange between the quantum system and the reservoirs is governed by the laws of thermodynamics. The energy change in the open system is equal to the energy current coming from the reservoirs and the term $J_{\mathrm{ac}}(t)$:

$$\partial_t \langle \mathscr{E} \rangle = \sum_\nu J_{\mathrm{E}}^{(\nu)} + J_{\mathrm{ac}}(t) = \left[\sum_\nu J_{\mathrm{E}}^{(\nu)} - \mu_\nu J_{\mathrm{N}}^{(\nu)}\right] + \left[\sum_\nu \mu_\nu J_{\mathrm{N}}^{(\nu)}\right] + J_{\mathrm{ac}}(t) = \dot{Q} + \dot{W} + J_{\mathrm{ac}}(t) \tag{1.40}$$

with $\dot{Q} = \sum_\nu J_{\mathrm{H}}^{(\nu)}$ and $\dot{W} = \sum_\nu \mu_\nu J_{\mathrm{N}}^{(\nu)}$. $\dot{Q}$ is positive when the reservoirs inject heat into the system and negative otherwise. $\dot{W}$ is positive when the power is extracted from reservoirs to the system, and is negative when power is extracted from the system to the reservoirs by transporting particles against the chemical potential bias direction.
The definition of the entropy comes from the Shannon entropy: $S(t) = \sum_i \langle \psi_i|\rho(t)|\psi_i\rangle \log\left[\langle \psi_i|\rho(t)|\psi_i\rangle\right]$. With some algebra the total entropy production reads:

$$\dot{S}(t) = \dot{S}_i(t) - \sum_\nu J_{\mathrm{H}}^{(\nu)}(t)\frac{1}{T_\nu} \tag{1.41}$$

where $\dot{S}_i(t) \geq 0$ is the internal entropy production. For $\dot{S}_i(t) = 0$ the system fulfills the detailed balance condition (reversible process)[125].

1.4 Driven quantum dots

In this section, the system is driven by an ac-gate [126–128] . An oscillatory term, $\hat{\mathrm{H}}_{\mathrm{ac}}(t)$, changes the on-site energies of the Hamiltonian in a sinusoidal way. The general form for the on-site part

of the Hamiltonian under the presence of an ac-gate is:

$$\hat{\mathrm{H}}_c + \hat{\mathrm{H}}_{\mathrm{ac}}(t) = \sum_i (\epsilon_i + \mathrm{V}_i \cos[\omega_i t + \phi_i])\hat{\mathrm{c}}_i^\dagger \hat{\mathrm{c}}_i \tag{1.42}$$

where V_i is the amplitude, ω_i is the frequency of the driving and ϕ_i is the phase of each on-site driving. In general, the on-site states of the Hamiltonian are used as the orthonormal basis of the states and operators, so it is convenient to have their energies constant in time. Transforming the system to the rotating frame

$$\mathscr{U}(t) = \mathrm{Exp}\left[i\int_0^t \hat{\mathrm{H}}_{\mathrm{ac}}(t')dt'\right] = \prod_i \mathrm{Exp}\left[i\frac{\mathrm{V}_i}{\omega_i}\sin(\omega_i t + \phi_i)\hat{\mathrm{c}}_i^\dagger \hat{\mathrm{c}}_i\right]\mathrm{Exp}\left[-i\frac{\mathrm{V}_i}{\omega_i}\sin(\phi_i)\hat{\mathrm{c}}_i^\dagger \hat{\mathrm{c}}_i\right] \tag{1.43}$$

the transformed Hamiltonian $\hat{\mathrm{H}}_{\mathrm{S}\S}(t) = \mathscr{U}(t)[\hat{\mathrm{H}}_{\mathrm{S}} - i\partial_t]\mathscr{U}^\dagger(t) = \hat{\mathrm{H}}_\varepsilon + \hat{\mathrm{H}}_{\mathrm{e-e}} + \mathscr{U}(t)\hat{\mathrm{H}}_\tau(t)\mathscr{U}^\dagger(t)$ takes the effect of the ac-gate from the on-site to the interdot coupling part of the Hamiltonian. Using the commutation relations, $\left[\hat{\mathrm{c}}_i^\dagger \hat{c}_j, \hat{\mathrm{n}}_{j(i)}\right] = +(-)\hat{\mathrm{c}}_i^\dagger \hat{c}_j$ and the *Jacobi-Anger expansion*:

$$\hat{\mathrm{H}}_{\tau\S}(t) = \mathscr{U}\hat{\mathrm{H}}_\tau(t)\mathscr{U}^\dagger = \sum_{\{i,j\}} \tau_{ij}\mathrm{C}_{ij}\sum_{l,s} B_l\left[\frac{\mathrm{V}_i}{\omega_i}\right]B_s\left[\frac{\mathrm{V}_j}{\omega_j}\right]\mathrm{e}^{il(\omega_i t+\phi_i)}\mathrm{e}^{-is(\omega_j t+\phi_j)}\hat{c}_i^\dagger \hat{c}_j + h.c. \tag{1.44}$$

where $\{i,j\}$ indicates all the tunnel couplings combinations between two dots in the QD system. $B_n(\alpha)$ is the n-Bessel function of first kind. The expression C_{ij} contains the term:

$$\mathrm{C}_{ij} = \mathrm{Exp}\left[-i\frac{\mathrm{V}_i}{\omega_i}\sin(\phi_i)\right]\mathrm{Exp}\left[-i\frac{\mathrm{V}_j}{\omega_j}\sin(\phi_j)\right] \tag{1.45}$$

which is equal to one for the cases that $\phi_{i,j} = \{0,\pi\}$. However, for systems with one, two or very symmetric drivings $\mathrm{V}_i = \mathrm{V}_j$ and $\omega_i = \omega_j$; this coefficient is a general phase that will not change the transport and dynamical behavior of the system. The only important information is the phase difference between the drivings.

Exploring the properties of the Bessel function, for two cases, the inner summation in Eq. (1.44) can be simplified when the two drivings have the same frequency $\omega_i = \omega_j \equiv \omega$. (i) the phase opposition case $\phi_j - \phi_i = (2n+1)\pi$ ($n \in \mathbb{Z}$):

$$\sum_{l,s} B_l\left[\frac{\mathrm{V}_i}{\omega}\right]B_s\left[\frac{\mathrm{V}_j}{\omega}\right]\mathrm{e}^{il(\omega t+\phi_i)}\mathrm{e}^{-is(\omega t+\phi_i+[2n+1]\pi)} = \sum_l B_l\left[\frac{\mathrm{V}_i+\mathrm{V}_j}{\omega}\right]\mathrm{e}^{il(\omega t+\phi_i)} \tag{1.46}$$

and (ii) the in-phase case $\phi_j - \phi_i = 2n\pi$ ($n \in \mathbb{Z}$):

$$\sum_{l,s} B_l\left[\frac{\mathrm{V}_i}{\omega}\right]B_s\left[\frac{\mathrm{V}_j}{\omega}\right]\mathrm{e}^{il(\omega t+\phi_i)}\mathrm{e}^{-is(\omega t+\phi_i+2n\pi)} = \sum_l B_l\left[\frac{\mathrm{V}_i-\mathrm{V}_j}{\omega}\right]\mathrm{e}^{il(\omega t+\phi_i)} \tag{1.47}$$

With this two simplifications is concluded that when the driving have opposite phase, its effect is enhanced with the summation of both amplitudes; while in the on-phase case the effect is decreased, the amplitudes are subtracted with the limit of no driving when $\mathrm{V}_i = \mathrm{V}_j$, i.e., the driving is a global oscillation which do not produce any internal dynamics.

In Eq. (1.44) the time dependent exponentials Exp[$in\omega t$] assert that when there is a energy difference between the non-driven on-site energy states of $|\epsilon_i - \epsilon_j| = n\hbar\omega$ the transport is resonant. The resonances involving the emission or absorption of an integer number of photons are called sidebands. For fast driving, $\hbar\omega \gg \tau_{ij}$, the strength of the coupling is mainly controlled by the corresponding, n-Bessel function $B_n(\mathrm{V}/\omega)$, which depends on the value of the amplitude and the frequency.

For $\hbar\omega \gg \{\tau, |\epsilon_i - \epsilon_j| - n\hbar\omega\}$, usually only the resonant sideband contributes. One can then neglect the off-resonant sidebands by assuming a Rotating Wave Approximation (RWA). It transforms the Hamiltonian into the rotating frame and neglects all the fast oscillatory therms. The rotation to the n-sideband of the on-site states i, j is

$$\hat{\mathrm{H}}_{\mathrm{S\S rot}}(t) = \mathcal{V}(t)\Big(\hat{\mathrm{H}}_{\mathrm{S\S}}(t) - i\partial_t\Big)\mathcal{V}^\dagger(t), \qquad \mathcal{V}(t) = \mathrm{Exp}[in\omega t\hat{\mathrm{c}}_i^\dagger\hat{\mathrm{c}}_i] \tag{1.48}$$

The part of the Hamiltonian in the RWA that contains the coupling between the states i, j reads:

$$\hat{\mathrm{H}}_{\mathrm{RWA}} = \begin{pmatrix} \ddots & \vdots & \vdots & \\ \dots & \epsilon_i + n\hbar\omega & \tau_{ij}B_n\left[\frac{V}{\omega}\right] & \dots \\ \dots & \tau_{ij}^* B_n\left[\frac{V}{\omega}\right] & \epsilon_j & \dots \\ & \vdots & \vdots & \ddots \end{pmatrix} \tag{1.49}$$

where it has been approximated $\mathrm{e}^{-in\omega t}\langle i|\hat{\mathrm{H}}_{\tau\S}(t)|j\rangle \approx \tau_{ij}B_n\left[\frac{V}{\omega}\right]$. The diagonal term $n\hbar\omega$ implies that at an energy difference of $|\epsilon_i - \epsilon_j| = n\hbar\omega$ the transport between the states is resonant with a renormalized coupling depending on the parameters of the ac-field.

1.4.1 Cotunnel approach in time dependent Hamiltonians

In Section 1.2.3, the cotunnel approach for a time independent Hamiltonians was explained. In this section it is extended to time dependent periodic Hamiltonians. The effective Hamiltonian has the same form:

$$\hat{\mathrm{H}}_{\mathrm{eff}}(t) = \sum_{n=0}^{\infty}\frac{1}{2n!}\left[\hat{\mathrm{H}}_0 + \hat{\mathrm{H}}_1, \mathrm{S}\right]^{(2n)} + \sum_{m=0}^{\infty}\frac{1}{(2m+1)!}\left[\hat{\mathrm{H}}_{AB}, \mathrm{S}\right]^{(2m+1)}. \tag{1.50}$$

But the ordinary equations used to obtain the operator S are now differential equations, which may be difficult to solve analitically.

$$-\frac{i}{\hbar}\frac{\partial}{\partial t}\mathrm{S}(t) = \sum_{n=0}^{\infty}\frac{1}{(2n+1)!}\left[\hat{\mathrm{H}}_0 + \hat{\mathrm{H}}_1, \mathrm{S}\right]^{(2n+1)} + \sum_{n=0}^{\infty}\frac{1}{2n!}\left[\hat{\mathrm{H}}_{AB}, \mathrm{S}\right]^{(2n)}. \tag{1.51}$$

The expression for the first order in $\mathrm{S}(t)$ reads

$$\begin{cases} \hat{\mathrm{H}}_{AB}(t) + \left[\hat{\mathrm{H}}_0(t), \mathrm{S}^{(1)}(t)\right] = -\frac{i}{\hbar}\frac{\partial}{\partial t}\mathrm{S}^{(1)}(t) \\ \hat{\mathrm{H}}_{AB}(0) + \left[\hat{\mathrm{H}}_0(0), \mathrm{S}^{(1)}(0)\right] = 0 \end{cases} \tag{1.52}$$

where it is needed an additional equation to obtain the initial conditions of the elements within the $S^{(1)}(t)$ matrix.
As an example the Effective Hamiltonian form Chapter 4 is going to be obtained. Starting from the Hamiltonian in the convenient basis (Eq. (1.44)), the transformed Hamiltonian reads

$$\hat{H}_{\S}(t) = \begin{bmatrix} \epsilon_L & 0 & \tau_{LC}\sum_n B_n\left(\frac{V}{\omega}\right)e^{in\omega t} \\ 0 & \epsilon_R & \tau_{CR} \\ \tau_{LC}\sum_n B_n\left(\frac{V}{\omega}\right)e^{-in\omega t} & \tau_{CR} & \epsilon_C \end{bmatrix}. \tag{1.53}$$

The blue zone is sub-set **A** and the orange zone is the sub-set **B**. The rest is the weak interaction $\hat{H}_{AB}$. The result of Eq. (1.52) reads

$$S^{(1)}(t) = \begin{bmatrix} 0 & 0 & \sum_n \frac{\tau_{LC}B_n^2\left(\frac{V}{\omega}\right)e^{-in\omega t}}{\epsilon_C-\epsilon_L-n\hbar\omega} \\ 0 & 0 & \frac{\tau_{CR}}{\epsilon_C-\epsilon_R} \\ -\sum_n \frac{\tau_{LC}B_n\left(\frac{V}{\omega}\right)e^{-in\omega t}}{\epsilon_C-\epsilon_L-n\hbar\omega} & -\frac{\tau_{CR}}{\epsilon_C-\epsilon_R} & 0 \end{bmatrix}. \tag{1.54}$$

The effective Hamiltonian projected to the states from subset A reads:

$$\hat{H}_{\text{eff}}(t) = \begin{bmatrix} \epsilon_L - \sum_n \frac{\tau_{CR}^2 B_n^2\left(\frac{V}{\omega}\right)}{\epsilon_C-\epsilon_L-n\hbar\omega} & -\sum_n t_n e^{-in\omega t} \\ -\sum_n t_n e^{in\omega t} & \epsilon_R - \frac{\tau_{CR}^2}{\epsilon_C-\epsilon_L} \end{bmatrix} \tag{1.55}$$

where $t_n = \frac{1}{2}\tau_{CR}\tau_{LC}B_n\left(\frac{V}{\omega}\right)\left(\frac{1}{\epsilon_C-\epsilon_R}+\frac{1}{\epsilon_C-\epsilon_L-n\hbar\omega}\right)$. One can additionally consider that $\epsilon_C-\epsilon_R \approx \epsilon_C-\epsilon_L-n\hbar\omega$.

For more complex set-ups this procedure may be not very useful, instead one can use the Magnus expansion. The ansatz $|\Psi(t)\rangle = \text{Exp}[\Theta(t,t_0)]|\Psi(t_0)\rangle$ with $\Theta(t,t_0)=\sum_n \Theta_n(t,t_0)$ is proposed for the solution of the Schrödinger equation. Substituting, it is deduced

$$\hat{H}(t) = \frac{d}{dt}\left[e^{\Theta(t,t_0)}\right]e^{-\Theta(t,t_0)}; \tag{1.56}$$

from this expression the Magnus expansion is obtained. The first terms read

$$\Theta_1(t,t_0) = \int_0^t \hat{H}(t_1)dt_1, \quad \Theta_2(t,t_0) = \frac{1}{2}\int_0^t\int_0^{t_1}\left[\hat{H}(t_1),\hat{H}(t_2)\right]dt_1dt_2. \tag{1.57}$$

The cotunnel approximations are done in the terms of Eq. (1.57), then the effective Hamiltonian is calculated with Eq. (1.56). The long-range couplings in Chapter 5 are obtained with this method.

1.4.2 Floquet Master Equation Approach

Starting from Eq. (A.15) after doing the Born-Markov approximation, the operators are projected to the Floquet states (see Appendix C) at $t=0$: $\{|\phi_\alpha(0)\rangle\}_\alpha$. In the following the notation is reduced

$|\phi_\alpha\rangle \equiv |\phi_\alpha(0)\rangle$.

$$\dot{\rho}_S(t) = \sum_{\alpha\mu}\sum_{a,b,c,d}\int_0^\infty \Big\{ C_{\mu\alpha}(\tau)\langle\phi_a|\hat{A}_\mu(t)|\phi_b\rangle\langle\phi_c|\hat{A}_\alpha(t-\tau)|\phi_d\rangle \times \Big[|\phi_a\rangle\langle\phi_b||\phi_c\rangle\langle\phi_d|\rho_S(t) - |\phi_c\rangle\langle\phi_d|\rho_S(t)|\phi_a\rangle\langle\phi_b|\Big] + \text{h.c.}\Big\} d\tau \tag{1.58}$$

Using the Floquet propertie $|\phi_\alpha(t)\rangle \text{Exp}[-iq_\alpha t] = \text{Exp}\left[-i\int_0^t \hat{H}_S(t_1)dt_1\right]|\phi_\alpha(0)\rangle$ the equation reads

$$\begin{aligned}\dot{\rho}_S(t) = \sum_{\alpha\mu}\sum_{a,b,c,d}\int_0^\infty \Big\{ & C_{\mu\alpha}(\tau)e^{i(q_d-q_c)\tau}e^{i(q_a-q_b+q_c-q_d)t} \\ & \times\langle\phi_a(t)|\hat{A}_\mu|\phi_b(t)\rangle\langle\phi_c(t-\tau)|\hat{A}_\alpha|\phi_d(t-\tau)\rangle \\ & \times\Big[|\phi_a\rangle\langle\phi_b||\phi_c\rangle\langle\phi_d|\rho_S(t) - |\phi_c\rangle\langle\phi_d|\rho_S(t)|\phi_a\rangle\langle\phi_b|\Big] + \text{h.c.}\Big\} d\tau \\ = \sum_{\alpha\mu}\sum_{a,b,c,d}\sum_{n,m,l,p}\int_0^\infty \Big\{ & C_{\mu\alpha}(\tau)e^{i(q_d-q_c)\tau}e^{i(q_a-q_b+q_c-q_d)t}e^{i(l-p)\omega\tau}e^{i(m-n+p-l)\omega t} \\ & \times\langle\Phi_a^n|\hat{A}_\mu|\Phi_b^m\rangle\langle\Phi_c^l|\hat{A}_\alpha|\Phi_d^p\rangle \\ & \Big[|\phi_a\rangle\langle\phi_b||\phi_c\rangle\langle\phi_d|\rho_S(t) - |\phi_c\rangle\langle\phi_d|\rho_S(t)|\phi_a\rangle\langle\phi_b|\Big] + \text{h.c.}\Big\} d\tau\end{aligned} \tag{1.59}$$

1.4.3 Floquet-Secular approximation

Additionally to the secular approximation of the previous case, now it is considered that the ac-field oscillates much faster than the system-bath dynamics, i.e., $\omega \gg |\lambda|^2$, obtaining the Floquet-secular approximation:

$$\begin{aligned}\dot{\rho}_S(t) = \sum_{\alpha\mu}\sum_{a,b,c,d}\sum_{n,m,l,p}\Gamma_{\mu\alpha}(q_d - q_c + (l-p)\omega)\delta_{q_a-q_b+q_c-q_d-(n-m+l-p)\omega}\langle\phi_a^n|\hat{A}_\mu|\phi_b^m\rangle\langle\phi_c^l|\hat{A}_\alpha|\phi_d^p\rangle \\ \Big[|\phi_a\rangle\langle\phi_b||\phi_c\rangle\langle\phi_d|\rho_S(t) - |\phi_c\rangle\langle\phi_d|\rho_S(t)|\phi_a\rangle\langle\phi_b|\Big] + \text{h.c.}\end{aligned} \tag{1.60}$$

with $\Gamma_{\mu\alpha}(\varepsilon) = \int_0^\infty C_{\mu\nu}(\tau)e^{i\varepsilon\tau}d\tau$. Like in the non-driven case (see Sec. 1.2.4) the anti-hermitian part is neglected, obtaining:

$$\dot{\rho}_S(t) = -\sum_{a,b,c,d}\gamma_{ab,cd}\Big[|\phi_c\rangle\langle\phi_d|\rho_S(t)(|\phi_b\rangle\langle\phi_a|)^\dagger - \frac{1}{2}\Big\{(|\phi_b\rangle\langle\phi_a|)^\dagger|\phi_c\rangle\langle\phi_d|, \rho_S(t)\Big\}\Big] \tag{1.61}$$

with $\gamma_{ab,cd} = \sum_{\alpha\mu}\sum_{n,m,l,p}\Gamma_{\mu\alpha}(q_d - q_c + (l-p)\omega)\delta_{q_a-q_b+q_c-q_d-(n-m+l-p)\omega}\langle\phi_b^m|\hat{A}_\mu|\phi_a^n\rangle^*\langle\phi_c^l|\hat{A}_\alpha|\phi_d^p\rangle$. Using the same derivation as in Eq. (A.23), the expression for $\Gamma_{\mu\alpha}(\varepsilon)$ reads:

$$\Gamma_{\mu\alpha}(q_d - q_c + (l-p)\omega) = \sum_{\eta\xi}2\pi\delta_{q_d-q_c+(l-p)\omega+\epsilon_\eta-\epsilon_\xi}\langle\xi|\hat{B}_\mu|\eta\rangle^*\langle\xi|\hat{B}_\alpha|\eta\rangle\langle\eta|\bar{\rho}_B|\eta\rangle \tag{1.62}$$

Then $\gamma_{ab,cd}$ reads

$$\gamma_{ab,cd} = \sum_{n,m,l,p}\sum_{\eta\xi}2\pi\delta_{q_d-q_c+(l-p)\omega+\epsilon_\eta-\epsilon_\xi}\delta_{q_a-q_b+q_c-q_d-(n-m+l-p)\omega}\langle\phi_b^m\xi|\hat{H}_{\text{int}}|\phi_a^n\eta\rangle^*\langle\phi_c^l\xi|\hat{H}_{\text{int}}|\phi_d^p\eta\rangle\langle\eta|\bar{\rho}_B|\eta\rangle \tag{1.63}$$

To fulfill energy conservation: $a = d$, $b = c$, $n = p$ and $m = l$; hence:

$$\gamma_{ab,ba} = \sum_{n,m} \sum_{\eta\xi} 2\pi\delta_{q_a - q_b + (m-n)\omega + \epsilon_\eta - \epsilon_\xi} \left| \langle \phi_b^m \xi | \hat{\mathrm{H}}_{\mathrm{int}} | \phi_a^n \eta \rangle \right|^2 \langle \eta | \bar{\rho}_{\mathrm{B}} | \eta \rangle \tag{1.64}$$

The master equation finally reads

$$\dot{\rho}_{\mathrm{S}}(t) = -\sum_{a,b} \gamma_{ba} \Big[|\phi_b\rangle \langle \phi_a| \rho_{\mathrm{S}}(t) (|\phi_b\rangle \langle \phi_a|)^\dagger - \frac{1}{2} \Big\{ (|\phi_b\rangle \langle \phi_a|)^\dagger |\phi_b\rangle \langle \phi_a|, \rho_{\mathrm{S}}(t) \Big\} \Big] \tag{1.65}$$

Going back to the Schrödinger picture is finally obtained

$$\begin{aligned} \dot{\rho}_{\mathrm{S}}(t) = -i \left[\hat{\mathrm{H}}_{\mathrm{S}}(t), \rho_{\mathrm{S}}(t) \right] + \sum_{a,b} \gamma_{ba} \Big[& |\phi_b(t)\rangle \langle \phi_a(t)| \rho_{\mathrm{S}}(t) (|\phi_b(t)\rangle \langle \phi_a(t)|)^\dagger \\ & - \frac{1}{2} \Big\{ (|\phi_b(t)\rangle \langle \phi_a(t)|)^\dagger |\phi_b(t)\rangle \langle \phi_a(t)|, \rho_{\mathrm{S}}(t) \Big\} \Big] \end{aligned} \tag{1.66}$$

1.4.3.1 Example

To show an example, a driven quantum dot weakly coupled to a reservoir is considered. With a interacting Hamiltonian of the form $\hat{\mathrm{H}}_{\mathrm{int}} = \sum_k \lambda \left(\hat{d}_k^\dagger \hat{c}_{\mathrm{L}} + \hat{c}_{\mathrm{L}}^\dagger \hat{d}_k \right)$, where $\hat{d}$ is the destructive operator of the reservoir, $\hat{c}$ is the destructive operator of the system and λ the coupling between them, the derivation of γ_{ba} is

$$\gamma_{ba} = \sum_{n,m} 2\pi |\lambda|^2 \mathscr{D}(\Delta_{ab,mn}) \left\{ \left| \langle \phi_b^m | \hat{c}_{\mathrm{L}} | \phi_a^n \rangle \right|^2 \left[1 - f(\Delta_{ab,mn}) \right] + \left| \langle \phi_b^m | \hat{c}_{\mathrm{L}}^\dagger | \phi_a^n \rangle \right|^2 f(\Delta_{ab,mn}) \right\} \tag{1.67}$$

with $\Delta_{ab,mn} = q_a - q_b + (m-n)\omega$. $\mathscr{D}(\omega)$ is the density of states and $f(\omega)$ the Fermi function. The first term corresponds to one electron going from the system to the reservoir and the second therm from the reservoir to the system.

1.4.4 Redfield Master Equation

In some cases, the secular approximation is not appropriate. For example in driven configurations some oscillating terms from the driving field are important to consider when coupling the system to the reservoirs. The Redfield-Master equation in the Schrödinger picture reads:

$$\begin{aligned} \dot{\rho}_{\mathrm{S}}(t) = -i \left[\hat{\mathrm{H}}_{\mathrm{S}}(t), \rho_{\mathrm{S}}(t) \right] + \sum_{a,b,c,d} \gamma_{ab,cd}(t) \Big[& |\phi_c(t)\rangle \langle \phi_d(t)| \rho_{\mathrm{S}}(t) (|\phi_b(t)\rangle \langle \phi_a(t)|)^\dagger \\ & - \frac{1}{2} \Big\{ (|\phi_b(t)\rangle \langle \phi_a(t)|)^\dagger |\phi_c(t)\rangle \langle \phi_d(t)|, \rho_{\mathrm{S}}(t) \Big\} \Big] \end{aligned} \tag{1.68}$$

which different to Eq. (1.66) has time dependent couplings:

$$\gamma_{ab,cd}(t) = \sum_{n,m,l,p} \sum_{\eta\xi} 2\pi\delta_{q_d - q_c + (l-p)\omega + \epsilon_\eta - \epsilon_\xi} e^{i(m-n+p-l)\omega t} \langle \Phi_b^m \xi | \hat{\mathrm{H}}_{\mathrm{int}} | \Phi_a^n \eta \rangle^* \langle \Phi_c^l \xi | \hat{\mathrm{H}}_{\mathrm{int}} | \Phi_d^p \eta \rangle \langle \eta | \bar{\rho}_{\mathrm{B}} | \eta \rangle . \tag{1.69}$$

1.4.4.1 Example used in the paper: Coherent Long-Range Thermoelectrics in Nonadiabatic Driven Quantum Systems

Considering $\hat{H}_{\text{int}} = \sum_k \lambda \left(\hat{d}_k^\dagger \hat{c}_L + \hat{c}_L^\dagger \hat{d}_k \right)$ where $\hat{d}$ is the annihilation operator of the reservoir, $\hat{c}$ is the annihilation operator of the system and λ the coupling between them. Let's see the derivation of $\gamma_{\text{ab,cd}}$ considering there are up to one electron in the system.

With just one electron in the system, either the final or the initial state of the system must be the empty state $|0\rangle$. So with some algebra it is straightforward to obtain that there are only two non-zero terms: $\gamma_{a0,0d}(t)$ and $\gamma_{0b,c0}(t)$,

$$\begin{aligned}\gamma_{a0,0d}(t) &= \sum_{n,p} 2\pi|\lambda|^2 e^{-i(n-p)\omega t} \sum_{k\eta\xi} \delta_{q_d - p\omega + \epsilon_\eta - \epsilon_\xi} \langle \phi_a^n \eta | \hat{d}_k \hat{c}_L^\dagger | 0\xi \rangle \langle 0\xi | \hat{d}_k^\dagger \hat{c}_L | \phi_d^p \eta \rangle \langle \eta | \bar{\rho}_B | \eta \rangle \\ &= \sum_{n,p} 2\pi|\lambda|^2 \mathscr{D}(\Delta_{d,p}) \Big\{ e^{-i(n-p)\omega t} \langle \phi_a^n | \hat{c}_L^\dagger | 0 \rangle \langle 0 | \hat{c}_L | \phi_d^p \rangle \Big\} [1 - f(\Delta_{d,p})] \qquad (1.70) \\ \gamma_{0b,c0}(t) &= \sum_{m,l} 2\pi|\lambda|^2 e^{-i(l-m)\omega t} \sum_{k\eta\xi} \delta_{-q_c + l\omega + \epsilon_\eta - \epsilon_\xi} \langle 0\eta | \hat{c}_L \hat{d}_k^\dagger | \phi_b^m \xi \rangle \langle \phi_c^l \xi | \hat{c}_L^\dagger \hat{d}_k | 0\eta \rangle \langle \eta | \bar{\rho}_B | \eta \rangle \\ &= \sum_{m,l} 2\pi|\lambda|^2 \mathscr{D}(\Delta_{c,l}) \Big\{ e^{-i(l-m)\omega t} \langle 0 | \hat{c}_L | \phi_b^m \rangle \langle \phi_c^l | \hat{c}_L^\dagger | 0 \rangle \Big\} f(\Delta_{c,l}) \qquad (1.71)\end{aligned}$$

with $\Delta_{i,s} = q_i - s\omega$. $\mathscr{D}(\omega)$ is the density of states and $f(\omega)$ the Fermi function.

Defining the density matrix in the Floquet basis $\rho_S(t) = \sum_{\alpha=0}^{N} p_\alpha |\phi_\alpha(t)\rangle \langle \phi_\alpha(t)|$, where N is the number of states in the system plus the empty state: $\alpha = 0$. To obtain the occupations of the Floquet eigenstates is just needed the part with $a = d$ and $b = c$:

$$\dot{\rho}_S(t) = \sum_{a,b} \gamma_{ba}(t) \Big[|\phi_b(t)\rangle \langle \phi_a(t)| \rho_S(t) (|\phi_b(t)\rangle \langle \phi_a(t)|)^\dagger - \frac{1}{2} \Big\{ (|\phi_b(t)\rangle \langle \phi_a(t)|)^\dagger |\phi_b(t)\rangle \langle \phi_a(t)|, \rho_S(t) \Big\} \Big] \qquad (1.72)$$

$$\langle \phi_\alpha(t)| \dot{\rho}_S(t) |\phi_\alpha(t)\rangle = \sum_a \gamma_{a\alpha}(t) \langle \phi_a(t)| \rho_S(t) |\phi_a(t)\rangle - \sum_b \gamma_{b\alpha}(t) \langle \phi_\alpha(t)| \rho_S(t) |\phi_\alpha(t)\rangle \qquad (1.73)$$

The γ with $\beta \neq 0$ reads

$$\gamma_{0\beta}(t) = \sum_{n,p} 2\pi|\lambda|^2 \mathscr{D}(\Delta_{\beta,p}) \Big\{ e^{-i(n-p)\omega t} \langle \phi_\beta^n | \hat{c}_L^\dagger | 0 \rangle \langle 0 | \hat{c}_L | \phi_\beta^p \rangle \Big\} [1 - f(\Delta_{\beta,p})] \qquad (1.74)$$

$$\gamma_{\beta 0}(t) = \sum_{m,l} 2\pi|\lambda|^2 \mathscr{D}(\Delta_{\beta,l}) \Big\{ e^{-i(l-m)\omega t} \langle 0 | \hat{c}_L | \phi_\beta^m \rangle \langle \phi_\beta^l | \hat{c}_L^\dagger | 0 \rangle \Big\} f(\Delta_{\beta,l}) \qquad (1.75)$$

Replacing them in Eq. (1.73) is obtained:

$$\langle \phi_\beta(t)| \dot{\rho}_S(t) |\phi_\beta(t)\rangle = \gamma_{\beta 0}(t) \langle 0| \rho_S(t) |0\rangle - \gamma_{0\beta}(t) \langle \phi_\beta(t)| \rho_S(t) |\phi_\beta(t)\rangle \qquad (1.76)$$

$$\langle 0| \dot{\rho}_S(t) |0\rangle = \sum_\beta \gamma_{0\beta}(t) \langle \phi_\beta(t)| \rho_S(t) |\phi_\beta(t)\rangle - \sum_\beta \gamma_{\beta 0}(t) \langle 0| \rho_S(t) |0\rangle \qquad (1.77)$$

CHAPTER 2

NONEQUILIBRIUM RELAXATION TRANSPORT OF ULTRACOLD ATOMS

Fernando Gallego-Marcos, Christian Nietner, Gernot Schaller, Gloria Platero & Tobias Brandes
Physical Review A **90**, 033614 (2014)

All the authors authorize Fernando Gallego Marcos to include this work in his dissertation.

2.1 Objectives

In recent years it has been possible to isolate and control quantum systems to a very high degree. The equilibrium properties of isolated quantum systems are well known, but when these systems are initialized out of equilibrium, the thermalization and relaxation process to the steady state are no totally understood. It has revived the necessity of reconsidering and developing the theory of such processes [129–133]. There are some obstacles for the observation and manipulation of quantum systems: Firstly, due to their isolation, the thermodynamical variables of such systems are not tunneable externally, they are determined by the properties of the quantum system; therefore, in the theory they have to be calculated self-consistently. Secondly measuring the properties of these systems without modifying it (or even destroying) is very challenging.
To avoid measuring the properties of the system, one possibility is to observe transport processes. Transport in isolated quantum systems has already been analyzed in some theoretical works, for instance, in [134] bosonic transport is measured through a chain of quantum dots coupled to two bosonic reservoirs that keep the system far from equilibrium. In other work [135], the dynamics

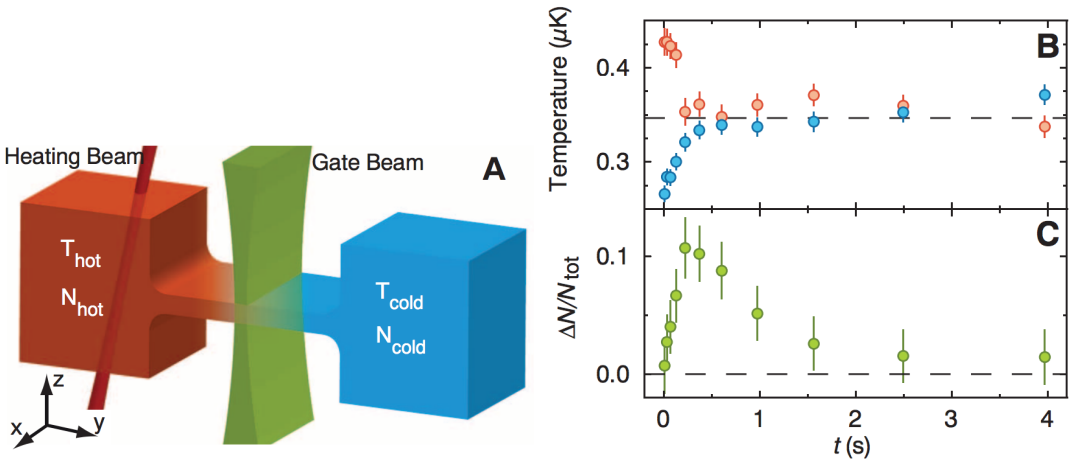

Figure 2.1: Sketch and experimental measurements taken from Ref. [142]. Two identical reservoirs of ultra-cold atoms are coupled through a quasi two dimensional channel. A gate beam blocks the the particle and heat transport between the reservoirs while one of the reservoirs is heated up with a laser heating beam. After the laser beam, the transport between the two reservoirs (now with different temperatures) is permitted again and the relaxation dynamics is studied. In the graphics, the temperature and the particle difference between the reservoirs are measured during the relaxation process.

between a quantum dot and a single superfluid reservoir is calculated, and in a previous work of some of the authors [136]. Other transport setups are also investigated: relaxation of two identical atomic reservoirs prepared at different temperatures which are directly coupled [137], fermionic transport connecting two finite one dimensional fermionic reservoirs through a lattice system [138], or two bosonic reservoirs connected through a one dimensional potential trap [139]. The experiments which investigate transport properties in isolated quantum systems are of high interest. The motivation of this work comes from experiments between two ultracold atomic clouds [140–142] (See Fig. 2.1). The objective is to analyze both numerical and analytically, with a linearized theory, the thermalization and relaxation transport dynamics with a set-up of two ultracold particle reservoirs coupled through a few-level quantum system. The introduction of this few-level quantum system enhance the quantum character of the transport and allows, in principle, to control the thermalization process externally by just changing the properties of this intermediate quantum system.

2.2 Model and set up

The setup of this work is a two ultracold atomic baths coupled through a few level quantum system. The ultracold atom reservoirs are modeled as an spin-less ideal quantum gas trapped in a 3D harmonic potential. The three macroscopic equilibrium variables of the reservoirs, temperature (T_ν), chemical potential (μ_ν) and average particle number (N_ν) are derived with the

grand-canonical ensemble. Within this theory a relation between the three variables and a expression for the average internal energy of the reservoir are obtained. These are the two self-consistent equations. Doing the total differential of these relations, the temperature and chemical potential change in time is derived. The equations are defined for both fermionic and bosonic particles.

The coupling between the reservoirs and the system is considered weak and the fastest timescale in the system is the equilibration of the reservoir to a thermal state. This permits to use the Born-Markov-Secular master equation between the intermediate quantum system and the reservoirs. Particle, and energy current through the few level quantum system is calculated with Eq. (1.21). The energy and particle current are then used to obtain the temperature and chemical potential change of the reservoirs.

The analysis of the systems out of equilibrium are very complex, all the thermodynamic variables of the reservoirs and the occupations in the quantum system are time dependent. In order to clearly understand the insights of the dynamics between the two reservoirs, a linearized model is considered, that allows to understand the most important features of the relaxation process. One of the first approximations made to linearize the system is that the intermediate few-level quantum system reaches a quasi-steady-state in a time scale much faster than the thermalization among the two reservoirs. Hence, the density matrix of the few level quantum system is considered as almost stationary, and thus, the energy and particle current are substituted by their quasi-steady-state values. This allows to reduce the dimensions of the system by just considering the evolution of the differences between the variables of both reservoirs: temperature, chemical potential and particle number differences. Additionally is considered that the thermodynamic variables of each reservoirs are symmetric to their average values. These two approximations permit to linearize the particle and energy currents between the reservoirs with respect to the temperature and particle number bias.

The linearized theory describes the characteristics of the intermediate system with know transport coefficients as the conductance, heat conductivity and Seebeck coefficient. Analytical timescales of the non-equilibrium dynamics are obtained. They explain two exponential processes: the saturation process and the exponential decay of the system.

In the analysis of the dynamics between the reservoirs, the case for one single transport channel and the case for multiple transport channels are considered. Both of them treated for bosons and fermions. In the single channel case the time scale related to the exponential decay is infinite, which leads to the saturated steady-sate, i.e., a maximally biased final state. Heat engines are defined with this set up, which are controlled by the energy of the intermediate region. An study of this process is done calculating its efficiency. For two or multiple channels both time scales play a role in the relaxation process between the two reservoirs; thus, after the saturation process, the two reservoirs eventually reach the full thermal equilibrium.

2.3 Spin degree of freedom

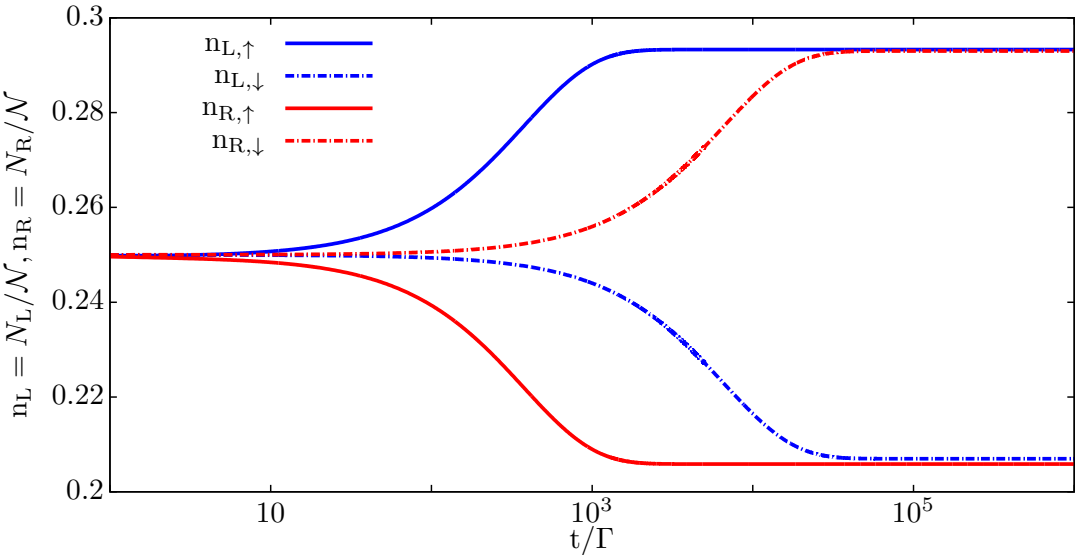

Figure 2.2: Time evolution of the particle density $n_{\nu,\sigma} = N_{\nu,\sigma}/\mathcal{N}$ in both reservoirs for each spin. The quantum system that connect the two reservoirs suffers a Zeeman splitting breaking the spin degeneracy in its energy level, the $\uparrow$ particles travels through the lower level at $\omega_\uparrow = 0.9\bar{\omega}$ and the $\downarrow$ particles at $\omega_\downarrow = 2.1\bar{\omega}$. At $t = 0$ the particle number in each reservoir and for each spin are equal $n_{\nu,\sigma} = 0.25$ and there is a temperature gradient between the reservoirs $T_L = 0.45\bar{\omega}$, $T_R = 0.25\bar{\omega}$.

An extension to this work has been done for the spin dynamics between the two ultra cold atoms reservoirs. Each reservoir has a number of spins up and spins down: $N_{\nu,\sigma}$, where $\nu = \{\mathrm{L},\mathrm{R}\}$ refers to the reservoir and $\sigma = \{\uparrow,\downarrow\}$ the spin. Particles in the same reservoir with different spin have same temperatures and in general different particle number; hence, in order to fulfill the self-consistent equations, they have different chemical potentials. Initially the particle density is the same in the L and R reservoir with the same amount of spins $\uparrow$ and $\downarrow$. The quantum system has one level that suffers a Zeeman splitting breaking the spin degeneracy. Each spin can just travel through one of the channels. The system behavior is like a two parallel systems going toward a saturated steady-state. Then, the steady-state is a maximally biased state where the spins gradient between the reservoirs has increased. In Fig. 2.2 the initial temperature gradient generates a spin gradient between the left and right reservoirs during its relaxation process through the quantum system, which is maximal in the steady-state.

2.4 Conclusions

In this paper, it was analyzed the equilibration process between two reservoirs, which are initialized in a non-equilibrium configuration and that are weakly thermally connected via a few-level quantum system. To this end, it was established the full equations of motion describing the

evolution of the density matrix elements of the quantum system, as well as the evolution of the thermodynamic variables of the attached reservoirs. Subsequently, these equations were solved, both numerically and analytically, by a linearized theory. It is observed a qualitative dependence of the equilibration on the number of available transport channels. Only setups with more than one accessible transport channel show a thermodynamic equilibration for long times, whereas a non-thermal steady state is reached in systems with only a single transport channel. This fundamentally different behavior might be used to construct a transistor or capacitor for ultracold atoms. Such a machine would also work quite efficiently, as it is confirmed from the calculation of the heat current and power output. Finally, it is compared the equilibration process in thermal fermionic and bosonic transport setups, where one qualitatively observe the same behavior.

Transient and far non-equilibrium dynamics of isolated quantum systems of ultra cold atoms has been extensively studied both experimentally and theoretically for a wide range of fields. Ultracold atom systems have open a new research in the field of quantum simulators, for understanding the complex behavior of quantum systems [143]. In an impressive experiment from the Esslinger group [144] it has been observed a quantized conductance of neutral mater through a quantum point contact connecting two ultra cold atom reservoirs. There have been proposals to realize, in the work presented here, ac-driven thermodynamic engines [145]. In the paper presented here, the bosonic reservoirs are always above the values where the bosons start to condensate in the lowest energy level, hence the phase transition to the condensate is not studied. In [146] the phase transition to the condensate is studied using the same set-up, showing the generation and evaporation of a Bose Einstein condensate during the transient regime. In a different set-up, where all the atoms are initially contained in one of the reservoirs, it has been studied the expansion/relaxation of the atomic cloud to the drain [147]. During the expansion is observed that the current drop below a critical value where a superfluid Bose-Einstein condensate is established [148] in the drain reservoir. The complex extension to strong coupling systems that follows non-Markovian dynamics has also been studied in a recent work [149]. There are theoretical proposals of transport experiment with ultra cold atoms which shows signatures of the orbital Kondo effect [150].

PHYSICAL REVIEW A **90**, 033614 (2014)

Nonequilibrium relaxation transport of ultracold atoms

Fernando Gallego-Marcos* and Gloria Platero
Instituto de Ciencia de Materiales, CSIC, Cantoblanco, 28049 Madrid, Spain

Christian Nietner,† Gernot Schaller, and Tobias Brandes
Institut für Theoretische Physik, Technische Universität Berlin, Hardenbergstr. 36, 10623 Berlin, Germany
(Received 10 July 2014; published 15 September 2014)

We analyze the equilibration process between two either fermionic or bosonic reservoirs containing ultracold atoms with a fixed total number of particles that are weakly connected via a few-level quantum system. We allow for both the temperatures and particle densities of the reservoirs to evolve in time. Subsequently, linearizing the resulting equations enables us to characterize the equilibration process and its time scales in terms of equilibrium reservoir properties and linear-response transport coefficients. Additionally, we investigate the use of such a device as particle transistor or particle capacitor and analyze its efficiency.

DOI: 10.1103/PhysRevA.90.033614 PACS number(s): 67.85.−d, 51.10.+y, 05.60.Gg, 05.30.Rt

I. INTRODUCTION

Transport phenomena are of utmost importance in a whole variety of scientific research fields such as biology, chemistry, and physics. Here, systems which are initialized in nonequilibrium strive to equilibrate with their surrounding by exchanging energy and particles until a stationary state is reached. This equilibration is quite well understood for classical systems, where it usually results in a thermal steady state. However, despite its importance, relaxation and thermalization in closed quantum systems are still not fully understood [1–5].

In recent years it has become possible to isolate and control quantum systems to a very high degree. Namely, there has been a lot of progress in the production and manipulation of ultracold quantum gases in ultrahigh vacuum chambers, using optomagnetical traps [6,7] and lasers [8–10]. Here, the system of interest is isolated from its environment to such a high degree that thermodynamic variables are not tunable externally, but are solely determined implicitly by the system itself. Therefore, in such systems it is necessary to calculate the thermodynamic variables self-consistently in order to correctly describe their equilibration properties.

Thereby, the quantum mechanical peculiarities become relevant and potentially observable and measurable in an experiment. This has been impressively confirmed by the creation of the famous Bose-Einstein condensate [11,12]. After successfully studying setups with ultracold atoms in equilibrium configurations for quite a while, nowadays, the focus shifts to investigating their nonequilibrium properties [13–22]. However, measuring the properties of such systems is quite complicated and usually results in the destruction of the system. A possible evasion of this problem could be the observation of transport processes, as has been also theoretically researched for setups involving atomic reservoirs coupled to, e.g., each other [23], a lattice system [24], a potential trap [25], or even quantum dot systems [26–28]. Following this idea, recent experiments [29–31], which investigate the transport properties between two ultracold atomic clouds, are especially noteworthy.

Motivated by these experiments, we analyze within this paper a transport setup consisting of a mesoscopic few-level quantum system in contact with two ultracold particle reservoirs, whose thermodynamic variables are calculated self-consistently. We explicitly include a few-level system in our model since it enhances the quantum character of the transport setup, as is well known from electronic and photonic mesoscopic transport, where one observes effects such as the Kondo effect [32–35], Coulomb blockade [36–39], coherent population trapping [40,41], and dark states [42–44], to name but a few. Furthermore, this approach, in principle, allows for an external control of the equilibration process via the few-level quantum system.

In Sec. II, we start by presenting the general theoretical framework which we use throughout this paper. Here, we first review the properties of ideal quantum gases in Sec. II A, and in Sec. II B, we derive the master-equation formalism which we use to describe the transport through an open quantum system. In Sec. II C, we deduce the resulting system of equations of motion and additionally establish a linear-response theory in Sec. II D. Subsequently, we apply this formalism to different setups and present the respective results in Sec. III. In particular, we investigate fermionic systems with one and two transition energies in Secs. III A and III B, respectively. In comparison, we additionally analyze a bosonic system with two transition energies in Sec. III C. Finally, we summarize our results in Sec. IV.

Note that throughout this paper we use the natural units with $\hbar = k_B = 1$.

II. THEORETICAL FRAMEWORK

In real experiments with cold atoms the chemical potential can not be tuned directly by applying an external voltage as usually considered for electronic transport. Instead, one can introduce a thermal or density gradient which causes a bias in the chemical potentials of the reservoirs.

In order to describe this bias correctly, we need to determine the chemical potential self-consistently from the reservoir

*fergallmar@hotmail.com
†cnietner@itp.tu-berlin.de

CHAPTER 3

SUPEREXCHANGE BLOCKADE IN TRIPLE QUANTUM DOTS

Rafael Sánchez, Fernando Gallego-Marcos & Gloria Platero
Physical Review B **89**, 161402(R) (2014)

All the authors authorize Fernando Gallego Marcos to include this work in his dissertation.

3.1 Objectives

Long Range (LR) transport mechanism is essential in many fields: for donor-acceptor reactions through bridge states, which is relevant for molecules as complex as photosynthetic centers or DNA to explain transport and order in magnetic compounds, and for the Kondo problem to name a few (see Sec. 1.1.4 for more details). The complexity of the physics underlying this transition makes it difficult to study the insights of these long distant coherent states. The motivation of this work is to study the LR transition in a simpler model of three quantum dots, where its coherence and dynamics can be fully understood.

The objective of this work is to control the LR coupling between QDs, studying virtual transitions between non-directly coupled quantum states. The LR coupling has been measured as current resonances [101, 102] and by real time charge detection [103] (see Fig. 3.1). The transitions go through energetically forbidden intermediate quantum states that are only virtually occupied. The virtual transitions are a consequence of the uncertainty principle, which allows electrons to access energetically forbidden states if they do so on a sufficiently fast timescale [151]. There is a high interest on the control of these transitions for quantum information transfer [80] and for the control of LR interaction between qubits [75, 104].

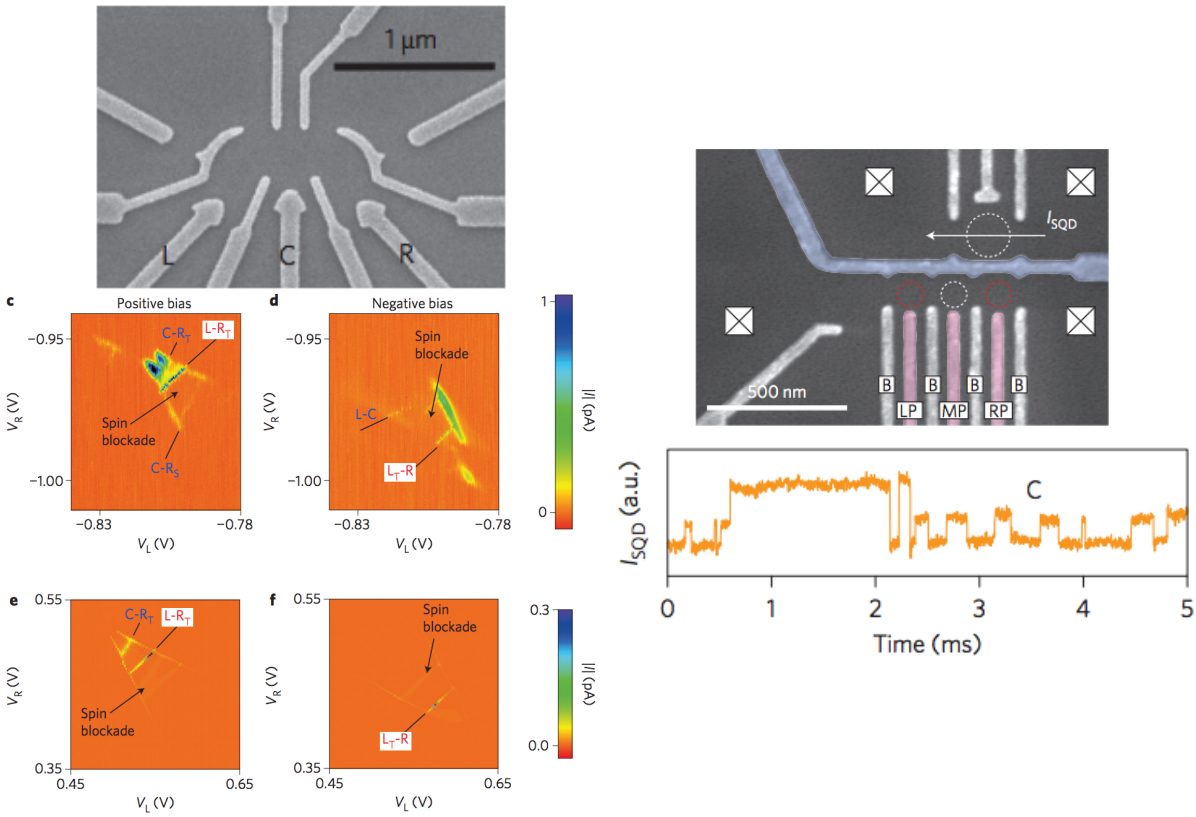

Figure 3.1: *Left*- Figures from Ref. [101]. In the upper figure, the image of the used TQD sample is shown. The bottom picture shows the transport triangles for finite bias, where resonance transport lines are observed for the LR transition ($L-R_T$ and L_T-R) between the states $(1,1,2)$ and $(2,1,1)$. *Right*- Figures from Ref. [103]. The upper figure shows the TQD sample used in the experiment. A QPC is located in the proximity to detect the charges within the system. At the bottom, the real-time trace of the QPC current exhibits fast steps that appear to correspond to single electron transfer between the states $(1,1,0)$ and $(0,1,1)$.

In particular, the effect of the interference [103] is studied in a two electron set-up as a consequence of interaction and the spin of the particles. The electron-electron interaction leads to two different transport paths in the Hilbert space between the reservoirs, defining the two arms of an interferometer. One of the paths contains an state of double occupancy; hence, due to the Pauli exclusion principle, only singlet states are permitted on it. Depending on the spin of the two electrons, either a singlet or triplet state is formed in the system. The singlets are allowed to go through the two paths while the triplets only flow through one of them. The interferences are studied and a new current blocking effect is observed in the singlet subspace. Additionally, the effect of spin decoherence and relaxation in the dynamics and interactions among the quantum states is studied.

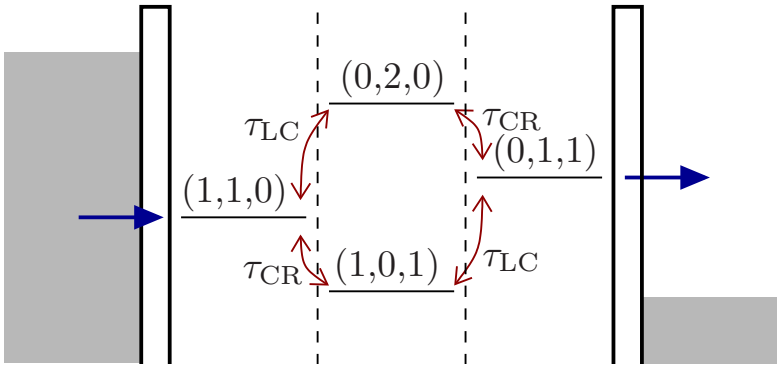

Figure 3.2: Two electron states structure within the TQD.

3.2 Model and set up

The proposed minimal transport set up is a two electron linear TQD. QD arrays are ideal for their scalability, high degree of tuneability [2] and long coherence times. The states of the TQD that participate in transport are composed by one energy state in each outer dot and one quantum state with double occupancy in the central dot, the rest of the energy states are in the CB regime and do not play a role in transport. This system, sketched in Fig. 3.2, is modeled as a three site Anderson Hamiltonian, where the dots are tunnel coupled only with their neighbor sites. The density matrix formalism is used to study the dynamical evolution of the quantum states and the coherences among them.

The quantum states connected to the reservoirs are the singlets and triplets $\left\{|S_{LC}\rangle, |T^{0,\pm}_{LC}\rangle\right\}$ for $(1,1,0)$, and $\left\{|S_{CR}\rangle, |T^{0,\pm}_{CR}\rangle\right\}$ for $(0,1,1)$. The states are labeled as (N_L, N_C, N_R), where N_i is the number of particles in the i-dot. The spin degree of freedom is represented as $\sigma = \{\uparrow, \downarrow\}$. They are connected via the intermediate sates $|S\rangle = (0, \uparrow\downarrow, 0)$ and $(1,0,1)$. $|S\rangle$ is a singlet state; hence, it is only coupled to the singlet states $|S_{LC}\rangle$ and $|S_{CR}\rangle$. On the other hand, the state $(1,0,1)$ is coupled to both triplets and singlets. Therefore, the singlets are connected by two channels and the triplet sates only by one. The double path in the singlet component:

$$(0,1,0) \rightarrow |S_{LC}\rangle \rightarrow \left\{ \begin{array}{c} |S\rangle \\ |S_{LR}\rangle \end{array} \right\} \rightarrow |S_{CR}\rangle \rightarrow (0,1,0) \tag{3.1}$$

leads to interferences that can be destructive and lead to the suppression of the current.

The destructive interference of the two paths going from $|S_{LC}\rangle$ to $|S_{CR}\rangle$ generates an eigenstate $|DS\rangle$ with zero occupation probability in $|S_{CR}\rangle$. In the infinite bias regime that is considered here, the state $|S_{CR}\rangle$ is not populated from the reservoirs. Electrons are only entering the system to the state $(1,1,0)$ and are leaving from $(0,1,1)$, i.e., unidirectional transport. Therefore, at the conditions of destructive interference, it is assured that in the steady state the system will be in the pure state $|DS\rangle$, and the current will be blocked [152–154]. Note the analogy with dark states in quantum optics, which are non-emitting superpositions that decouple from the driving fields

[155–157]

To study the long-range transport, the intermediate states $(0,\uparrow\downarrow,0)$ and $(1,0,1)$ are considered to be sufficiently far in energy from the outer states to neglect particle occupation on them, i.e., $|E_{outer} - E_{inter}| \gg |\tau|$, where $E_{inter,outer}$ is the energy of the state and τ is the coupling between the outer and intermediate states; hence, the intermediate states are energetically unaccessible from the outer states $(1,1,0)$ and $(0,1,1)$. Projecting the Hamiltonian into the outer states and considering higher order transitions between these states, an effective Hamiltonian is obtained which couples them directly:

As an example, the effective Hamiltonian of the singlet sub-space is derivated. In matrix form, the Hamiltonian for the singlet sub-space reads:

$$\hat{H}_S = \begin{bmatrix} E_{|S_{LC}\rangle} & 0 & \tau_{CR} & -\sqrt{2}\tau_{LC} \\ 0 & E_{|S_{CR}\rangle} & \tau_{LC} & -\sqrt{2}\tau_{CR} \\ \tau_{CR} & \tau_{LC} & E_{|S_{LR}\rangle} & 0 \\ -\sqrt{2}\tau_{LC} & -\sqrt{2}\tau_{CR} & 0 & E_{|S\rangle} \end{bmatrix} \tag{3.2}$$

where the blue shadowed area is the subset of the outer states $(1,1,0)$ and $(0,1,1)$, and the orange one is the subset of the intermediate states $(0,2,0)$ and $(1,0,1)$. The interaction between them is the green shadowed area. Using the theory from Appendix B the effective Hamiltonian is calculated. Considering the same energy for the states $E_{|S_{LC}\rangle} = E_{|S_{CR}\rangle} \equiv E$. From Eq. (1.15), $S^{(1)}$ reads:

$$\hat{S}^{(1)} = \begin{bmatrix} 0 & \hat{S}^{(1)}_{AB} \\ -\hat{S}^{(1)*}_{AB} & 0 \end{bmatrix} \text{ with } \hat{S}^{(1)}_{AB} = \begin{bmatrix} \frac{\tau_{CR}}{E_{|S_{LR}\rangle}-E} & \frac{-\sqrt{2}\tau_{LC}}{E_{|S\rangle}-E} \\ \frac{\tau_{LC}}{E_{|S_{LR}\rangle}-E} & \frac{-\sqrt{2}\tau_{CR}}{E_{|S\rangle}-E} \end{bmatrix} \tag{3.3}$$

Calculating the effective Hamiltonian from (1.13) and projecting it into the outer-states subspace, it becomes:

$$\mathscr{P}\hat{H}^{(2)}_{eff}\mathscr{P} = \begin{bmatrix} E - \frac{\tau^2_{CR}}{E_{|S_{LR}\rangle}-E} - \frac{2\tau^2_{LC}}{E_{|S\rangle}-E} & -\frac{\tau_{CR}\tau_{LC}}{E_{|S_{LR}\rangle}-E} - \frac{2\tau_{CR}\tau_{LC}}{E_{|S\rangle}-E} \\ -\frac{\tau_{CR}\tau_{LC}}{E_{|S_{LR}\rangle}-E} - \frac{2\tau_{CR}\tau_{LC}}{E_{|S\rangle}-E} & E - \frac{\tau^2_{LC}}{E_{|S_{LR}\rangle}-E} - \frac{2\tau^2_{CR}}{E_{|S\rangle}-E} \end{bmatrix} \tag{3.4}$$

An effective coupling has been obtained between the two disconnected states and their energies have been renormalized. The outer states are effectively coupled with two different tunnel couplings:

$$\tau^S_{eff} = -\frac{\tau_{CR}\tau_{LC}}{E_{|S_{LR}\rangle} - E} - \frac{2\tau_{CR}\tau_{LC}}{E_{|S\rangle} - E} \tag{3.5}$$

$$\tau^T_{eff} = -\frac{\tau_{CR}\tau_{LC}}{E_{|T_{LR}\rangle} - E} \tag{3.6}$$

depending on the total spin, s = 0 (singlets) or s = 1 (triplets). The effective coupling for the triplets is calculated with a similar derivation. With this effective Hamiltonian, a resonant long

range current intensity is predicted analytically even for a large detuning with the central states, when direct tunneling between the three dots is suppressed.
The destructive interference, DS, is predicted between the two paths in the singlet space. The DS does not carry current; therefore, it will eventually block the transport through the TQD. It will be occupied with probability 1 for $t \to \infty$.
The interferences that lead to the DS depend on the spin correlations. For that reason the effect of spin decoherence and relaxation is explored. The spin decoherence and relaxation mix the triplets and singlets which lift the spin blockade. It strongly affects the charge and spin dynamics. The DS is then coupled to triplets states which are connected with the drain and consequently, it is quenched and the system starts transporting particles again. An additional current transport path which was previously forbidden due to spin blockade appears, it comes from the transition between the triplets and the intermediate state $(0,\uparrow\downarrow,0)$.

3.3 Experimental detection of the *dark state*

The DS is sensitive to spin and charge fluctuations. In this section the effect of the DS on a measurement with the standard experimental techniques: QPC and lock-in transport measurements is studied. In the published paper just the infinite bias limit and up to two particles in the TQD is considered. Here, a less restricted set-up is used. The simulation will be done at finite bias with up to three electrons in the system (the state (1,1,1) is considered). The on-site energies of the TQD are tunned with three gate voltages: U_L, U_M and U_R, each one of them is capacitively coupled with different strengths to all the quantum dots. There are two possible transport sequences

$$|S_{LC}\rangle \to \left\{ \begin{array}{c} |S_C\rangle \\ |S_{LR}\rangle \end{array} \right\} \to |S_{CR}\rangle \to (1,1,1) \to |S_{LC}\rangle, \qquad \text{throught the } (1,1,1) \text{ state} \tag{3.7}$$

$$|S_{LC}\rangle \to \left\{ \begin{array}{c} |S_C\rangle \\ |S_{LR}\rangle \end{array} \right\} \to |S_{CR}\rangle \to (0,1,0) \to |S_{LC}\rangle, \qquad \text{throught the } (0,1,0) \text{ state} \tag{3.8}$$

The sequences in the previous equations are for *left-right* transport direction, for the opposite direction one has to flip the arrows. In the large bias limit, where just one direction is possible, the system evolves towards the DS for the conditions of destructive interference. In the finite bias, the particles also flow from the drain to the source. Thus, the steady state of the system is not the in the pure state $|DS\rangle$ because electrons can now tunnel back to the left lead thus introducing a finite lifetime of the dark state. In the steady-state the system is a mixed state, a combination of the different eigenstates present in the Hamiltonian, where the eigenstate that corresponds to $|DS\rangle$ is only partially occupied.
The level configuration of the triple dot structure vs. U_L is displayed in Fig.3.3(a).To increase the occupation of the DS a configuration where the DSs for the *left→right* and *right→left* transport directions coincide at the same U_M and U_L is selected. This specific case is plotted in Fig.3.3(a)(b)

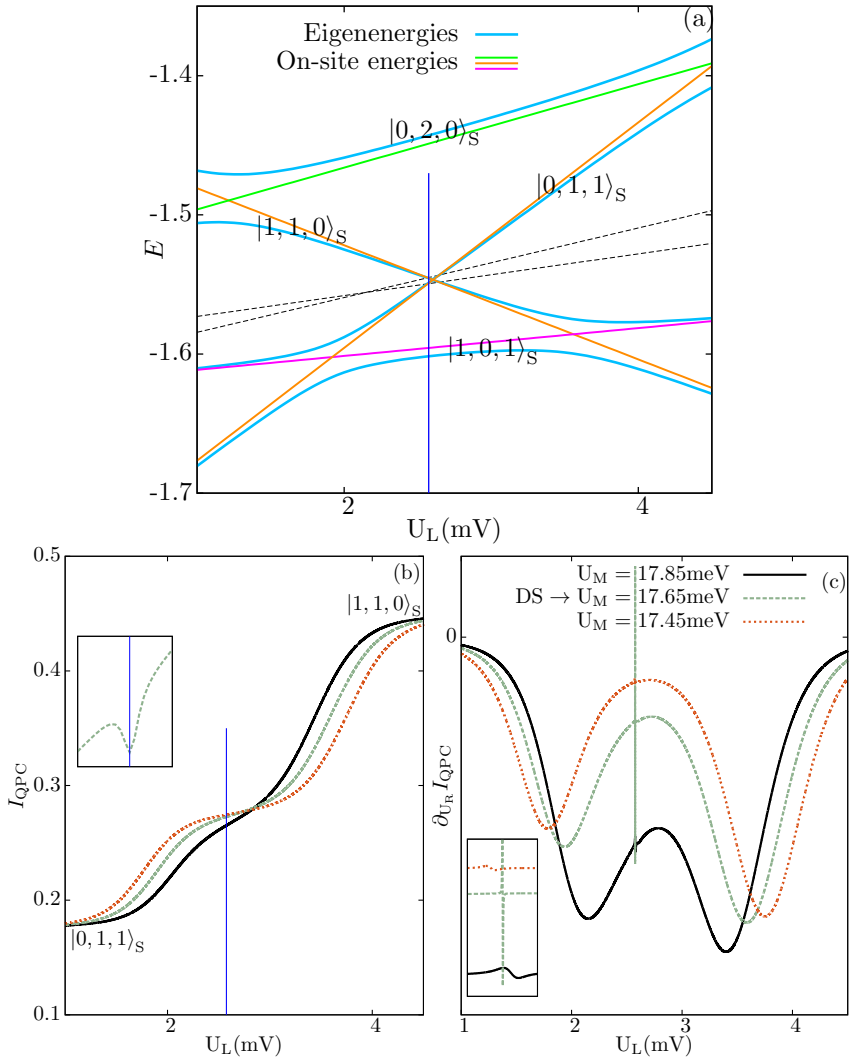

Figure 3.3: In (a) the level configuration for the different values of U_L is plotted. The blue vertical line is the U_L corresponding to the DS configuration. The dashed lines are the chemical potentials of the leads. In (b) the current through the QPC is plotted vs. U_L for three different values of U_M. A decrease of the QPC current is observed in the DS due to a decrease of the occupation of the state $|0,1,0\rangle$ in the TQD. In (c) we plot the lock-in simulation. The inset shows the structure around the DS condition.

and (c) for the value of $U_M = 17.65$meV. In these figures the condition where the system has a DS is marked with a blue vertical line, which is for $U_L \approx 2.58$ At a different value of U_M the two DS don't coincide anymore and their occupation decrease.

In Fig.3.3(b) the current through the QPC is plotted, it depends on the charge occupation and energy configuration of the quantum dot system. One can distinguish three current steps, the lower one corresponding to the state $|1,1,0\rangle$ that blocks the QPC current more strongly, then the $|1,0,1\rangle$ and finally $|1,1,0\rangle$, the weakest coupled to the QPC. Closer to the DS condition a small

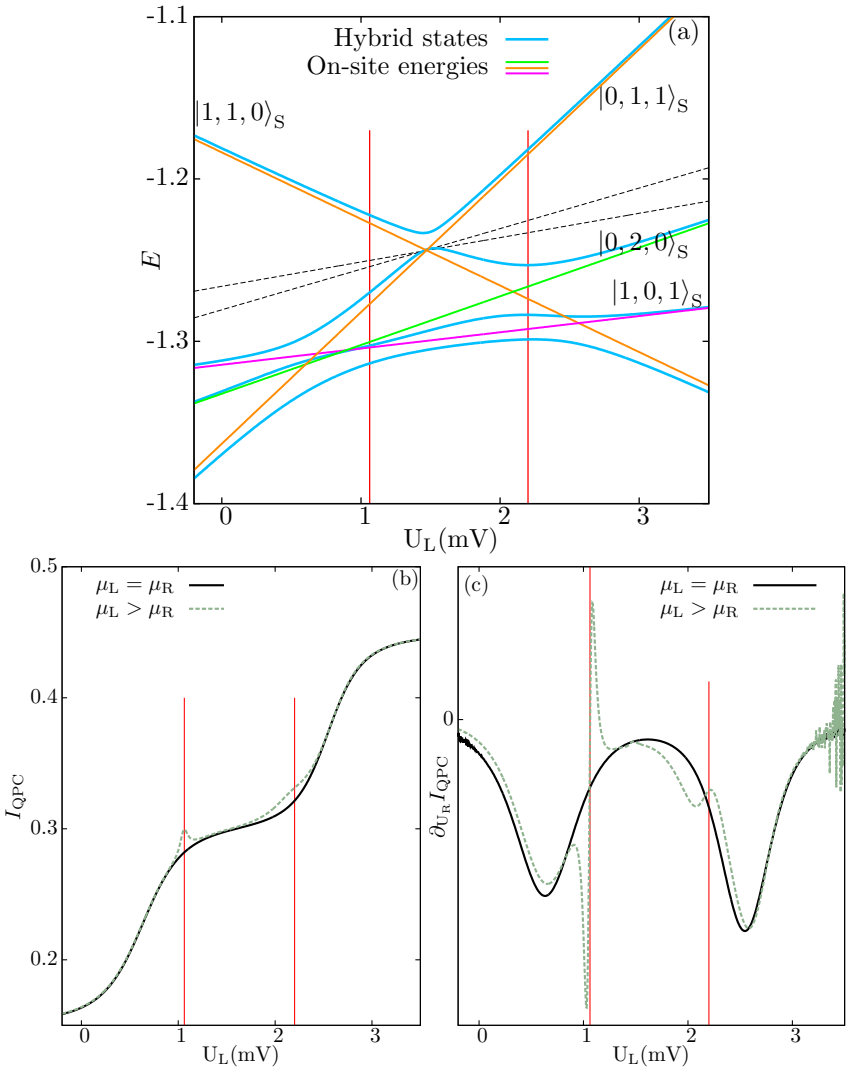

Figure 3.4: Same simulations as in Fig.3.3, with a level configuration where the DS and LR do not coincide at the same value of U_L and importantly, for the detection of the DS, the DS's energy is far below the chemical potential of the leads. The vertical red lines indicates the value of U_L for the DS.

decrease of the QPC current is observed. The DS partially blocks the transport channel in Eq. 3.8 so the state with one electron decreases its occupation while the two electron states increase their occupation and consequently the QPC current intensity is reduced. The other transport channel through the triple occupancy Eq. 3.7 is not playing a role for these parameters.
In Fig.3.3(b) the lock-in signal is plotted. It is calculated with the following equation

$$\text{Lock-in} = \Big[I_{QPC}(U_R = \alpha + \Delta_\alpha) - I_{QPC}(U_R = \alpha)\Big]/\Delta_\alpha,\ \Delta_\alpha > 0. \tag{3.9}$$

As one can observe, at the value of the DS a narrow and clear perturbation appears in Fig.3.3(c). The small effect of the DS in the QPC figure is magnified with the lock-in technique.

In Fig.3.4 the energy of the DS is more below the chemical potential of the leads than in Fig.3.3, so the DS gets more occupied. In this situation the transport sequence contains the three electron state, Eq. 3.7. In Fig.3.4(b)(c) the effect of the DS on the I_{QPC} is observed and the lock-in detection is stronger than in the previous situation.

3.4 Conclusions

It has been proposed a triple quantum dot setup within today's experimental reach where superexchange interactions can be detected and manipulated. Current resonances involving only states with merely indirect coupling have been found and analyzed. The transport mechanism is described in terms of higher order superexchange transitions. In the resonance of states with left-right inverted charge distribution, an electron is delocalized between the outermost quantum dots with the center dot being only virtually occupied. A dark superposition of spin singlets is predicted which is formed at a point of destructive interference of virtual transitions. It is manifested in a total current suppression (the superexchange blockade). We emphasize the relevance of spin correlations for systems with more than one electron. In particular, resonances which are suppressed by Pauli spin blockade show lifetime enhanced coherent transport in the presence of decoherence. We identify another configuration where left-right symmetric superpositions of spin states are formed which pave the way for CTAP of Bell states.
On later works there has been an increasing interest in TQD systems, the TQD is the smallest qubit chain and it permits to study interference and coherent effects in a controllable manner in experiments and theory [68, 72, 79, 85, 91, 103]. The results obtained in this work can be extended to longer arrays that begin to be accessible in the present technology [158].
In other works the study of long-range interactions has been extended and also measured to long-range charge and well defined spin transfer between the outer dots of the TQD, where the spin electron acts as an spin bus [102]. It has also been driven by an external field which gives advantages for the spin qubit control and can increase the operation speed [159]. In a very recent publication it has been demonstrated the first working example of a direct quantum gate between solid-state spins at a distance via the virtual occupation of an intermediate quantum region [160]. There are other extensions to this work by the same author of this dissertation, they have been discussed in the introduction and in more detail in their corresponding sections.

PHYSICAL REVIEW B **89**, 161402(R) (2014)

Superexchange blockade in triple quantum dots

Rafael Sánchez,[1] Fernando Gallego-Marcos,[1,2] and Gloria Platero[1]
[1]*Instituto de Ciencia de Materiales de Madrid, CSIC, Cantoblanco, 28049 Madrid, Spain*
[2]*Institut für Theoretische Physik, Technische Universität Berlin, D-10623 Berlin, Germany*
(Received 20 December 2013; revised manuscript received 5 March 2014; published 4 April 2014)

We propose the interaction of two electrons in a triple quantum dot as a minimal system to control long-range superexchange transitions. These are probed by transport spectroscopy. Narrow resonances appear indicating the transfer of charge from one side of the sample to the other with the central one being occupied only virtually. We predict that two different intermediate states establish the two arms of a one-dimensional interferometer. We find configurations where destructive interference of the two superexchange trajectories totally blocks the current through the system. We emphasize the role of spin correlations giving rise to lifetime-enhanced resonances.

DOI: 10.1103/PhysRevB.89.161402 PACS number(s): 73.63.Kv, 75.10.Jm, 85.35.Be, 85.35.Ds

Introduction. Transitions mediated by long-range quantum coherence in two or more particle systems are an essential concept in many different fields. Superexchange, the interaction of orbitals whose overlap is small but is mediated by intermediate virtual states, was introduced by Pauling in his resonance theory of the molecular bond [1]. Delocalization due to long-range electron transfer mechanisms is responsible for donor-acceptor reactions through bridge states [2,3] relevant for molecules as complex as photosynthetic centers [4] or DNA [5,6]. In the solid state, seminal works by Zener [7] and Anderson [8] introduced long-range exchange interactions to explain transport and order in magnetic compounds. Related ideas led to models of the Kondo problem [9,10]. Resonance valence bond models [11] have found recently an increased interest in the context of topological phases in triangular lattices [12].

The complex physics involved in the above mentioned systems can be unraveled by investigating simpler configurations that can be realized experimentally. For that purpose, quantum dot arrays are ideal for their scalability, high degree of tunability, and long coherence times [13]. Coupled quantum dots behave as artificial molecules and their coupling is naturally described by hopping Hamiltonians. These characteristics nominate them for simulations of chemical reactions [14] or lattice models [15–17]. The interplay of charge and spin correlations introduces unique transport dynamics as the mesoscopic Kondo effect [18] or Pauli spin blockade [19]. The impressive gate control of few-electron triple quantum dots [20–23] has succeeded the operation of three-electron exchange-only qubits [24–26]. In situations where tunneling to the center dot is energetically forbidden, superexchange is responsible for the indirect coupling of the two outer quantum dots, mediated by virtual transitions through the middle one. Evidences of such transitions have been recently reported in the form of sharp current resonances [27,28] and by real-time charge detection [29]. Thus quantum dots offer not only a way to experimentally control superexchange but also the possibility to explore new phenomena based on long-range interactions [30,31].

Here we investigate the minimal system with long-range superexchange interactions affected by charge and spin correlations. It requires three sites and two electrons. In particular, two-particle correlations introduce a mechanism for the quantum interference of superexchange transitions. At the degeneracy of $(N_L,N_C,N_R) = (1,1,0)$ and $(0,1,1)$ states—N_l being the number of electrons in quantum dot l—charge is delocalized between the two edge dots via the virtual occupation of *two* possible intermediate states, (0,2,0) and (1,0,1), which are detuned, as sketched in Fig. 1.

We focus on a configuration where the two different virtual transitions coexist and lead to interference. Remarkably, we find conditions where the destructive interference of transitions through the (1,0,1) and (0,2,0) branches completely cancels the transport, which we term superexchange blockade. We emphasize the role of spin correlations. The two-path interference only occurs for singlet states: the Pauli exclusion principle avoids triplets to tunnel into the (0,2,0) state. As a consequence, at the condition for superexchange blockade, triplets contribute to transport assisted by long-range tunneling through (1,0,1), while the occupation of singlet states cancels the current. This mechanism is in utter contrast with spin blockade in coupled quantum dots, where triplets block the current.

Model. We describe the triple quantum dot with the three-site Anderson Hamiltonian ($i = \mathrm{L,C,R}$):

$$\hat{H}_{\mathrm{TQD}} = \sum_{i\sigma} \varepsilon_i \hat{c}^{\dagger}_{i\sigma}\hat{c}_{i\sigma} + \sum_i U_i \hat{n}_{i\uparrow}\hat{n}_{i\downarrow} + \frac{1}{2}\sum_{i\neq j} U_{ij}\hat{n}_i\hat{n}_j - \sum_{i\neq j,\sigma} \tau_{ij}\hat{c}^{\dagger}_{i\sigma}\hat{c}_{j\sigma} + \mathrm{H.c.}, \quad (1)$$

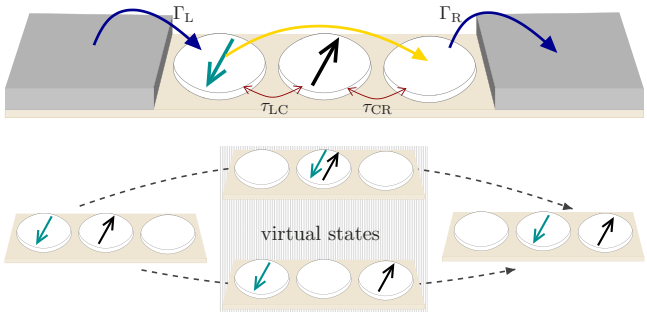

FIG. 1. (Color online) A triple quantum dot with superexchange mediated transport. Electrons tunnel from the source lead into the left dot and from the right dot into the drain lead with rates $\Gamma_{L,R}$. Interdot tunneling is described by the hopping terms τ_{LC} and τ_{CR}. When states (1,1,0) and (0,1,1) are degenerate, charge is transferred via higher order tunneling processes in which the intermediate states are only virtually occupied. The two intermediate states, whose energy is tunable by gate voltages, define the two arms of a superexchange interferometer.

CHAPTER 4

PHOTON ASSISTED LONG-RANGE TUNNELING

Fernando Gallego-Marcos, Rafael Sánchez & Gloria Platero
J. Appl. Phys. **117**, 112808 (2015)

All the authors authorize Fernando Gallego Marcos to include this work in his dissertation.

4.1 Objectives

In systems weakly coupled to reservoirs and isolated from the rest of the environment, transitions between discrete energy levels occur when the two sates have the same energy. If they are not in resonance, transitions can still be induced by the interaction with a time dependent field. A fast time dependent field is introduced with time dependent gate voltages (see Sec.1.1.3). They change the on-site energy levels of the quantum dots. Transitions occur between crossing quantum dot states, the so called Landau-Zener Transitionss (LZTs) (see Sec. 1.1.3). A periodic field generates multiple LZTs between the states within the quantum dot system, which gives rise to the LZS interferences. They become constructive for an energy difference between the undriven coherent states equal to an integer number of the frequency of the ac-field $\Delta E = n\hbar\omega$. The driven transition can be interpreted as an absorption or emission of n photons and is known as Photo Assisted Transition (PAT). The probability of a transition absorbing n photons is controlled by the amplitude of the driving, which renormalizes the tunnel coupling with the n-Bessel function (see Eq. (1.44) and (1.49)). For the values of the driving amplitude giving zeros of the Bessel functions, the renormalized coupling vanishes. Tunneling is then suppressed, what is known as Coherent Destruction of Tunneling (CDT) [66, 67]. The renormalized couplings depend on the

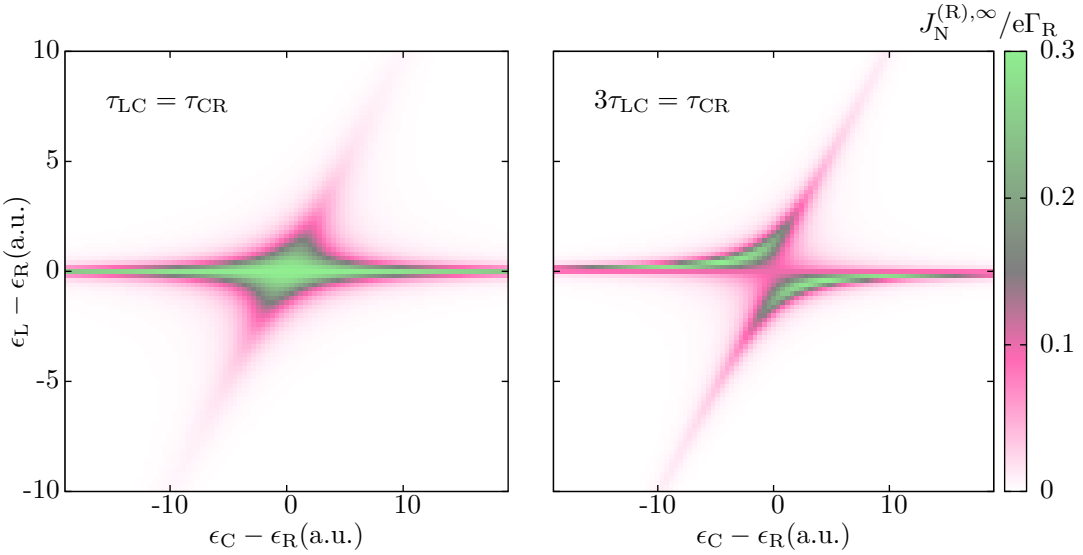

Figure 4.1: Transport through a linear TQD weakly coupled to reservoirs on its ends vs. the energy differences between the energy levels of the dots. Each quantum dot has a single energy level and the number of electrons within the TQD is up to one. The simulation is done with the Master equation theory (see Sec. 1.2.4). High current intensity is observed in both figures at $\epsilon_L - \epsilon_R = 0$ while the energy difference with the central dot is large. (a)- The couplings between the dots are symmetric. A central peak is observed when all the dots are on resonance. (b)- The couplings are asymmetric. This fact produces a molecular behavior between the dots that are more strongly coupled, showing an anticrossing shape in the resonance of the three dots.

parameters of the ac-field, which gives a clear dependence of the probability of the transition on the amplitude of the driving. The ac driving is an easy external control of the system by just changing its parameters.

Long-range interactions have already been studied and introduced in a previous work of the candidate (see Chapter 3) for quantum dot systems. They are transitions between states that are non-directly coupled, despite the intermediate energy regions are energetically forbidden, these central regions are just virtually occupied. It is shown in this paper that such transitions can be induced and controlled with a time dependent driving.

The objective of this paper is to study the photon assisted transition between discrete energy levels that are non-directly coupled. This work also provides the theoretical base for forthcoming works, which treat different aspects of long-range transport.

4.2 Model and set up

In this work, a linear TQD is considered as the minimal chain where long-range transitions can be defined. The strong Coulomb blockade regime is assumed, where each quantum dot has a single available energy level with up to one electron in the whole TQD system. The left dot is coupled to a fast oscillating field, while living static the rest of the dots. The linear triple quantum

dot is weakly coupled in its ends to two electronic reservoirs with a sufficient large bias. The Born-Markov-Secular approximation is then considered to calculate the transport between the triple quantum dot and the reservoirs.

With the master equation, transport is studied analytically and numerically between the two reservoirs at the region of the stability diagram where all the TQD energy states coincide $\epsilon_{|1,0,0\rangle} = \epsilon_{|0,1,0\rangle} = \epsilon_{|0,0,1\rangle}$ and the empty state is within the bias region, i.e., a quadruple point. The regions where just two states of the TQD coincide (triple points) are also studied. Driven and undriven simulation are compared in order to understand the effects of the ac-driving. In the undriven measurement, high current intensity is observed at the quadruple point, a exponential decay in transport at the region where the outer states are tunned off resonance, and long-range transport where the outer states are in resonance while the central one is off resonance. The long-range transport persists for high energy difference with the central site. For the driven simulation, the same behavior observed in the undriven case is reproduced with a renormalized tunneling at each energy difference $n\hbar\omega$ between the states. The additional resonant transport paths produced by the absorption or emission of photons are named sidebands. Replicas of the quadruple points appear at each crossing of two sidebands. Some of them have the appearance of an anticrossing. This happens when the tunneling coupling between the on-site energies is asymmetric (see Fig . 4.1); which is the case, since the hopping parameters have distinct renormalization values. This renormalization effect of the drivings can be observed at the quadruple point of the undriven measurement: while the undriven signal presents a crossing-like signal, the corresponding driven configuration is an anticrossing.

Once the driven and undriven case is analyzed the work focuses in the driven long-range state. The central site is taken far away in energy and the transport simulation is calculated using the effective Hamiltonian. The effective model considers the second order processes dominate over the first order. By tunning the parameters of the system, the LZS long-range interference pattern (see Sec. 1.1.3) is obtained between the two ends of the chain. In order to get a time independent analytical solution of the transport through the driven TQD the rotating wave approximation is applied in the effective Hamiltonian for each specific resonance between the outer states:

$$\mathrm{I}^{(n)}_{\mathrm{RWA}} = e\frac{g_{\mathrm{LR},n}\Gamma_{\mathrm{L}}\Gamma_{\mathrm{R}}}{g_{\mathrm{LR},n}(2\Gamma_{\mathrm{L}}+\Gamma_{\mathrm{R}})+\Gamma_{\mathrm{L}}\left[\Gamma_{\mathrm{R}}^2+4(\Delta-n\hbar\omega)^2\right]} \tag{4.1}$$

This analytical result is the charge current between the leads through a long-range PAT in the n sideband. $g_{\mathrm{LR},n} = \tau_{\mathrm{LC}}\tau_{\mathrm{CR}}B_n(\mathrm{V}/\omega)/(\epsilon_{\mathrm{L}}-\epsilon_{\mathrm{C}}+n\hbar\omega)$ is the renormalized cotunnel couplings for the sideband n and Δ is the on-site energy difference between distant coupled states. The information of the energy difference with the virtual (intermediate) state is implicit in the renormalized cotunnel coupling g. In the article, the transport simulated with the Master equation is compared with the general Hamiltonian, the effective Hamiltonian, and the one with the rotating wave approximation. They show a perfect agreement for their validity range.

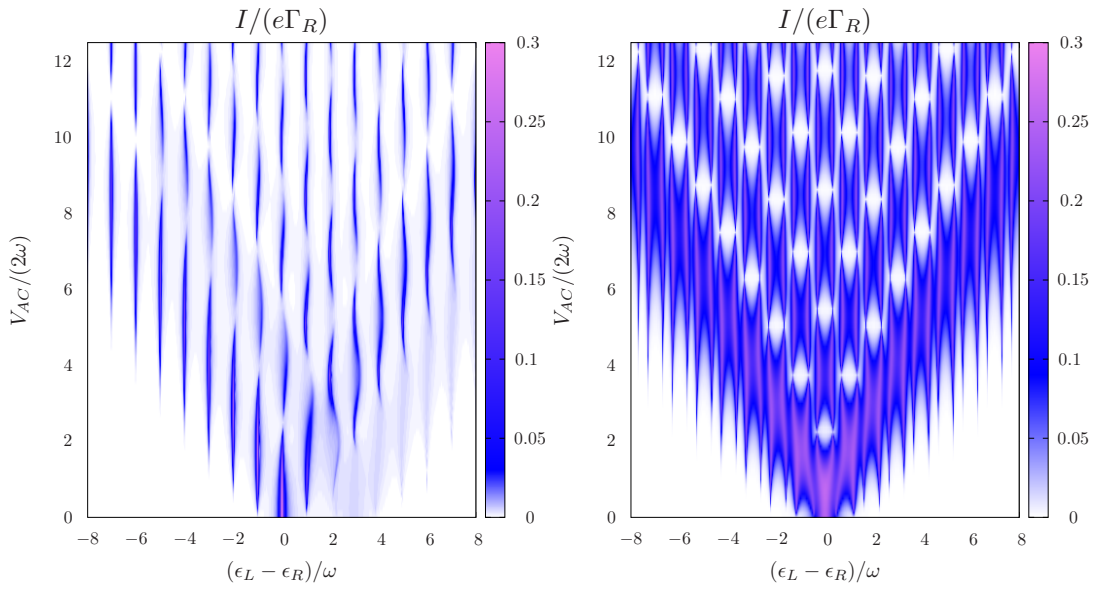

Figure 4.2: Charge transport between reservoirs in the infinite bias limit through the TQD vs. the amplitude of the ac-field and the energy differences between the outer dots. The left dot of the TQD is coupled to an ac-field. The LZS pattern shows the participation of the three states within the TQD system. *Left:* Central dot in resonance with the left dot for $\epsilon_L - \epsilon_R = 3\hbar\omega = \epsilon_C$. *Right:* Full triple quantum dot resonance at $\epsilon_L - \epsilon_R = 0 = \epsilon_C$. In both cases $\tau = 1$, $\hbar\omega = 3.3\tau$ and $\epsilon_R = 0$.

4.3 Resonant Landau-Zener-Stückelberg (LZS) pattern

In the previous sections and in the article presented in this chapter the LZS interference pattern is only studied for the LR transition, where the charge goes virtually through the central site. In this section the central site is considered in resonance of $m\hbar\omega$ with the driven left dot.

The coupling between the central and right dot is not driven by any ac-field; thus, to get a significant direct coupling between them, they have to be at an energy difference comparable to the coupling between them: $|\epsilon_C - \epsilon_R| \lessapprox |\tau|$. In Fig. 4.2 the LZS pattern is plotted for different energy configurations of the central and right dots while tunning the energy of the left dot: In the left figure, the center and right dots are out of resonance and in the right figure, they are on resonance. In the left figure, a main interference pattern of the charge transport is observed centered at $\epsilon_L - \epsilon_R = 0$ which is going through the driven LR transition, and a second interference pattern when the central site is in resonance with the left quantum dot. However, the effect of this second pattern on the main one is not very strong, because, as explained before, the coupling between the central and the right dots is really weak for this energy configuration, very much reducing the charge transport through this channel. In the right figure, the central site is always on resonance with the right quantum dot, forming two molecular states separated an energy 2τ (see Eq. (1.3)). Each molecular state is coupled through the renormalized couplings to the sidebands of the left quantum dot. Therefore, the system is an effective double quantum dot with a driving in the left dot and two states separated an energy 2τ in the right quantum dot. This is

the reason why in the LZS picture all the resonances are splitted in two.
In summary, with a single driving in the left part of the TQD, the LR LZS pattern is only strongly modified for a resonance between the right and the central dots. Any other configuration with the left and central dot in driven resonant transition, but not in resonant with the right dot, will just make the charge oscillate between the left and central dots, modifying slightly the LR LZS pattern.

4.4 Conclusions

In summary, photon assisted long range transport is analyzed through a linearly coupled triple quantum dot. The transport between the edge quantum dots is assisted by the ac field and gives rise to resonances between the left and right quantum dot energy levels differing in n photons. The ac driving also renormalizes the interdot hopping and hence the level hybridization. Therefore, the ac field determines the current spectrum and allows its control by tuning the ac field parameters. We present as well a theoretical model of photon assisted second order transitions (cotunnel) and propose an effective Hamiltonian. We have considered the simplest model with up to one electron. The analysis of other regions in the stability diagram with more electrons will be affected by charge and spin correlations.

Nowadays the microwaves used for the photo assisted transport have shown benefits over the usual gate control, that additionally with the long-range transport can act non-locally over the different states of the system. The study of photo assisted long-range transport has been extended to an energy level distribution where the energy detuning with the central is partially reduced by the absorption of n-photons from the field. Therefore, the charge transfer maintain the virtual trajectory through the central site, but now it is faster since the detuning with the central level is reduced. This configuration offers an efficient and non-local manipulation of spin qubits [159]. This study may have some corrections due to the charge occupation on the central states if they are tunned close to a sideband of the long-range transport. The occupation of the virtual state is considered in an article of the same author, which is presented in Chapter 5 of the thesis [161].

Photon assisted long-range tunneling

Fernando Gallego-Marcos, Rafael Sánchez, and Gloria Platero
Instituto de Ciencia de Materiales, CSIC, Cantoblanco, 28049 Madrid, Spain

(Received 9 August 2014; accepted 9 October 2014; published online 16 March 2015)

We analyze long-range transport through an ac driven triple quantum dot with a single electron. Resonant transitions between separated and detuned dots are mediated by the exchange of n photons with the time-dependent field. An effective model is proposed in terms of second order (cotunneling) processes which dominate the long-range transport between the edge quantum dots. The ac field renormalizes the inter dot hopping, modifying the level hybridization. It results in a non-trivial behavior of the current with the frequency and amplitude of the external ac field. © *2015 AIP Publishing LLC*. [http://dx.doi.org/10.1063/1.4913834]

I. INTRODUCTION

Quantum transitions between two coupled systems with discrete levels occur when the two levels have the same energy. This is naturally the case in molecules and solids where coherent oscillations are induced. In quantum dots, these oscillations can be manipulated by the tuning of both level energies and tunnel couplings with gate voltages.[1] In a double quantum dot, an electron is delocalized between the two dots giving rise to molecular-like orbitals. When the levels are not resonant, transitions can still be induced by the interaction with time dependent fields. The required energy is provided by the absorption or emission of photons with the appropriate frequency, as sketched in Fig. 1(b). In transport, this effect is known as photon-assisted tunneling[2,3] and is accomplished by applying time dependent gate voltages. Remarkably, it allowed for the demonstration of coherent tunneling in semiconductor double quantum dots.[4] Photon assisted transport in nanostructures has been the objective of intense research.[2] We mention only those references close to this work considering double barriers[5–10] and quantum dots.[4,11–23] An additional and important effect of photon assisted tunneling is the renormalization of the tunnel couplings which become dependent on the parameters of the driving. This way, a fine tuning of the different couplings, and therefore the control of the hybridized superpositions, is possible by simply acting on the amplitude of the oscillations.

Tunneling between distant states that are not directly coupled (e.g., like next to nearest neighbours in a chain) is also possible even if transitions into the intermediate sites are energetically forbidden. The delocalization in that case is due to higher order transitions[24] when the initial and final states are resonant, with the virtual only occupation of the intermediates, cf. Fig. 1(c). Such a long-range charge transfer is relevant for chemical reactions[25] and has analogues in quantum optics.[24] The recent advances in the tunability of triple quantum dots (TQDs)[26–32] has remarkably achieved the observation of this effect.[33–35] It entails the transfer of charge or spin between the two ends of the triple dot via superpositions that do not include the central one,[36] opening the way to the transfer of quantum information between distant qubits with low decoherence. In transport through quantum dots, long-range coupling has found interest for the prediction of the interference of spin-dependent trajectories,[36] the generation of entangled currents,[37] or the influence of dephasing.[38] It is also involved in the occurrence of dark states.[39–43]

In this paper, we investigate transport via the long-range coupling of the outmost sites of a serial triple quantum dot mediated by the interaction with a time dependent potential. This configuration allows for the characterization of single-electron virtual transitions involving discrete levels only. Note the difference with cotunneling events where electrons are transferred from or into a continuum.[8,9,44] In particular, we consider a configuration where the time dependent signal is applied to one extreme of the array (say the left dot) with the opposite one staying static, cf. Fig. 1(e). We discuss how, surprisingly, an electron in the right dot being static and energetically detuned is coupled resonantly with the left dot via a non-local interaction with the driving. Furthermore, the renormalization of the hopping implies the control of the hybridization which leads to a splitting of the transport resonance. As a consequence of the driving, Stückelberg interference patterns arise for the multiphotonic long-range excitations.[34] As triple dots constitute a tunable three level

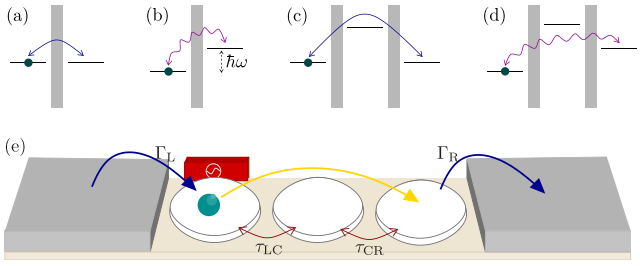

FIG. 1. (a)-(d) Different tunneling processes: (a) Resonant Rabi oscillations, (b) photon assisted tunneling, (c) long-range tunneling, (d) photon assisted long-range tunneling. (e) Scheme of a TQD coupled in series to a source and drain. We consider high bias between the reservoirs such that charge transport is unidirectional from left to right. A time dependent voltage is applied to the left quantum dot only. Long-range tunneling transitions will be induced by the interaction with the ac signal enabling resonant transport in strongly detuned configurations.

CHAPTER 5

COUPLED LANDAU-ZENER-STÜCKELBERG QUANTUM DOT INTERFEROMETERS

Fernando Gallego-Marcos, Rafael Sánchez & Gloria Platero
Phys. Rev. B **93**, 075424 (2016)

All the authors authorize Fernando Gallego Marcos to include this work in his dissertation.

5.1 Objectives

In Chapter 3 interference effects of two LR paths defined by electron-electron correlations are discussed in a linear TQD. In Chapter 4 the left dot is coupled to an ac gate. Then, the transitions between the left and central dot were driven by the ac-gate. However, since the energy difference between them was much higher than the coupling and than the amplitude of the field: $|\epsilon_L - \epsilon_C| \gg \{|\tau_{LC}|, V\}$, and it was not in resonance with an integer number of photons, the occupation on the central site was negligible. Even if the ac field drove resonant transitions between the left and center dots, they would not contribute to transport as the center-right tunneling is not affected by the driving. Therefore, just the second order process to the other end was relevant in transport, obtaining a driving LR tunnel coupling. The driving generates sidebands by the absorption and emission of photons from the driving field. If the amplitude is increased, the PAT between the left and central site will become more probable and the central site will began to get populated. However, as said before, this transition will not contribute to the charge current between the reservoirs, since there is no PAT between the central-right transition.

Therefore, the transport between the contacts will be again exclusively contained in the LR driven transition.

The idea of this work is to couple another ac field to the right dot in order to permit the PAT between the central and right quantum dot, opening a new path to the reservoir. The two outer dots are driven by ac gates. The two drivings generate a driving LR transition and a driving direct transition through the central site. The interference for a single electron going through the two driven paths is studied.

With the extra ac-field the transitions become more complex. The LR driven transition takes place between all the combinations of the left and right sidebands, while there is an additional driven direct transition with the central site through a single sideband. This introduces an additional channel for transport, parallel to the long-range PAT. In this work the interplay between long-range and direct photon-assisted transport is investigated in a triple quantum dot chain. The phase different between the two ac fields considered in a triple quantum dot becomes another important parameter. In the work presented in this article, the phase difference between the two ac voltage is proposed as an external parameter, which can be easily tuned to manipulate the current characteristics.

5.2 Model and set up

The set-up is a linear triple quantum dot (TQD) system with two ac-fields coupled to each end of the chain. They have same frequency and same amplitude and they differ by a phase difference ϕ. The system is assumed to be in the Coulomb blockade regime, where only one electron is allowed in the TQD at a time. For $\phi \neq 0$, the ac-field performs direct energy anti-crossings between the on-site states L-C and C-R and a long-range anti-crossing between L-R. This set up is a two parallel Landau-Zener-Stückelberh interferometer between the two ends of the chain: one interferometer comes from the L-C and C-R transition, which is called the direct transition, and the other is the LR transition at the L-R anti-crossing. The ends of the TQD system are weakly coupled to two reservoirs in the large bias limit, i.e., unidirectional transport. Therefore, for the study of the transport is used the Born-Markov-Secular Master Equation.
Differently from previous works in this set-up the occupation of the central energy level is not neglected, it is considered as another transport path between the reservoirs. For the simplify model all the energy levels are in photo assisted resonance with an integer number of photons: $\Delta E_{LC} = m\hbar\omega$, $\Delta E_{LR} = n\hbar\omega$, $\Delta E_{LR} = (n+m)\hbar\omega$. The amplitude of the ac-field assures that all the PAT between the three states contribute to the dynamics in the same level, i.e., the amplitude is larger than the energy differences of the states within the TQD. For $n \neq m$, the corresponding sidebands for the direct and long-range transition are different and thus the transport channels can be separated. To study the dynamics in detail, approximations are done. The different transitions are described by different orders in the tunneling expansion. The first order terms

contain the L-C and C-R direct transitions. LR transitions are only contained by the second order expansion. The effective Hamiltonian contains the two transitions, coupling all the three states directly. The Hamiltonian is then similar to an undriven triangular triple quantum dot whose tunneling couplings depend on the parameters of the driving. For $\phi = \pi$, the renormalized tunnel couplings are not complex, and the same dark states which are only present between the different paths of undriven triangular structures are obtained.
At the special case of $\phi = 0$ the ac-drivings oscillate on phase; thus, there is no LR PAT between the L-R states. The tunneling between the outer dots is effectively undriven, so resonant LR tunneling only occurs at $n = 0$. At $n = 0$ and $\phi = 0$ the TQD is fully symmetric and for sufficient large bias the system is equivalent to a TQD with undriven outer dots and a single ac driving in the central region. Using this equivalence, an effective Hamiltonian is obtained, where the transition between the outer dots goes through the multiple sidebands of the central site. These multiple transitions interfere destructively at some values the amplitude, generating a blockade of the current. The values of the destructive interference is compared with an analytical result, showing a perfect agreement.

5.3 Conclusions

In summary, quantum interferences that depend in a nontrivial way on the phase difference of the locally applied drivings are predicted. For gate voltages in phase opposition, destructive interferences are found between direct and long-range transitions which are analogous to dark states in closed-loop undriven triple dot molecules. As the edge dot levels oscillate in phase, quantum paths mediated by positive and negative detuned sidebands interfere, leading to multiple dark states in the Landau-Zener-Stückelberg pattern. These destructive interferences can be experimentally detected as they are of the same nature as long-range current resonances which have been unambiguously observed. A transport configuration is proposed, where all parameters are experimentally controllable, in which these features can be measured as cancellations of the current. This is particularly accessible in quantum dot arrays which are within experimental reach [103, 162, 163] for electric drivings. The results can be extended to electron transfer through larger chains, with important implications in quantum information architectures.

PHYSICAL REVIEW B **93**, 075424 (2016)

Coupled Landau-Zener-Stückelberg quantum dot interferometers

Fernando Gallego-Marcos,[1,2] Rafael Sánchez,[1,3] and Gloria Platero[1]
[1]*Instituto de Ciencia de Materiales de Madrid, CSIC, Cantoblanco, 28049 Madrid, Spain*
[2]*Institut für Festkörperphysik, Leibniz Universität Hannover, Appelstrasse 2, 30167 Hannover, Germany*
[3]*Instituto Gregorio Millán, Universidad Carlos III de Madrid, 28911 Leganés, Madrid, Spain*
(Received 20 August 2015; revised manuscript received 25 January 2016; published 16 February 2016)

We investigate the interplay between long-range and direct photon-assisted transport in a triple quantum dot chain where local ac voltages are applied to the outer dots. We propose the phase difference between the two ac voltages as an external parameter, which can be easily tuned to manipulate the current characteristics. For gate voltages in phase opposition we find quantum destructive interferences analogous to the interferences in closed-loop undriven triple dots. As the voltages oscillate in phase, interferences between multiple paths give rise to dark states. Those totally cancel the current, and could be experimentally resolved.

DOI: 10.1103/PhysRevB.93.075424

I. INTRODUCTION

A system that is driven nonadiabatically through the avoided crossing of two states undergoes a transition [1–4]. The probability of the transition depends on the parameters of the driving and the splitting at the crossing. The latest is given by the coupling between the diabatic states. Repeating the passing through the crossing introduces different paths to end in a given state, which gives rise to constructive interference. The control of this mechanism in solid state qubits has become a standard tool in the manipulation of quantum states [5–7], the generation of entanglement [8], or the measurement of the qubit coherence time scales [9].

In periodically driven quantum dot systems, this effect is measured as photon-assisted tunneling resonances [10]. An electron is hence delocalized between tunnel coupled quantum dots when the detuning of their energy levels is a multiple of the driving frequency $n\hbar\omega$ [11]. The tunnel coupling is renormalized by the ac field by a factor which depends on the amplitude and frequency of the driving [12,13]. Recently, striking electron spin resonance measurements in quantum dot systems [14] have been interpreted in terms of multilevel crossings [15]. Three-level crossings may also lead to peculiar phenomena, such as dark resonances [16,17].

Triple quantum dots (TQDs) are ideal systems for the investigation of such processes. On one hand, the spatial separation of three states [18,19], one in each dot (L, C, and R), makes it possible to manipulate them individually by means of gate voltages [20]. Hence, different drivings can be applied to the different levels by applying localized time-dependent gate voltages to each quantum dot [21]. Thus, not only do the amplitude and frequency of the driving [10,22], but also the phase differences [23] become important.

On the other hand, the tunnel coupling between all three states can be tuned, also between those that are not directly coupled. Indeed, long-range transport between the edge dots of a linear TQD has been very recently detected [24–26]. During these higher-order (cotunneling) transitions, the center dot is only virtually occupied. Hence they involve the direct transfer of a charge or a spin qubit between distant sites, avoiding decoherence and relaxation in the intermediate region [27].

By applying sinusoidal signals to the outer dot gates, the system can be driven through anticrossings among the three states, performing Landau-Zener transitions: L-C, C-R, and L-R [cf. Fig. 1(b)]. Note that the long-range L-R transition is parallel to the direct-tunneling L-C, C-R trajectory. The system then behaves as a combination of coupled interferometers. The interference patterns, coming from real or virtual paths,

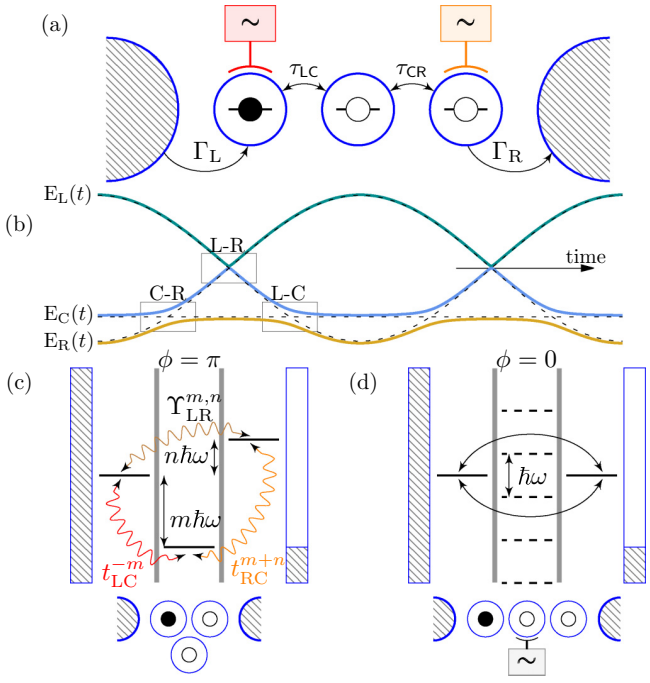

FIG. 1. (a) TQD in series connected to leads. Two ac voltages are applied to the outer dots, with a phase difference ϕ. (b) Time evolution of the energy levels for the left, center, and right dots for $\phi = \pi$, showing the different crossings mediated by direct (L-C and C-R) and virtual tunneling (L-R). (c) For $\phi = \pi$ the driving induces resonant transitions (either direct, t_{ik}^n, or virtual, $\Upsilon_{LR}^{m,n}$) between all the levels. The system can thus be mapped to an undriven triangular TQD depicted below. (d) The case where the edge dot levels oscillate in phase ($\phi = 0$) is equivalent to that where only the center dot is driven. Transport is then governed by sidebands in the center dot.

CHAPTER 6

COHERENT LONG-RANGE THERMOELECTRICS IN NONADIABATIC DRIVEN QUANTUM SYSTEMS

Fernando Gallego-Marcos & Gloria Platero
arXiv. Accepted in Phys. Rev. B.

All the authors authorize Fernando Gallego Marcos to include this work in his dissertation.

6.1 Objectives

Nowadays the size of the thermal and electrical devices are reducing to the nanoscale, consequently their properties have to be treated quantum mechanically. Recently, nanoscale structures started to receive attention for their applications as thermoelectric devices [125, 164–170]. Experiments already permit to study in such systems quantized heat transport [171] and manipulate heat currents using external fields [172, 173]. Quantum dots are an ideal playground for testing these devices since the control by external gates and external fields of their energy level structure, tuneability and in general, their coherent properties has high versatility and stability. Most of the studies of driven-thermoelectric transport in triple quantum dots have been done using adiabatic low frequency time dependent fields. In these studies with low frequency, work is done against an external force, in general, pumping particles against the chemical potential bias .
The objective is to implement and study a thermo-electric device in a triple quantum dot strongly driven by an electric field, that transfers energy through a long-range state between the two ends of the chain. One of the main goals is to define driven long-range heat and cooling engines. The

application of external electric field to quantum thermal devices has mostly addressed the low frequency driving (adiabatic regime) [174–179]. This work is using all the techniques used in previous works of the candidate.

6.2 Model and set up

The system is a linear triple quantum dot, where the left dot is interacting with an ac-gate with whom it only exchanges energy; charge is not exchanged with it. Strong Coulomb interaction is assumed, so up to one electron is allowed in the system. In the manuscript a detailed study of the energy dynamics within the closed TQD (decoupled from the reservoirs) coupled to the ac-field is done. The mechanism of how the ac-field introduces energy to the TQD and in which manner this energy is stored within the system is explained. Within the cotunnel regime is proposed a long-range energy transfer from the ac-field to the other end of the chain. The oscillations of the ac-field are considered much faster than the internal Rabi oscillations between the different states in the triple quantum dot. For this reason the values of the variables are generally averaged for each oscillation of the field.

In the open system the time dependence of the TQD Hamiltonian is treated with Floquet theory, in order to solve the evolution operator as a matrix diagonalization. Differently to the rotating wave approximation that only considers a single sideband, this method includes in the Hamiltonian all the sidebands which have a significant occupation. The reservoirs are coupled to the outermost dots and are modeled as an ideal Fermi bath. The coupling between the TQD and reservoirs is considered weak in comparison with their internal relaxation time. Hence, the reservoirs thermalize much faster than the interval of two transport events between the quantum dots and the reservoirs. Therefore, the Born-Markov Master equation is used for the calculation of the density matrix elements of the triple quantum dot system. With this theory a Floquet Master equation is obtained which allows one to calculate heat and charge transport under the effect of the ac-field. Notice that the secular approximation is not done since the energy level oscillation plays an important role in the energy and heat transport for small or zero bias voltage between the reservoirs (see Sec. 1.4.4).

The case where the two reservoirs are at the same temperature is considered. This emphasizes the role of the ac driving as the source of nonequilibrium. Three different energy currents are relevant two from the reservoirs and one from the ac-gate, that flow through the TQD for different values of the chemical potential bias between the reservoirs. The ac-field induces at zero bias an energy current through the TQD to the reservoirs without particle exchange.

Finally, for both temperature and chemical potential bias, heat and cooling engines are defined. Their efficiencies are calculated for all the time evolution towards the steady-state and are limited by a modified Carnot efficiency which takes into account the ac-field.

6.3 Conclusions

Direct energy and heat transfer between outer dots without visiting (but virtually) the central site in a locally ac-driven TQD is predicted. In this way, energy dissipation in the intermediate region is avoided. Furthermore we show how to efficiently store the energy the TQD gained from the ac-gate in the right dot. As the system is attached to contacts the LR energy transport coming from three energy sources is investigated: the two contacts attached to the TQD and the ac-gate. We propose long-range quantum heat and cooling engines, driven by high frequency, where additional tunneling channels, side bands, allow the energy and heat transfer. Those engines operate without intermediate region energy losses.
Our results open a new way to transfer efficiently energy and heat minimizing losses in the intermediate region. This work is easily extensible to longer array of quantum dots, which are within experimental reach [158, 180, 181].

Coherent Long-Range Thermoelectrics in Nonadiabatic Driven Quantum Systems

F. Gallego-Marcos* and G. Platero
Instituto de Ciencia de Materiales, CSIC, Cantoblanco, 28049 Madrid, Spain
(Dated: November 26, 2016)

We investigate direct energy and heat transfer between two distant sites of a triple quantum dot connected to reservoirs, where one of the edge dots is driven by an ac-gate voltage. We theoretically propose how to implement heat and cooling engines mediated by long range photoassisted transport. Additionally we propose a simple set up to heat up coherently the two reservoirs symmetrically and a mechanism to store energy in the closed system. The present proposals can be experimentally implemented and easily controlled by tunning the external parameters.

Quantum thermoelectric transport in nanoscale devices has gained importance due to the needs of current technology[1]. Quantum dots (QDs) have shown to be perfect platforms to study quantum thermoelectric properties which allow to design thermoelectric engines[2–8], refrigerators[9,10] and heat rectifiers[11,12]. AC driven thermoelectric transport has been investigated recently but mainly in the adiabatic regime[13–18].
Recently, experimental evidence shows direct charge transfer between edges in arrays of QDs by means of quantum superpositions[19–21]. Long range (LR) quantum transitions mediate different physical processes which are essential in many fields: in solid state were introduced to explain transport and order in magnetic compounds[22,23], Kondo physics[24,25] or spin qubit transfer in arrays of quantum dots[20] and recently in resonant valence bonds models[26] for the analysis of topological phases in triangular lattices[27]; they are present in donor-acceptor reactions through bridge states[28,29] relevant for molecules[30] or DNA[31,32]. LR photoassisted charge transfer in triple quantum dots (TQDs) has also been investigated[19–21,33]
One open question which has not yet been addressed is if LR energy and heat transfer could be achieved in quantum dot arrays, which are quantum simulators of real atoms and molecules.
In this work we present a detailed analysis of coherent LR energy and heat transfer in a TQD[34,35] driven by a fast oscillating field, where we observe genuine properties of thermoelectric transport which are attributed to coherent effects. A nonadiabatic driving with frequency ω induces photon assisted transitions (PAT) between non resonant states detuned by $n\hbar\omega$[21,36–39]. We propose the PAT between LR states detuned $n\hbar\omega$ as the quantum paths to transfer coherently a controlled amount of energy between them, with only the virtual participation of the intermediate region. A mechanism to store energy in one of the quantum dots is also proposed. Furthermore, when the outer dots are coupled to leads, we propose that these systems could work as heat and cooling engines whose transfer mechanism is based in photo-assisted quantum superpositions between the edges. Then, a cooling engine, that we term LR cooling engine, works transferring heat directly from the cold lead attached to the left dot to the hot lead attached to the right dot. A LR heat engine transfers charge directly from the source to the drain dot against chemical potential bias. We demonstrate as well a way to symmetrically transfer energy to both leads at zero bias voltage.

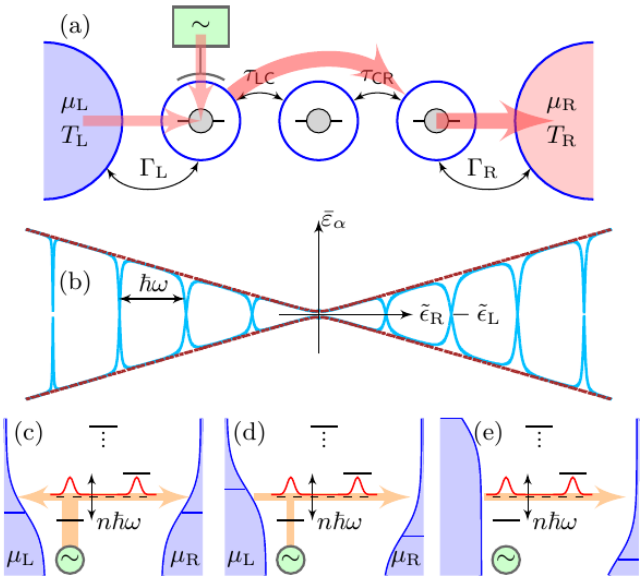

FIG. 1. (a)- A linear TQD where the left dot is driven with an ac voltage. The thick arrows show long-range energy transfer. The energy coming from the ac voltage and dc source is transfered directly to the right dot and then to the right contact. (b)- Average value of the eigenenergies (see Eq. (C4)) vs. detuning (Δ) between $|L\rangle$ and $|R\rangle$ states. For zero ac driving (red dashed lines) there is a single anticrossing of the left and right levels while for finite driving (solid blue lines) there are anticrossings at $\Delta = n\hbar\omega$ coming from the absorption or emission of n-photons. These anticrossings are responsible of long-range energy transfer. (c,d,e)- Average energy current direction in one period of the ac-field (orange arrows) for zero (c), finite (d) and infinite (e) bias voltage.

I. DRIVEN TRIPLE QUANTUM DOT

For simplicity we consider up to one electron in the TQD system; hence, the Hamiltonian reads: $H_{TQD} = \sum_{i=\{L,C,R\}} \epsilon_i \hat{c}_i^\dagger \hat{c}_i + \tau_{LC}\hat{c}_L^\dagger \hat{c}_C + \tau_{CR}\hat{c}_C^\dagger \hat{c}_R + h.c.$, which is written in the on-site orthonormal basis: $|L\rangle \equiv |1,0,0\rangle$, $|C\rangle \equiv |0,1,0\rangle$, $|R\rangle \equiv |0,0,1\rangle$. $\hat{c}_i$ is the fermionic destruc-

CHAPTER 7

CHANNEL BLOCKADE IN A TWO-PATH TRIPLE-QUANTUM-DOT SYSTEM

Monika Kotzian, Fernando Gallego-Marcos, Gloria Platero & Rolf J. Haug
Phys. Rev. B **94**, 035442 (2016)

All the authors authorize Fernando Gallego Marcos to include this work in his dissertation.

7.1 Objectives

Double quantum dots are widely studied theoretically and experimentally, they are motivated by their use in quantum computing, since one can define and manipulate within the DQD a charge or spin qubit [11]. With an additional dot, triple quantum dots are the smallest qubit chain, where the dynamics and coherences between two qubits are the goals of their study. There are a lot of theoretical predictions for triple quantum dots, such as destructive interferences for linear [182] and triangular configurations [86, 89, 90, 153], long-range coherent transport [101–103, 182] and several applications in quantum information processing as exchange-controlled spin qubits [37, 72, 102] or as a current rectifier [78, 79]. Experiments have recently overcome the difficulties for their fabrication, some of the first experiments are [68, 69, 79]. The understanding of all the effects in the experiments is not totally clear since the coherences and dynamics are much more complex that in double quantum dots and, as they are bigger structures, they are much more affected by the interaction and decoherence from the environment.
There are several studies of the the interaction between two paths and how the charge occupation

in one of the paths blocks the transport through the other. This process is known as dynamical channel blockade [183–187]. The origin of this effect comes from multilevel (multichannel) quantum dots, where one of them blocks or reduces the transport through the system [185]. It is also observed in systems with one channel but which are coupled capacitivally to another one that blocks the transport [188–190]. Also the spin play a mayor role leading to the spin blockade which is actually a type of dynamical blockade [191]. The detection of this effect has been proposed by its impact on the shot noise characteristics. Super-Poissonian noise observed in self-assembled double quantum dot samples [192] can be interpreted in terms of dynamical channel blockade [190].

The motivation of this work is to understand a two interacting double quantum dots which share one of the dots, forming a triple quantum dot. Triangular TQDs has a geometry that permits to define a two path transport formed by DQDs, the device has one source reservoir coupled to each path and a common drain reservoir. The study is focused in the Coulomb correlations between the charges flowing through the two transport channels which share one of the dots. In this dynamical process, the electron occupation probability of the shared dot from one path determines the conductance through the other path.

7.2 Model and set up

In this experimental and theoretical study the set up is a triangular shaped triple quantum dot with one gate attached to each dot, i.e., three terminals. The advantages of using multiple gates are that both double and triple quantum dot physics are measured in transport experiments. The tunnel coupling between the dots and their on-site energies controls the double or triple dot behavior. This device due to its versatility is very suitable for studying coherent dynamics for quantum information processing.

Two of the contacts are set as a source and the other one as a drain. The two dots coupled to the sources are only capacitively coupled, i.e., there are no direct charge transitions between them. Hence, one can define two transport paths from the sources to the drain going through two of the quantum dots present in the TQD. The electrons from the different paths compete for the occupation of the dot coupled to the drain, which is the one shared by both paths. In this device, multiple dark-states are theoretically predicted for specific conditions of the tunnel coupling between the dots and their on-site energies [77, 86, 89]; however, in the experiment these conditions are not fulfilled or the effect of the environment destroy them.

Particle transport conductance from both paths are measured simultaneously, making a distinction depending from which source the electrons are coming. Double dot physics are observed when the two dots present in the path are on resonance conditions. The characteristics of each dot as the capacitive couplings with the gates and other dots are then measured with a quantum point contact located in the proximity of the system. When the resonance of the two double quantum

dots coincide, the two paths interact, forming a triple quantum dot with quadruple points, i.e., four states of the two paths are coexisting in the same region of the stability diagram. This is the region of interest for the experiment.
To model this system, the three site Anderson Hamiltonian is used. Each quantum dot can have up to one electron, hence there are up to three electrons within the TQD. The values of the capacitive couplings with the gates are taken from the experimental measurements. The couplings between the dots are extracted from a fit to the experimental data. The couplings with the leads are considered weak, thus the Born-Markov-Secular approximation is applied. Two different lock-in frequencies are applied to each source terminal. This way the contribution of electrons coming from the two different reservoirs can be resolved. Hence, to be as close as possible to the experiments, in the model the electrons coming from different sources are labeled with different indices. With this model and using the density matrix theory, the stability region of each state and the conductance from the different paths are calculated.
The theory shows that the dynamical blockade between the different paths in the shared dot, depends on the ratio between the tunneling probabilities through the two paths. When the bias voltage is increased the path with higher tunneling probability raises the electron occupation in the shared dot, making that dot less accessible to electrons in the other path. Therefore, transport conductance through the other path decreases with increasing bias voltage. This is shown in the theory and the experiment as negative differential conductance for the blocked path.

7.3 Conclusions

In summary, channel blockade is experimentally demonstrated for the first time. This is done in electronic transport through a TQD system with two source leads, which leads to nonlinear transport characteristics in such a setup. Interchannel Coulomb interaction between electrons coming from the two sources gives rise to a blockade of transport through one path, when the other path has high conductance, and affects in this way the transport properties of the multiterminal device. This work provides a step towards a better understanding of transport properties in complex multidot systems.
This paper is formed at zero bias voltage configuration. The same setup is used afterwards to investigate finite bias transport, where the bias of each paths is tunned separately. In recent experiments the size of the quantum dots arrays defined in a two dimensional electron gas is extended to four and five dots [158, 180, 181]. The coherence of these devices are still being tested but are a promising set-up for quantum operations among several qubits in a more real scale getting closer to the realization of the quantum computer.

PHYSICAL REVIEW B **94**, 035442 (2016)

Channel blockade in a two-path triple-quantum-dot system

M. Kotzian,[1,*] F. Gallego-Marcos,[2,1] G. Platero,[2] and R. J. Haug[1]
[1]*Institut für Festkörperphysik, Leibniz Universität Hannover, Appelstrasse 2, 30167 Hannover, Germany*
[2]*Instituto de Ciencia de Materiales, CSIC, Cantoblanco, 28049 Madrid, Spain*
(Received 14 July 2015; revised manuscript received 10 June 2016; published 26 July 2016)

Electronic transport through a two-path triple-quantum-dot system with two source leads and one drain is studied and the interaction between the two paths is analyzed. We observe a channel blockade as a result of interchannel Coulombic interaction. The experimental results are understood with the help of a theoretical model which allows one to obtain the parameters of the system, the stability regions of each state, and the full dynamical transport in the triple-dot resonances.

DOI: 10.1103/PhysRevB.94.035442

Triple quantum dots (TQDs), which have been implemented only recently [1–4], offer the possibility of analyzing new fascinating properties which are not present in double-quantum-dot systems. These new properties, to name a few, include interference phenomena between different transport channels giving rise to dark states in triangular [5–8] and linear [9] dot distributions and long distant coherent states in TQDs [9–13]. TQDs are, as the smallest qubit chain, a step towards the more complex architectures needed in quantum computation. They allow for novel applications in the field of quantum information processing, for example, as exchange-controlled spin qubits [14,15] or as current rectifiers [1,16]. They provide as well the implementation of quantum cellular automata processes, a combination of charging and reconfiguration events in the system being a crucial process in quantum information [17,18]. Coherent electron transfer using adiabatic passage was proposed for TQDs in series [19]. Furthermore, decoherence due to charge fluctuations is reduced in a TQD-based coded qubit as it involves a decoherence-free subspace [15,20].

Our system is a triangular-shaped TQD with one lead attached to each dot and two of the dots only capacitively coupled [Fig. 1(a)]. A triangular geometry is suitable for studying entanglement and effects of interference which makes it an interesting device for quantum information processing. The flexibility of this setup makes it a convenient tool for investigating the transport properties of a TQD. In particular we study the interaction between two double dot paths within the TQD structure. Transport can be measured separately and simultaneously for the two double dot paths and be compared or combined to study the whole TQDs physics on the basis of the double dots.

In contrast to former published works [4] where one source and two drain leads were used, we now use one drain and two source leads. In this configuration of two-path transport the electrons from the different paths compete for the occupation of dot A, which is shared by both paths [Fig. 1(a)]. This competition gives rise to a current-blocking effect, produced by the interchannel Coulombic interaction. By applying different ac frequencies with a lock-in to the paths, the interaction between the paths becomes apparent in a more distinct manner.

*kotzian@nano.uni-hannover.de

We analyze the role of interactions between the charge flowing through the two different paths by transport measurements. We observe, as a consequence of interchannel Coulombic interaction, channel blockade in transport.

I. TQD SAMPLE AND CHARACTERIZATION

The measurements were performed on a lateral TQD made with local anodic oxidation by atomic force microscopy (AFM) on a GaAs/AlGaAs heterostructure [21–23]. A two-dimensional electron gas with an electron concentration of $n_e = 3.47 \times 10^{15}$ m^{-2} is located at 33 nm depth below the surface. The dots A,B,C are arranged in a triangular geometry [4] with each dot placed next to the other two and one lead attached to each dot [Fig. 1(a)]. Dots A and B and also A and C are tunnel coupled; dots B and C are only capacitively coupled. The source leads S_1 and S_2 are connected to dots B and C, respectively, and dot A is connected to the drain lead D. We have two transport paths: path 1 with dots A and B and path 2 with dots A and C. The sample has four in-plane gates $G_1 - G_4$ [Fig. 1(b)] to control the potential of the dots, interdot, and dot-lead couplings. A quantum point contact (QPC) sensitive to all three dots is placed next to dots B and C to perform charge measurements. The measurements were conducted in a dilution refrigerator. To measure the differential conductance of the two transport paths simultaneously but separately, a lock-in technique was used with ac voltages with two different frequencies $f_1 = 83.3$ Hz and $f_2 = 18.3$ Hz, with $U_{AC} = 10$ μV applied to S_1 and S_2, respectively. In addition, different dc voltages are applied to the source contacts. The QPC was operated by applying a dc voltage to the source of the QPC, S_{QPC}, and measuring a dc current at the drain of the QPC, D_{QPC}. The QPC is tuned by the gate G_{QPC}. In our transport measurement range the dots contain several tens of electrons on the whole. The charging energies are $E_{ch,A} = 2$ meV, $E_{ch,B} = 6$ meV, and $E_{ch,C} = 3$ meV for dots A, B, and C, respectively.

A. Charge measurements

To characterize the device, the charging is studied by using the QPC as a detector. The derivative of the QPC current is plotted as a function of gate voltages U_{G1} and U_{G3} (Fig. 2) with denoted charge configurations $|N_A, N_B, N_C\rangle$, where N_i are the occupations of dots A,B,C. The electrons in the core of the

APPENDIX A

MASTER EQUATION

In this appendix, the derivation of the Master Equation is obtained. The Hamiltonian for a system weakly coupled to reservoirs is:

$$\hat{H} = \hat{H}_S(t) \otimes \mathbb{1}_B + \mathbb{1}_S \otimes \hat{H}_B(t) + \hat{H}_{int}(t), \tag{A.1}$$

where $\hat{H}_B$ is the Hamiltonian for the baths and $\hat{H}_{int}$ is the interaction between the baths and the quantum dot system. The solution for the dynamics of (A.1) is:

$$\frac{\partial}{\partial t}\rho(t) = -i\left[\hat{H}(t), \rho(t)\right] \tag{A.2}$$

The Hamiltonian has so many degrees of freedom that in most of the cases it is not possible to solve it. Then, some approximations are needed. The approximations are based in the weak coupling regime with the reservoirs. To treat the interaction as a perturbation to the Hamiltonian, one goes to the interaction picture, this transformation constructs the solution of (A.2) as the solution for a free particle problem with some interaction. Defining $\hat{H} = \hat{H}_S \otimes \mathbb{1}_B + \mathbb{1}_S \otimes \hat{H}_B + \hat{H}_{int} \equiv \hat{H}_0 + \hat{H}_{int}$, the transformed Schrödinger equation reads:

$$e^{i\hat{H}_0 t}\left(\hat{H}_0 + \hat{H}_{int} - i\frac{\partial}{\partial t}\right)e^{-i\hat{H}_0 t}e^{i\hat{H}_0 t}|\Psi(t)\rangle = 0 \;\rightarrow\; \left(e^{i\hat{H}_0 t}\hat{H}_{int}e^{-i\hat{H}_0 t} - i\frac{\partial}{\partial t}\right)e^{i\hat{H}_0 t}|\Psi(t)\rangle = 0 \tag{A.3}$$

where:

$$\hat{H}_I(t) = e^{i\hat{H}_0 t}\hat{H}_{int}e^{-i\hat{H}_0 t},\ |\Psi_I(t)\rangle = e^{i\hat{H}_0 t}|\Psi(t)\rangle,\ \rho_I(t) = e^{i\hat{H}_0 t}\rho(t)e^{-i\hat{H}_0 t} \tag{A.4}$$

$$\dot{\rho}_I(t) = -i\left[\hat{H}_I, \rho_I(t)\right] \tag{A.5}$$

In the following the sub-index “I" will be deleted. $\hat{H}(t)$ acts over the system and the bath: $\hat{H}(t) = \sum_\alpha \hat{A}_\alpha(t) \otimes \hat{B}_\alpha(t)$. Without loss of generality is assumed the case of hermitian coupling

operators $\hat{A}_\alpha(t) = \hat{A}_\alpha^\dagger(t)$ and $\hat{B}_\alpha(t) = \hat{B}_\alpha^\dagger(t)$. Doing the Picard iteration and the *fundamental theorem of calculus*, the first term for (A.5) reads

$$\dot{\rho}(t) = -i\left[\hat{H}(t), \rho_0\right] - \int_0^t dt_1 \left[\hat{H}(t), \left[\hat{H}(t_1), \rho(t_1)\right]\right]. \tag{A.6}$$

This first order approximation (Born approximation) neglects the back action of the QD system to the bath, because $\hat{H}_B$ is so large that is not affected by the presence of the QD system. $\hat{H}_B$ is described as a thermal equilibrium distribution at constant temperature and chemical potential

$$\rho_B(t) = \bar{\rho}_B \propto \exp\left[-\hat{H}_B/k_B T\right] \quad \Rightarrow \quad \rho(t) = \rho_S(t) \otimes \bar{\rho}_B \tag{A.7}$$

To extract the information of $\hat{H}_B$ one performs a partial trace over the bath degrees of freedom

$$\dot{\rho}_S(t) = -i\mathrm{Tr}_B\left\{\left[\hat{H}(t), \rho_0\right]\right\} - \int_0^t \mathrm{Tr}_B\left\{dt_1\left[\hat{H}(t), \left[\hat{H}(t_1), \rho_S(t_1)\otimes\bar{\rho}_B\right]\right]\right\} \tag{A.8}$$

Using the mixed product property: $(A\otimes B)(C\otimes D) = AC\otimes BD$ one gets

$$\begin{aligned}
\dot{\rho}_S(t) =& -i\mathrm{Tr}_B\left\{\left[\sum_\alpha \hat{A}_\alpha(t)\otimes\hat{B}_\alpha(t), \rho_{S,0}\otimes\bar{\rho}_B\right]\right\} \\
&- \int_0^t \mathrm{Tr}_B\left\{dt_1\left[\sum_\alpha \hat{A}_\alpha(t)\otimes\hat{B}_\alpha(t), \left[\sum_\alpha \hat{A}_\alpha(t_1)\otimes\hat{B}_\alpha(t_1), \rho_S(t_1)\otimes\bar{\rho}_B\right]\right]\right\} \\
=& -i\sum_\alpha\left(\hat{A}_\alpha(t)\rho_{S,0}\otimes\mathrm{Tr}\left\{\hat{B}_\alpha(t)\bar{\rho}_B\right\} - \rho_{S,0}\hat{A}_\alpha(t)\otimes\mathrm{Tr}\left\{\bar{\rho}_B\hat{B}_\alpha(t)\right\}\right) \\
&- \sum_{\alpha\mu}\int_0^t \hat{A}_\mu(t)\hat{A}_\alpha(t_1)\rho_S(t_1)\otimes\mathrm{Tr}\left\{\hat{B}_\mu(t)\hat{B}_\alpha(t_1)\bar{\rho}_B\right\} - \hat{A}_\alpha(t_1)\rho_S(t_1)\hat{A}_\mu(t)\otimes\mathrm{Tr}\left\{\hat{B}_\alpha(t_1)\bar{\rho}_B\hat{B}_\mu(t)\right\} \\
&+ \sum_{\alpha\mu}\int_0^t \hat{A}_\mu(t)\rho_S(t_1)\hat{A}_\alpha(t_1)\otimes\mathrm{Tr}\left\{\hat{B}_\mu(t)\bar{\rho}_B\hat{B}_\alpha(t_1)\right\} - \rho_S(t_1)\hat{A}_\alpha(t_1)\hat{A}_\mu(t)\otimes\mathrm{Tr}\left\{\bar{\rho}_B\hat{B}_\alpha(t_1)\hat{B}_\mu(t)\right\}
\end{aligned} \tag{A.9}$$

To get rid of the first term in Eq. (A.9) is used the transformation $\hat{B}_\alpha \to \hat{B}_\alpha - g_\alpha\mathbb{1}$, $\hat{H}_S \to \hat{H}_S - \sum_\alpha \hat{A}_\alpha g_\alpha$, which leaves the total Hamiltonian invariant. Setting $g_\alpha = \mathrm{Tr}\left\{\hat{B}_\alpha\bar{\rho}_B\right\}$ the value of $\mathrm{Tr}\left\{(\hat{B}_\alpha - g_\alpha\mathbb{1})\bar{\rho}_B\right\} = 0$. Doing this transformation and using the cyclic property of the trace $\mathrm{Tr}\{ABC\} = \mathrm{Tr}\{BCA\} = \mathrm{Tr}\{CAB\}$, Eq. (A.9) reads:

$$\dot{\rho}_S(t) = -\sum_{\alpha\mu}\int_0^t \left[\hat{A}_\mu(t), \hat{A}_\alpha(t_1)\rho_S(t_1)\right]\otimes\mathrm{Tr}\left\{\hat{B}_\mu(t)\hat{B}_\alpha(t_1)\bar{\rho}_B\right\} + \left[\hat{A}_\mu(t), \rho_S(t_1)\hat{A}_\alpha(t_1)\right]\otimes\mathrm{Tr}\left\{\hat{B}_\alpha(t_1)\hat{B}_\mu(t)\bar{\rho}_B\right\} \tag{A.10}$$

$$\dot{\rho}_S(t) = -\sum_{\alpha\mu}\int_0^t \left\{C_{\mu\alpha}(t,t_1)\left[\hat{A}_\mu(t), \hat{A}_\alpha(t_1)\rho_S(t_1)\right] + C_{\alpha\mu}(t_1,t)\left[\rho_S(t_1)\hat{A}_\alpha(t_1), \hat{A}_\mu(t)\right]\right\}dt_1 \tag{A.11}$$

were $C_{\mu\alpha}(t,t_1)$ is the bath correlation function. As $[\hat{H}_B, \hat{B}_\alpha] = 0$, the correlation function only depends on the time difference,

$$\begin{aligned}
C_{\mu\alpha}(t,t_1) =& \mathrm{Tr}\left\{e^{i\hat{H}_B t}\hat{B}_\mu e^{-i\hat{H}_B t}e^{i\hat{H}_B t_1}\hat{B}_\alpha e^{-i\hat{H}_B t_1}\bar{\rho}_B\right\} \\
=& \mathrm{Tr}\left\{e^{i\hat{H}_B(t-t_1)}\hat{B}_\mu e^{-i\hat{H}_B(t-t_1)}\hat{B}_\alpha\bar{\rho}_B\right\} = \mathrm{Tr}\left\{\hat{B}_\mu(t-t_1)\hat{B}_\alpha\bar{\rho}_B\right\},
\end{aligned} \tag{A.12}$$

,i.e, $C_{\mu\alpha}(t,t_1) = C_{\mu\alpha}(t-t_1)$, and it has the symmetry relation $C_{\mu\alpha}(\tau) = C^*_{\alpha\mu}(-\tau)$. Assuming the bath correlation function decays rapidly and the density matrix varies much slower $|\lambda|^2 \ll k_B T$, where $|\lambda|^2$ is the coupling between the system and the bath. Hence, one can write $\rho_S(t_1)$ as $\rho_S(t)$ in Eq. (A.11)(first Markov approximation). Changing variables $t_1 \to t-\tau$:

$$\dot{\rho}_S(t) = \sum_{\alpha\mu} \int_0^t \left\{ C_{\mu\alpha}(\tau) \left[\hat{A}_\mu(t), \hat{A}_\alpha(t-\tau)\rho_S(t) \right] + C_{\alpha\mu}(-\tau) \left[\rho_S(t)\hat{A}_\alpha(t-\tau), \hat{A}_\mu(t) \right] \right\} d\tau \tag{A.13}$$

Using the same assumption, one can extend the integral limits to infinity (second Markov approximation):

$$\dot{\rho}_S(t) = \sum_{\alpha\mu} \int_0^\infty \left\{ C_{\mu\alpha}(\tau) \left[\hat{A}_\mu(t), \hat{A}_\alpha(t-\tau)\rho_S(t) \right] + C_{\alpha\mu}(-\tau) \left[\rho_S(t)\hat{A}_\alpha(t-\tau), \hat{A}_\mu(t) \right] \right\} d\tau \tag{A.14}$$

This is the Born-Markov equation, giving the so called Redfield Master Equation. With some algebra it is rewritten as

$$\dot{\rho}_S(t) = \sum_{\alpha\mu} \int_0^\infty \left\{ C_{\mu\alpha}(\tau) \left[\hat{A}_\mu(t), \hat{A}_\alpha(t-\tau)\rho_S(t) \right] + \text{h.c.} \right\} d\tau. \tag{A.15}$$

Now the operators are written with its time dependence explicitly. Writing Eq. (A.15) with the eigenvectors $\hat{H}_S |\psi_n\rangle = E_n |\psi_n\rangle$

$$\begin{aligned}
\dot{\rho}_S(t) = &\sum_{\alpha\mu} \sum_{a,b,c,d} \int_0^\infty \Big\{ \quad C_{\mu\alpha}(\tau) \left[|\psi_a\rangle\langle\psi_a|\hat{A}_\mu(t)|\psi_b\rangle\langle\psi_b|, |\psi_c\rangle\langle\psi_c|\hat{A}_\alpha(t-\tau)|\psi_d\rangle\langle\psi_d|\rho_S(t) \right] + \text{h.c.} \Big\} d\tau \\
= &\sum_{\alpha\mu} \sum_{a,b,c,d} \int_0^\infty \Big\{ \quad C_{\mu\alpha}(\tau) \Big[\langle\psi_a|\hat{A}_\mu(t)|\psi_b\rangle\langle\psi_c|\hat{A}_\alpha(t-\tau)|\psi_d\rangle |\psi_a\rangle\langle\psi_b||\psi_c\rangle\langle\psi_d|\rho_S(t) \\
&\qquad - \langle\psi_a|\hat{A}_\mu(t)|\psi_b\rangle\langle\psi_c|\hat{A}_\alpha(t-\tau)|\psi_d\rangle |\psi_c\rangle\langle\psi_d|\rho_S(t)|\psi_a\rangle\langle\psi_b| \Big| \text{h.c.} \Big\} d\tau \\
= &\sum_{\alpha\mu} \sum_{a,b,c,d} \int_0^\infty \Big\{ \quad C_{\mu\alpha}(\tau) \langle\psi_a|\hat{A}_\mu(t)|\psi_b\rangle\langle\psi_c|\hat{A}_\alpha(t-\tau)|\psi_d\rangle \\
&\qquad \times \Big[|\psi_a\rangle\langle\psi_b||\psi_c\rangle\langle\psi_d|\rho_S(t) - |\psi_c\rangle\langle\psi_d|\rho_S(t)|\psi_a\rangle\langle\psi_b| \Big] + \text{h.c.} \Big\} d\tau \\
= &\sum_{\alpha\mu} \sum_{a,b,c,d} \int_0^\infty \Big\{ \quad C_{\mu\alpha}(\tau) e^{i(E_d - E_c)\tau} e^{i(E_a - E_b + E_c - E_d)t} \langle\psi_a|\hat{A}_\mu|\psi_b\rangle\langle\psi_c|\hat{A}_\alpha|\psi_d\rangle \\
&\qquad \times \Big[|\psi_a\rangle\langle\psi_b||\psi_c\rangle\langle\psi_d|\rho_S(t) - |\psi_c\rangle\langle\psi_d|\rho_S(t)|\psi_a\rangle\langle\psi_b| \Big] + \text{h.c.} \Big\} d\tau
\end{aligned} \tag{A.16}$$

When the dynamics associated to the system-bath coupling is much slower than the QD system dynamics, i.e., $|\lambda|^2 \ll |\tau|$, where τ is the coupling between the different parts of the QD system, a secular approximation (long time average) is valid. It neglects all the oscillating terms. Without this approximation the Markovian equation (A.14) is the Redfield equation. After doing the secular approximation (A.16) reads:

$$\begin{aligned}
\dot{\rho}_S(t) = \sum_{\alpha\mu} \sum_{a,b,c,d} \quad &\Gamma_{\mu\alpha}(E_d - E_c)\delta_{E_a - E_b + E_c - E_d} \langle\psi_b|\hat{A}_\mu|\psi_a\rangle^* \langle\psi_c|\hat{A}_\alpha|\psi_d\rangle \\
&\times \Big[\left(|\psi_b\rangle\langle\psi_a|\right)^\dagger |\psi_c\rangle\langle\psi_d|\rho_S(t) - |\psi_c\rangle\langle\psi_d|\rho_S(t)\left(|\psi_b\rangle\langle\psi_a|\right)^\dagger \Big] + \text{h.c.}
\end{aligned} \tag{A.17}$$

with $\Gamma_{\mu\alpha}(\omega) = \int_0^\infty C_{\mu\alpha}(\tau) e^{i\omega\tau} d\tau$. Expanding Eq. (A.17) and doing the transformation$\{a \leftrightarrow d, b \leftrightarrow c, \alpha \leftrightarrow \beta\}$:

$$\begin{aligned}
\dot{\rho}_S(t) = \sum_{\alpha\mu} \sum_{a,b,c,d} & \Gamma_{\mu\alpha}(E_d - E_c)\delta_{E_a - E_b + E_c - E_d} \langle\psi_b|\hat{A}_\mu|\psi_a\rangle^* \langle\psi_c|\hat{A}_\alpha|\psi_d\rangle \\
& \times \left[\left(|\psi_b\rangle\langle\psi_a|\right)^\dagger |\psi_c\rangle\langle\psi_d|\rho_S(t) - |\psi_c\rangle\langle\psi_d|\rho_S(t)\left(|\psi_b\rangle\langle\psi_a|\right)^\dagger \right] \\
+ \sum_{\alpha\mu} \sum_{a,b,c,d} & \Gamma^*_{\mu\alpha}(E_d - E_c)\delta_{E_a - E_b + E_c - E_d} \langle\psi_b|\hat{A}_\mu|\psi_a\rangle\langle\psi_c|\hat{A}_\alpha|\psi_d\rangle^* \\
& \times \left[\rho_S(t)\left(|\psi_c\rangle\langle\psi_d|\right)^\dagger |\psi_b\rangle\langle\psi_a| - |\psi_b\rangle\langle\psi_a|\rho_S(t)\left(|\psi_c\rangle\langle\psi_d|\right)^\dagger \right] \qquad \text{(A.18)} \\
= -\sum_{\alpha\mu} \sum_{a,b,c,d} & \left[\Gamma_{\mu\alpha}(E_d - E_c) + \Gamma^*_{\alpha\mu}(E_d - E_c)\right]\delta_{E_a - E_b + E_c - E_d} \langle\psi_b|\hat{A}_\mu|\psi_a\rangle^* \langle\psi_c|\hat{A}_\alpha|\psi_d\rangle \\
& \times |\psi_c\rangle\langle\psi_d|\rho_S(t)\left(|\psi_b\rangle\langle\psi_a|\right)^\dagger \\
+ \sum_{\alpha\mu} \sum_{a,b,c,d} & \Gamma_{\mu\alpha}(E_d - E_c)\delta_{E_a - E_b + E_c - E_d} \langle\psi_b|\hat{A}_\mu|\psi_a\rangle^* \langle\psi_c|\hat{A}_\alpha|\psi_d\rangle \left(|\psi_b\rangle\langle\psi_a|\right)^\dagger |\psi_c\rangle\langle\psi_d|\rho_S(t) \\
+ \sum_{\alpha\mu} \sum_{a,b,c,d} & \Gamma^*_{\mu\alpha}(E_d - E_c)\delta_{E_a - E_b + E_c - E_d} \langle\psi_b|\hat{A}_\mu|\psi_a\rangle\langle\psi_c|\hat{A}_\alpha|\psi_d\rangle^* \rho_S(t)\left(|\psi_c\rangle\langle\psi_d|\right)^\dagger |\psi_b\rangle\langle\psi_a| \\
& \qquad \text{(A.19)}
\end{aligned}$$

The function $\Gamma_{\mu\alpha}(\omega)$ is split in its Hermitian and anti-Hermitian parts

$$\left.\begin{aligned} \Gamma_{\mu\alpha}(\omega) &= \tfrac{1}{2}\zeta_{\mu\alpha}(\omega) + \tfrac{1}{2}\sigma_{\mu\alpha}(\omega) \\ \Gamma^*_{\alpha\mu}(\omega) &= \tfrac{1}{2}\zeta_{\mu\alpha}(\omega) - \tfrac{1}{2}\sigma_{\mu\alpha}(\omega) \end{aligned}\right\} \Rightarrow \left\{\begin{aligned} \zeta_{\mu\alpha}(\omega) &= \zeta^*_{\alpha\mu}(\omega) \\ \sigma_{\alpha\mu}(\omega) &= -\sigma^*_{\alpha\mu}(\omega) \end{aligned}\right\} \Rightarrow \left\{\begin{aligned} \zeta_{\mu\alpha}(\omega) &= \Gamma_{\mu\alpha}(\omega) + \Gamma^*_{\alpha\mu}(\omega) = \int_{-\infty}^{\infty} C_{\mu\alpha}(\tau) e^{i\omega\tau} d\tau \\ \sigma_{\alpha\mu}(\omega) &= \Gamma_{\mu\alpha}(\omega) - \Gamma^*_{\alpha\mu}(\omega) = \int_{-\infty}^{\infty} C_{\mu\alpha}(\tau)\mathrm{sgn}(\tau) e^{i} \end{aligned}\right. \qquad \text{(A.20)}$$

The anti-Hermitian part introduces a small renormalization of the energy levels (Lamb-Shift), which are neglected. Then, Eq. (A.19) reads:

$$\dot{\rho}_S(t) = -\sum_{a,b,c,d} \gamma_{ab,cd}\left[|\psi_c\rangle\langle\psi_d|\rho_S(t)\left(|\psi_b\rangle\langle\psi_a|\right)^\dagger - \frac{1}{2}\left\{\left(|\psi_b\rangle\langle\psi_a|\right)^\dagger |\psi_c\rangle\langle\psi_d|, \rho_S(t)\right\}\right] \qquad \text{(A.21)}$$

with $\gamma_{ab,cd} = \sum_{\alpha\mu} \zeta_{\mu\alpha}(E_d - E_c)\delta_{E_a - E_b + E_c - E_d} \langle\psi_b|\hat{A}_\mu|\psi_a\rangle^* \langle\psi_c|\hat{A}_\alpha|\psi_d\rangle$ Going back to the Schrödinger picture

$$\dot{\rho}_S(t) = -i\left[\hat{H}_S, \rho_S(t)\right] + \sum_{a,b,c,d} \gamma_{ab,cd}\left[|\psi_c\rangle\langle\psi_d|\rho_S(t)\left(|\psi_b\rangle\langle\psi_a|\right)^\dagger - \frac{1}{2}\left\{\left(|\psi_b\rangle\langle\psi_a|\right)^\dagger |\psi_c\rangle\langle\psi_d|, \rho_S(t)\right\}\right] \qquad \text{(A.22)}$$

the Born-Markov-Secular Master equation is finally obtained.
The evaluation of $\zeta_{\mu\alpha}(\mathrm{E_d}-\mathrm{E_c})$ reads

$$\begin{aligned}\zeta_{\mu\alpha}(\mathrm{E_d}-\mathrm{E_c}) &= \int_{-\infty}^{\infty} e^{i(\mathrm{E_d}-\mathrm{E_c})\tau}\mathrm{Tr}\left\{e^{i\hat{\mathrm{H}}_\mathrm{B}\tau}\hat{\mathrm{B}}_\mu e^{-i\hat{\mathrm{H}}_\mathrm{B}\tau}\hat{\mathrm{B}}_\alpha\bar{\rho}_\mathrm{B}\right\}d\tau \\ &= \int_{-\infty}^{\infty} e^{i(\mathrm{E_d}-\mathrm{E_c})\tau}\sum_{\eta\xi}\langle\eta|\, e^{i\hat{\mathrm{H}}_\mathrm{B}\tau}\hat{\mathrm{B}}_\mu e^{-i\hat{\mathrm{H}}_\mathrm{B}\tau}\,|\xi\rangle\,\langle\xi|\,\hat{\mathrm{B}}_\alpha\bar{\rho}_\mathrm{B}\,|\eta\rangle\,d\tau \\ &= \sum_{\eta\xi}\int_{-\infty}^{\infty} e^{i(\mathrm{E_d}-\mathrm{E_c}+\epsilon_\eta-\epsilon_\xi)\tau}\,\langle\eta|\,\hat{\mathrm{B}}_\mu\,|\xi\rangle\,\langle\xi|\,\hat{\mathrm{B}}_\alpha\bar{\rho}_\mathrm{B}\,|\eta\rangle\,d\tau \\ &= \sum_{\eta\xi} 2\pi\delta_{\mathrm{E_d}-\mathrm{E_c}+\epsilon_\eta-\epsilon_\xi}\,\langle\xi|\,\hat{\mathrm{B}}_\mu\,|\eta\rangle^*\,\langle\xi|\,\hat{\mathrm{B}}_\alpha\,|\eta\rangle\,\langle\eta|\,\bar{\rho}_\mathrm{B}\,|\eta\rangle \end{aligned} \tag{A.23}$$

hence, the expression for $\gamma_{\mathrm{ab,cd}}$ reads

$$\begin{aligned}\gamma_{\mathrm{ab,cd}} =& 2\pi\delta_{\mathrm{E_a}-\mathrm{E_b}+\mathrm{E_c}-\mathrm{E_d}}\sum_{\eta\xi}\delta_{\mathrm{E_d}-\mathrm{E_c}+\epsilon_\eta-\epsilon_\xi}\sum_{\alpha\mu}\langle\psi_\mathrm{b}\xi|\,\hat{\mathrm{A}}_\mu\hat{\mathrm{B}}_\mu\,|\psi_\mathrm{a}\eta\rangle^*\,\langle\psi_\mathrm{c}\xi|\,\hat{\mathrm{A}}_\alpha\hat{\mathrm{B}}_\alpha\,|\psi_\mathrm{d}\eta\rangle\,\langle\eta|\,\bar{\rho}_\mathrm{B}\,|\eta\rangle \\ =& 2\pi\delta_{\mathrm{E_a}-\mathrm{E_b}+\mathrm{E_c}-\mathrm{E_d}}\sum_{\eta\xi}\delta_{\mathrm{E_d}-\mathrm{E_c}+\epsilon_\eta-\epsilon_\xi}\,\langle\psi_\mathrm{b}\xi|\,\hat{\mathrm{H}}_\mathrm{int}\,|\psi_\mathrm{a}\eta\rangle^*\,\langle\psi_\mathrm{c}\xi|\,\hat{\mathrm{H}}_\mathrm{int}\,|\psi_\mathrm{d}\eta\rangle\,\langle\eta|\,\bar{\rho}_\mathrm{B}\,|\eta\rangle\,. \end{aligned} \tag{A.24}$$

In general $\hat{\mathrm{H}}_\mathrm{int}$ changes from one state of $\hat{\mathrm{H}}_\mathrm{S}$ to another, so $a\neq b$ and $c\neq d$ and to fulfill energy conservation ($\delta_{\mathrm{E_a}-\mathrm{E_b}+\mathrm{E_c}-\mathrm{E_d}}$) it is needed $a=d$ and $b=c$. To this point $\gamma_{\mathrm{ab,cd}}$ has two sub-indexes $\gamma_{\mathrm{ab,ba}}\equiv\gamma_{\mathrm{ba}}$:

$$\begin{aligned}\gamma_{\mathrm{ba}} =& \sum_{\eta\xi} 2\pi\delta_{\mathrm{E_a}-\mathrm{E_b}+\epsilon_\eta-\epsilon_\xi}\,\langle\psi_\mathrm{b}\xi|\,\hat{\mathrm{H}}_\mathrm{int}\,|\psi_\mathrm{a}\eta\rangle^*\,\langle\psi_\mathrm{b}\xi|\,\hat{\mathrm{H}}_\mathrm{int}\,|\psi_\mathrm{a}\eta\rangle\,\langle\eta|\,\bar{\rho}_\mathrm{B}\,|\eta\rangle \\ =& \sum_{\eta\xi} 2\pi\delta_{\mathrm{E_a}-\mathrm{E_b}+\epsilon_\eta-\epsilon_\xi}\left|\langle\psi_\mathrm{b}\xi|\,\hat{\mathrm{H}}_\mathrm{int}\,|\psi_\mathrm{a}\eta\rangle\right|^2\langle\eta|\,\bar{\rho}_\mathrm{B}\,|\eta\rangle \end{aligned} \tag{A.25}$$

the delta function $\delta_{\mathrm{E_d}-\mathrm{E_c}+\epsilon_\eta-\epsilon_\xi}$ tells that the energy has to be conserved in a transition between the reservoirs and the quantum system. Finally the Master Equation reads

$$\dot{\rho}_\mathrm{S}(t) = -i\left[\hat{\mathrm{H}}_\mathrm{S},\rho_\mathrm{S}(t)\right] + \sum_{\mathrm{a,b}}\gamma_{\mathrm{ba}}\left[\,|\psi_\mathrm{b}\rangle\langle\psi_\mathrm{a}|\,\rho_\mathrm{S}(t)\left(|\psi_\mathrm{b}\rangle\langle\psi_\mathrm{a}|\right)^\dagger - \frac{1}{2}\left\{\left(|\psi_\mathrm{b}\rangle\langle\psi_\mathrm{a}|\right)^\dagger|\psi_\mathrm{b}\rangle\langle\psi_\mathrm{a}|\,,\rho_\mathrm{S}(t)\right\}\right] \tag{A.26}$$

This is the so called Lindblad Master Equation [123, 124], which is the most general type of Markovian and time-homogeneous master equation describing non-unitary evolution of the density matrix ρ that is trace-preserving and completely positive for any initial condition. This equation can also be written in a more compact way: $\dot{\rho}(t)=\mathscr{L}\rho(t)$, where $\mathscr{L}$ is the Liouvillian superoperator. Writing separately each element of the Master Equation:

$$\begin{aligned}\langle\psi_\mathrm{m}|\,\dot{\rho}_\mathrm{S}(t)\,|\psi_\mathrm{n}\rangle =& -i\,\langle\psi_\mathrm{m}|\left[\hat{\mathrm{H}}_\mathrm{S},\rho_\mathrm{S}(t)\right]|\psi_\mathrm{n}\rangle + \delta_{\mathrm{mn}}\left\{\sum_\mathrm{a}\gamma_{\mathrm{ma}}\,\langle\psi_\mathrm{a}|\,\rho_\mathrm{S}(t)\,|\psi_\mathrm{a}\rangle - \sum_\mathrm{b}\gamma_{\mathrm{bm}}\,\langle\psi_\mathrm{m}|\,\rho_\mathrm{S}(t)\,|\psi_\mathrm{m}\rangle\right\} \\ & -\frac{1}{2}(1-\delta_{\mathrm{mn}})\left\{\sum_\mathrm{b}\gamma_{\mathrm{bm}}\,\langle\psi_\mathrm{m}|\rho_\mathrm{S}(t)|\psi_\mathrm{n}\rangle + \gamma_{\mathrm{bn}}\,\langle\psi_\mathrm{m}|\rho_\mathrm{S}(t)|\psi_\mathrm{n}\rangle\right\} \end{aligned} \tag{A.27}$$

In the thesis it is also written as

$$\dot{\rho}_S(t) = -i\left[\hat{H}_S, \rho_S(t)\right] + \mathscr{L}_\Gamma \rho_S(t) \tag{A.28}$$

where $\mathscr{L}_\Gamma \rho_S(t)$ reads:

$$\langle \psi_m | \mathscr{L}_\Gamma \rho_S(t) | \psi_n \rangle = \delta_{mn} \sum_a \left(\gamma_{ma}\rho_{S,aa}(t) - \gamma_{am}\rho_{S,mm}(t)\right) - \frac{1}{2}(1-\delta_{mn})\left(\sum_b \gamma_{bm} + \gamma_{bn}\right)\rho_{S,mn}(t) \tag{A.29}$$

with $\rho_{S,mn} \equiv \langle \psi_m | \rho_S(t) | \psi_n \rangle$.

A.1 Redfield Master equation

In this section, the coupling with between the leads and the QDs, $|\lambda|^2$, is not considered to be much weaker than the internal dynamics τ: $|\lambda|^2 \approx \tau$. Hence, the secular approximation which neglects the oscillating terms can not be done. The derivation starts from Eq. (A.16), where the Born-Markov approximation is already done:

$$\begin{aligned}\dot{\rho}_S(t) = \sum_{\alpha\mu}\sum_{a,b,c,d}\int_0^\infty \Big\{ & C_{\mu\alpha}(\tau) e^{i(E_d - E_c)\tau} e^{i(E_a - E_b + E_c - E_d)t} \langle \psi_a | \hat{A}_\mu | \psi_b \rangle \langle \psi_c | \hat{A}_\alpha | \psi_d \rangle \\ & \times \Big[|\psi_a\rangle\langle\psi_b| |\psi_c\rangle\langle\psi_d| \rho_S(t) - |\psi_c\rangle\langle\psi_d| \rho_S(t) |\psi_a\rangle\langle\psi_b| \Big] + \text{h.c.} \Big\} d\tau\end{aligned} \tag{A.30}$$

with $\Gamma_{\mu\alpha}(\omega) = \int_0^\infty C_{\mu\alpha}(\tau) e^{i\omega\tau} d\tau$. Expanding Eq. (A.30) and doing the transformation$\{a \leftrightarrow d, b \leftrightarrow c, \alpha \leftrightarrow \beta\}$:

$$\begin{aligned}\dot{\rho}_S(t) = & \sum_{\alpha\mu}\sum_{a,b,c,d} \Gamma_{\mu\alpha}(E_d - E_c) e^{i(E_a - E_b + E_c - E_d)t} \langle \psi_b | \hat{A}_\mu | \psi_a \rangle^* \langle \psi_c | \hat{A}_\alpha | \psi_d \rangle \\ & \times \Big[\left(|\psi_b\rangle\langle\psi_a|\right)^\dagger |\psi_c\rangle\langle\psi_d| \rho_S(t) - |\psi_c\rangle\langle\psi_d| \rho_S(t) \left(|\psi_b\rangle\langle\psi_a|\right)^\dagger \Big] \\ & + \sum_{\alpha\mu}\sum_{a,b,c,d} \Gamma^*_{\mu\alpha}(E_d - E_c) e^{-i(E_a - E_b + E_c - E_d)t} \langle \psi_b | \hat{A}_\mu | \psi_a \rangle \langle \psi_c | \hat{A}_\alpha | \psi_d \rangle^* \\ & \times \Big[\rho_S(t) \left(|\psi_c\rangle\langle\psi_d|\right)^\dagger |\psi_b\rangle\langle\psi_a| - |\psi_b\rangle\langle\psi_a| \rho_S(t) \left(|\psi_c\rangle\langle\psi_d|\right)^\dagger \Big] \\ = & -\sum_{\alpha\mu}\sum_{a,b,c,d} \Big[\Gamma_{\mu\alpha}(E_d - E_c) + \Gamma^*_{\alpha\mu}(E_d - E_c)\Big] e^{i(E_a - E_b + E_c - E_d)t} \langle \psi_b | \hat{A}_\mu | \psi_a \rangle^* \langle \psi_c | \hat{A}_\alpha | \psi_d \rangle \\ & \times |\psi_c\rangle\langle\psi_d| \rho_S(t) \left(|\psi_b\rangle\langle\psi_a|\right)^\dagger \\ & + \sum_{\alpha\mu}\sum_{a,b,c,d} \Gamma_{\mu\alpha}(E_d - E_c) e^{i(E_a - E_b + E_c - E_d)t} \langle \psi_b | \hat{A}_\mu | \psi_a \rangle^* \langle \psi_c | \hat{A}_\alpha | \psi_d \rangle \left(|\psi_b\rangle\langle\psi_a|\right)^\dagger |\psi_c\rangle\langle\psi_d| \rho_S(t) \\ & + \sum_{\alpha\mu}\sum_{a,b,c,d} \Gamma^*_{\mu\alpha}(E_d - E_c) e^{i(E_a - E_b + E_c - E_d)t} \langle \psi_b | \hat{A}_\mu | \psi_a \rangle^* \langle \psi_c | \hat{A}_\alpha | \psi_d \rangle \rho_S(t) \left(|\psi_b\rangle\langle\psi_a|\right)^\dagger |\psi_c\rangle\langle\psi_d|\end{aligned} \tag{A.31}$$

Splitting $\Gamma_{\mu\alpha}(\omega)$ in the hermitian and anti-hermitian part (see Eq. (A.20)), and getting ride of the anti-hermitian part, Eq. (A.31) reads

$$\dot{\rho}_S(t) = -\sum_{a,b,c,d} \gamma_{ab,cd} e^{i(E_a - E_b + E_c - E_d)t} \left[|\psi_c\rangle\langle\psi_d| \rho_S(t) \left(|\psi_b\rangle\langle\psi_a|\right)^\dagger - \frac{1}{2}\left\{ \left(|\psi_b\rangle\langle\psi_a|\right)^\dagger |\psi_c\rangle\langle\psi_d|, \rho_S(t) \right\} \right] \tag{A.32}$$

with $\gamma_{\mathrm{ab,cd}} = \sum_{\alpha\mu}\zeta_{\mu\alpha}(\mathrm{E_d}-\mathrm{E_c})\langle\psi_\mathrm{b}|\hat{\mathrm{A}}_\mu|\psi_\mathrm{a}\rangle^*\langle\psi_\mathrm{c}|\hat{\mathrm{A}}_\alpha|\psi_\mathrm{d}\rangle$. For the same evaluation as in Eq. (A.23) the expression for $\gamma_{\mathrm{ab,cd}}$ reads:

$$\begin{aligned}\gamma_{\mathrm{ab,cd}} &= \sum_{\alpha\mu}\sum_{\eta\xi} 2\pi\delta_{\mathrm{E_d}-\mathrm{E_c}+\epsilon_\eta-\epsilon_\xi}\langle\psi_\mathrm{b}|\hat{\mathrm{A}}_\mu|\psi_\mathrm{a}\rangle^*\langle\psi_\mathrm{c}|\hat{\mathrm{A}}_\alpha|\psi_\mathrm{d}\rangle\langle\xi|\hat{\mathrm{B}}_\mu|\eta\rangle^*\langle\xi|\hat{\mathrm{B}}_\alpha|\eta\rangle\langle\eta|\bar{\rho}_\mathrm{B}|\eta\rangle \\ &= \sum_{\eta\xi} 2\pi\delta_{\mathrm{E_d}-\mathrm{E_c}+\epsilon_\eta-\epsilon_\xi}\langle\psi_\mathrm{b}\xi|\hat{\mathrm{H}}_\mathrm{int}|\psi_\mathrm{a}\eta\rangle^*\langle\psi_\mathrm{c}\xi|\hat{\mathrm{H}}_\mathrm{int}|\psi_\mathrm{d}\eta\rangle\langle\eta|\bar{\rho}_\mathrm{B}|\eta\rangle \end{aligned} \tag{A.33}$$

Eq. (A.32) in the Schrödinger picture reads:

$$\dot{\rho}_\mathrm{S}(t) = -i\left[\hat{\mathrm{H}}_\mathrm{S},\rho_\mathrm{S}(t)\right] + \sum_{\mathrm{a,b,c,d}}\gamma_{\mathrm{ab,cd}}\Big[|\psi_\mathrm{c}\rangle\langle\psi_\mathrm{d}|\rho_\mathrm{S}(t)\left(|\psi_\mathrm{b}\rangle\langle\psi_\mathrm{a}|\right)^\dagger - \frac{1}{2}\left\{\left(|\psi_\mathrm{b}\rangle\langle\psi_\mathrm{a}|\right)^\dagger|\psi_\mathrm{c}\rangle\langle\psi_\mathrm{d}|,\rho_\mathrm{S}(t)\right\}\Big] \tag{A.34}$$

A.1.1 Example for two reservoirs coupled to the left and right quantum dot

A QD system with up to one particle in the system is coupled to reservoirs with the Hamiltonian: $\hat{\mathrm{H}}_\mathrm{int} = \sum_{\nu=\{\mathrm{L,R}\}}\sum_k \lambda_\nu\left(\hat{d}^\dagger_{\nu,k}\hat{c}_\nu + \hat{c}^\dagger_\nu\hat{d}_{\nu,k}\right)$ where $\hat{d}_\nu$ is the destructive operator of the ν-reservoir, $\hat{c}_\nu$ is the destructive operator of the ν-site of the QD system and λ the coupling between them. The coupling terms $\gamma_{\mathrm{ab,cd}}$ read:

$$\begin{aligned}\gamma_{\mathrm{ab,cd}} = \sum_{\eta\xi}\sum_{kk'} 2\pi\delta_{\mathrm{E_d}-\mathrm{E_c}+\epsilon_\eta-\epsilon_\xi}&\langle\psi_\mathrm{b}\xi|\lambda_\mathrm{L}\left(\hat{d}^\dagger_{\mathrm{L},k}\hat{c}_\mathrm{L}+\hat{c}^\dagger_\mathrm{L}\hat{d}_{\mathrm{L},k}\right)+\lambda_\mathrm{R}\left(\hat{d}^\dagger_{\mathrm{R},k}\hat{c}_\mathrm{R}+\hat{c}^\dagger_\mathrm{R}\hat{d}_{\mathrm{R},k}\right)|\psi_\mathrm{a}\eta\rangle^* \\ &\langle\psi_\mathrm{c}\xi|\lambda_\mathrm{L}\left(\hat{d}^\dagger_{\mathrm{L},k'}\hat{c}_\mathrm{L}+\hat{c}^\dagger_\mathrm{L}\hat{d}_{\mathrm{L},k'}\right)+\lambda_\mathrm{R}\left(\hat{d}^\dagger_{\mathrm{R},k'}\hat{c}_\mathrm{R}+\hat{c}^\dagger_\mathrm{R}\hat{d}_{\mathrm{R},k'}\right)|\psi_\mathrm{d}\eta\rangle\langle\eta|\bar{\rho}_\mathrm{B}|\eta\rangle\end{aligned} \tag{A.35}$$

The terms with $\langle\eta|\hat{d}^\dagger_{\nu,k}\hat{d}_{\nu',k'}|\eta\rangle$ with $\nu\neq\nu'$ and/or $k\neq k'$ are zero. Using the anti-commutation relation for fermions $\{\hat{c}^\dagger_\alpha,\hat{c}_\beta\} = \delta_{\alpha\beta}$, the non-zero terms are:

$$\begin{aligned}\gamma_{\mathrm{ab,cd}} = \sum_\eta\sum_k 2\pi\delta_{\mathrm{E_d}-\mathrm{E_c}+\epsilon_k}\Big[&|\lambda_\mathrm{L}|^2\langle\psi_\mathrm{a}|\hat{c}_\mathrm{L}|\psi_\mathrm{b}\rangle\langle\psi_\mathrm{c}|\hat{c}^\dagger_\mathrm{L}|\psi_\mathrm{d}\rangle\langle\eta|\hat{d}^\dagger_{\mathrm{L},k}\hat{d}_{\mathrm{L},k}|\eta\rangle \\ &+|\lambda_\mathrm{L}|^2\langle\psi_\mathrm{a}|\hat{c}^\dagger_\mathrm{L}|\psi_\mathrm{b}\rangle\langle\psi_\mathrm{c}|\hat{c}_\mathrm{L}|\psi_\mathrm{d}\rangle\langle\eta|1-\hat{d}^\dagger_{\mathrm{L},k}\hat{d}_{\mathrm{L},k}|\eta\rangle \\ &+|\lambda_\mathrm{R}|^2\langle\psi_\mathrm{a}|\hat{c}_\mathrm{R}|\psi_\mathrm{b}\rangle\langle\psi_\mathrm{c}|\hat{c}^\dagger_\mathrm{R}|\psi_\mathrm{d}\rangle\langle\eta|\hat{d}^\dagger_{\mathrm{R},k}\hat{d}_{\mathrm{R},k}|\eta\rangle \\ &+|\lambda_\mathrm{R}|^2\langle\psi_\mathrm{a}|\hat{c}^\dagger_\mathrm{R}|\psi_\mathrm{b}\rangle\langle\psi_\mathrm{c}|\hat{c}_\mathrm{R}|\psi_\mathrm{d}\rangle\langle\eta|1-\hat{d}^\dagger_{\mathrm{R},k}\hat{d}_{\mathrm{R},k}|\eta\rangle\Big]\langle\eta|\bar{\rho}_\mathrm{B}|\eta\rangle\end{aligned} \tag{A.36}$$

For up to one particle in the system there are only two possibilities:

$$\begin{aligned}\gamma_{\mathrm{0b,c0}} &= \sum_{\nu=\{\mathrm{L,R}\}}\sum_\eta\sum_k 2\pi\delta_{\epsilon_k-\mathrm{E_c}}|\lambda_\nu|^2\langle 0|\hat{c}_\nu|\psi_\mathrm{b}\rangle\langle\psi_\mathrm{c}|\hat{c}^\dagger_\nu|0\rangle\langle\eta|\hat{d}^\dagger_{\nu,k}\hat{d}_{\nu,k}|\eta\rangle\langle\eta|\bar{\rho}_\mathrm{B}|\eta\rangle \\ \gamma_{\mathrm{a0,0d}} &= \sum_{\nu=\{\mathrm{L,R}\}}\sum_\eta\sum_k 2\pi\delta_{\mathrm{E_d}+\epsilon_k}|\lambda_\nu|^2\langle\psi_\mathrm{a}|\hat{c}^\dagger_\nu|0\rangle\langle 0|\hat{c}_\nu|\psi_\mathrm{d}\rangle\langle\eta|1-\hat{d}^\dagger_{\nu,k}\hat{d}_{\nu,k}|\eta\rangle\langle\eta|\bar{\rho}_\mathrm{B}|\eta\rangle\,.\end{aligned} \tag{A.37}$$

It finally reads

$$\gamma_{\mathrm{0b,c0}} = \sum_{\nu=\{\mathrm{L,R}\}} 2\pi|\lambda_\nu|^2\mathscr{D}_\nu(\mathrm{E_c})\langle\nu|\psi_\mathrm{b}\rangle\langle\psi_\mathrm{c}|\nu\rangle f_\nu(\mathrm{E_c}) \tag{A.38}$$

$$\gamma_{\mathrm{a0,0d}} = \sum_{\nu=\{\mathrm{L,R}\}} 2\pi|\lambda_\nu|^2\mathscr{D}_\nu(-\mathrm{E_d})\langle\psi_\mathrm{a}|\nu\rangle\langle\nu|\psi_\mathrm{d}\rangle(1-f_\nu(-\mathrm{E_d})) \tag{A.39}$$

A.2 Infinite bias limit

In the infinite bias limit, the energy difference between the chemical potential of the reservoirs fulfills: $|\mu_\alpha - \mu_{\alpha'}| \gg \{|\mathrm{E_a} - \mathrm{E_b}|, |\tau_{nm}|\}$ $\forall$a,b,m, n and $\mu_\alpha \gg \mathrm{E_a} \gg \mu_{\alpha'}$ $\forall$a; therefore, the values of the Fermi distribution functions and density of states of the reservoirs do not change if the reservoir energies are compared either with the quantum dot system eigenenergies or the quantum dot on-site energies, i.e, $f_\alpha(\mathrm{E_a} - \mathrm{E_b}) = f_\alpha(\epsilon_m - \epsilon_n)$, where $\mathrm{E_a}$ are eigenenergies and ϵ_n are on-site energies. To make this approximation one should consider the Redfield Master equation, because the coherences between the quantum states are not neglected. Doing this approximation, Eq. (A.33) reads:

$$\gamma^{\infty}_{\mathrm{ab,cd}} = \sum_{nmlr}\sum_{\eta\xi} 2\pi\delta_{\epsilon_s-\epsilon_l+\epsilon_\eta-\epsilon_\xi} \langle\psi_\mathrm{a}|n\rangle \langle m|\psi_\mathrm{b}\rangle \langle\psi_\mathrm{c}|l\rangle \langle s|\psi_\mathrm{d}\rangle \langle m\xi|\hat{\mathrm{H}}_{\mathrm{int}}|n\eta\rangle^* \langle l\xi|\hat{\mathrm{H}}_{\mathrm{int}}|s\eta\rangle \langle\eta|\bar{\rho}_\mathrm{B}|\eta\rangle . \tag{A.40}$$

where it has been included identities of the orthonormal set of the on-site states. The reservoirs are coupled to one single quantum dot, thus the only possible non-zero connection of $\hat{\mathrm{H}}_{\mathrm{int}}$ between η and ξ is through one unique $\{n,m\}$ pair:

$$\gamma^{\infty}_{\mathrm{ab,cd}} = \sum_{nm}\sum_{\eta\xi} 2\pi\delta_{\epsilon_n-\epsilon_m+\epsilon_\eta-\epsilon_\xi} \langle\psi_\mathrm{a}|n\rangle \langle m|\psi_\mathrm{b}\rangle \langle\psi_\mathrm{c}|m\rangle \langle n|\psi_\mathrm{d}\rangle |\langle m\xi|\hat{\mathrm{H}}_{\mathrm{int}}|n\eta\rangle|^2 \langle\eta|\bar{\rho}_\mathrm{B}|\eta\rangle . \tag{A.41}$$

substituting $\gamma^{\infty}_{\mathrm{ab,cd}}$ in Eq. (A.34):

$$\begin{aligned}
\dot{\rho}_\mathrm{S}(t) = &-i\left[\hat{\mathrm{H}}_\mathrm{S}, \rho_\mathrm{S}(t)\right] + \sum_{\mathrm{a,b,c,d}}\sum_{nm}\sum_{\eta\xi} 2\pi\delta_{\epsilon_n-\epsilon_m+\epsilon_\eta-\epsilon_\xi} \langle\psi_\mathrm{a}|n\rangle \langle m|\psi_\mathrm{b}\rangle \langle\psi_\mathrm{c}|m\rangle \langle n|\psi_\mathrm{d}\rangle |\langle m\xi|\hat{\mathrm{H}}_{\mathrm{int}}|n\eta\rangle|^2 \langle\eta|\bar{\rho}_\mathrm{B}|\eta\rangle \\
&\times\left[|\psi_\mathrm{c}\rangle\langle\psi_\mathrm{d}|\rho_\mathrm{S}(t)\left(|\psi_\mathrm{b}\rangle\langle\psi_\mathrm{a}|\right)^\dagger - \frac{1}{2}\left\{\left(|\psi_\mathrm{b}\rangle\langle\psi_\mathrm{a}|\right)^\dagger |\psi_\mathrm{c}\rangle\langle\psi_\mathrm{d}|, \rho_\mathrm{S}(t)\right\}\right] \\
= &-i\left[\hat{\mathrm{H}}_\mathrm{S}, \rho_\mathrm{S}(t)\right] + \sum_{nm}\left[\sum_{\eta\xi} 2\pi\delta_{\epsilon_n-\epsilon_m+\epsilon_\eta-\epsilon_\xi} |\langle m\xi|\hat{\mathrm{H}}_{\mathrm{int}}|n\eta\rangle|^2 \langle\eta|\bar{\rho}_\mathrm{B}|\eta\rangle\right] \\
&\times\left[|m\rangle\langle n|\rho_\mathrm{S}(t)(|m\rangle\langle n|)^\dagger - \frac{1}{2}\left\{(|m\rangle\langle n|)^\dagger |m\rangle\langle n|, \rho_\mathrm{S}(t)\right\}\right].
\end{aligned}$$

$\dot{\rho}_\mathrm{S}(t)$ finally reads in the on-site orthonormal base:

$$\dot{\rho}_\mathrm{S}(t) = -i\left[\hat{\mathrm{H}}_\mathrm{S}, \rho_\mathrm{S}(t)\right] + \sum_{nm}\tilde{\gamma}_{mn}\left[|m\rangle\langle n|\rho_\mathrm{S}(t)(|m\rangle\langle n|)^\dagger - \frac{1}{2}\left\{(|m\rangle\langle n|)^\dagger |m\rangle\langle n|, \rho_\mathrm{S}(t)\right\}\right] \tag{A.42}$$

$$\tilde{\gamma}_{mn} = \sum_{\eta\xi} 2\pi\delta_{\epsilon_n-\epsilon_m+\epsilon_\eta-\epsilon_\xi} |\langle m\xi|\hat{\mathrm{H}}_{\mathrm{int}}|n\eta\rangle|^2 \langle\eta|\bar{\rho}_\mathrm{B}|\eta\rangle \tag{A.43}$$

APPENDIX B

COTUNNEL APPROACH

To consider the cotunnel approximation, a weak interaction between two coupled sub-sets, say A and B, of the Hamiltonian is a necessary condition, i.e., $|\mathrm{E}_A - \mathrm{E}_B| \gg |\tau_{AB}|$, where $\mathrm{E}_{A,B}$ are the energies within each sub-set and τ_{AB} are the couplings between the states of the two subsets. The Hamiltonian is divided in three parts: $\hat{\mathrm{H}}_0$ with known eigenvectors, the interactions within each sub-set: $\hat{\mathrm{H}}_1$, and the weak interacting part between the two subsets: $\hat{\mathrm{H}}_{AB}$. The objective is to take the effect of $\hat{\mathrm{H}}_{AB}$ into the sets A and B. For that, the Hamiltonian is transformed with a unitary operator e^{S}, where S is an operator in the Hilber space of $\hat{\mathrm{H}}_{AB}$, to an effective Hamiltonian:

$$\hat{\mathrm{H}}_{\mathrm{eff}} = e^{-\mathrm{S}}\hat{\mathrm{H}}e^{\mathrm{S}} = \left(1 - \mathrm{S} + \frac{1}{2}\mathrm{S}^2 + \ldots\right)\left[\hat{\mathrm{H}}_0 + \hat{\mathrm{H}}_1 + \hat{\mathrm{H}}_{AB}\right]\left(1 + \mathrm{S} + \frac{1}{2}\mathrm{S}^2 + \ldots\right), \tag{B.1}$$

with the interacting part between the A and B sets is equal to zero. Whit this transformation the effect of the interaction between the sub-sets is taken into each sub-set:

$$\hat{\mathrm{H}} = \begin{bmatrix} A & \tau_{AB} \\ \tau_{AB} & B \end{bmatrix} \rightarrow \hat{\mathrm{H}}_{\mathrm{eff}} = \begin{bmatrix} \tilde{A} & 0 \\ 0 & \tilde{B} \end{bmatrix}. \quad S = \begin{bmatrix} 0 & \mathrm{S}_{AB} \\ -\mathrm{S}^*_{AB} & \end{bmatrix} \tag{B.2}$$

The S matrix is antihermitian. Each time the Hamiltonian $\hat{\mathrm{H}}_0$ and $\hat{\mathrm{H}}_1$ are multiplied by S: $\mathrm{S}\hat{\mathrm{H}}$ or $\hat{\mathrm{H}}\mathrm{S}$ the result is rotated to the Hilbert space of the interaction between the sub-sets. The opposite happens with $\hat{\mathrm{H}}_{AB}$, the result of $\mathrm{S}\hat{\mathrm{H}}_{AB}$ and $\hat{\mathrm{H}}_{AB}\mathrm{S}$ is contained within the Hilbert space of the sub-sets. Hence the result of a even number of S multiplications over $\hat{\mathrm{H}}_0$ and $\hat{\mathrm{H}}_1$, and the result of an odd number of S multiplications over $\hat{\mathrm{H}}_{AB}$ will be in the Hilbert space of the sub-sets. Therefore, Eq. (B.1) is divided in a part that must be zero and the part of the effective

Hamiltonian:

$$\hat{\mathrm{H}}_{\mathrm{eff}} = \sum_{n=0}^{\infty} \frac{1}{2n!} \left[\hat{\mathrm{H}}_0 + \hat{\mathrm{H}}_1, \mathrm{S}\right]^{(2n)} + \sum_{m=0}^{\infty} \frac{1}{(2m+1)!} \left[\hat{\mathrm{H}}_{AB}, \mathrm{S}\right]^{(2m+1)} \tag{B.3}$$

$$0 = \sum_{n=0}^{\infty} \frac{1}{(2n+1)!} \left[\hat{\mathrm{H}}_0 + \hat{\mathrm{H}}_1, \mathrm{S}\right]^{(2n+1)} + \sum_{n=0}^{\infty} \frac{1}{2n!} \left[\hat{\mathrm{H}}_{AB}, \mathrm{S}\right]^{(2n)} \tag{B.4}$$

The S is splitted in series $\mathrm{S} = \sum_{s=1}^{\infty} \mathrm{S}^{(s)}$ where $\mathrm{S}^{(s)}$ has and order $(\tau_{AB}/(\mathrm{E}_A - \mathrm{E}_B))^s$ of the energy difference between states from the different sets. In most of the cases considered in the present thesis is truncated to $s = 1$. The first order of S reads:

$$\hat{\mathrm{H}}_{AB} + \left[\hat{\mathrm{H}}_0, \mathrm{S}^{(1)}\right] = 0 \Rightarrow \langle \psi_\alpha^A | \mathrm{S}^{(1)} | \psi_\beta^B \rangle = -\frac{\langle \psi_\alpha^A | \hat{\mathrm{H}}_{AB} | \psi_\beta^B \rangle}{\mathrm{E}_\alpha^A - \mathrm{E}_\beta^B}. \tag{B.5}$$

With the result of Eq. (B.5), the expression of the Hamiltonian up to second order is obtained:

$$\hat{\mathrm{H}}_{\mathrm{eff}}^{(2)} = \hat{\mathrm{H}}_0 + \hat{\mathrm{H}}_1 + \left[\hat{\mathrm{H}}_{AB}, \mathrm{S}^{(1)}\right] + \left[\left[\hat{\mathrm{H}}_0 + \hat{\mathrm{H}}_1 +, \mathrm{S}^{(1)}\right], \mathrm{S}^{(1)}\right]. \tag{B.6}$$

where the first two terms are the original A and B subspaces, the single commutator accounts for the renormalization of the couplings among the states of each sub-set, and the double commutator is the renormalization of the energies.

B.1 Time dependent

In the last section, the cotunnel approach for a time independent Hamiltonians is explained. In this section it is extended to time dependent periodic Hamiltonians. For time periodic Hamiltonias the ordinary equations used to obtain the operator Exp[S] are now differential equations, which may be difficult to solve analitically. There are different ways of obtaining the effective Hamiltonian; in Chapter 4 it is obtained from the time evolution operator. The equation for the effective Hamiltonian reads

$$\begin{aligned}\hat{\mathrm{H}}_{\mathrm{eff}}(t) =& e^{-\mathrm{S}(t)} \hat{\mathrm{H}} e^{\mathrm{S}(t)} + \frac{i}{\hbar} \frac{\partial}{\partial t} \mathrm{S}(t) \\ =& \left(1 - \mathrm{S}(t) + \frac{1}{2}\mathrm{S}^2(t) + \ldots\right) \left[\hat{\mathrm{H}}_0(t) + \hat{\mathrm{H}}_1(t) + \hat{\mathrm{H}}_{AB}(t)\right] \left(1 + \mathrm{S}(t) + \frac{1}{2}\mathrm{S}^2(t) + \ldots\right) + \frac{i}{\hbar} \frac{\partial}{\partial t} \mathrm{S}(t).\end{aligned} \tag{B.7}$$

To solve this equation the procedure is similar to the time independent case.

$$\hat{\mathrm{H}}_{\mathrm{eff}}(t) = \sum_{n=0}^{\infty} \frac{1}{2n!} \left[\hat{\mathrm{H}}_0 + \hat{\mathrm{H}}_1, \mathrm{S}\right]^{(2n)} + \sum_{m=0}^{\infty} \frac{1}{(2m+1)!} \left[\hat{\mathrm{H}}_{AB}, \mathrm{S}\right]^{(2m+1)} \tag{B.8}$$

$$-\frac{i}{\hbar} \frac{\partial}{\partial t} \mathrm{S}(t) = \sum_{n=0}^{\infty} \frac{1}{(2n+1)!} \left[\hat{\mathrm{H}}_0 + \hat{\mathrm{H}}_1, \mathrm{S}\right]^{(2n+1)} + \sum_{n=0}^{\infty} \frac{1}{2n!} \left[\hat{\mathrm{H}}_{AB}, \mathrm{S}\right]^{(2n)} \tag{B.9}$$

The expression for the first order in $\mathrm{S}(t)$ reads

$$\begin{cases} \hat{\mathrm{H}}_{AB}(t) + \left[\hat{\mathrm{H}}_0(t), \mathrm{S}^{(1)}(t)\right] = -\frac{i}{\hbar} \frac{\partial}{\partial t} \mathrm{S}^{(1)}(t) \\ \hat{\mathrm{H}}_{AB}(0) + \left[\hat{\mathrm{H}}_0(0), \mathrm{S}^{(1)}(0)\right] = 0 \end{cases} \tag{B.10}$$

where it is needed an additional equation to obtain the initial conditions of the elements within the $S^{(1)}(t)$ matrix. Whit the result from Eq. (B.10) the effective Hamiltonian up to second order reads:

$$\hat{H}^{(2)}_{\text{eff}}(t) = \hat{H}_0(t) + \hat{H}_1(t) + \left[\hat{H}_{AB}(t), S(t)\right] + \left[\left[\hat{H}_0(t) + \hat{H}_1(t)+, S(t)\right], S(t)\right] + \ldots. \tag{B.11}$$

With the same set of states and assuming the approximations from the time independent case: $\{|E_\alpha - E_\beta|, |\tau_{\alpha\gamma}|, |\tau_{\gamma\beta}|\} \ll \{|E_\alpha - E_\gamma|, |E_\beta - E_\gamma|\}$; the following ones have to be additionally included: $\{V_\alpha, V_\beta, \hbar\omega\} \ll \{|E_\alpha - E_\gamma|, |E_\beta - E_\gamma|\}$. The analytical calculation is easier if it is performed the transformation (1.44) before obtaining the effective Hamiltonian.

APPENDIX C

FLOQUET THEORY

For time periodic Hamiltonians $\hat{\mathrm{H}}(t) = \hat{\mathrm{H}}(t+\mathscr{T})$ where $\mathscr{T} = 2\pi/\omega$ is the period, it is used Floquet theory to solve the evolution operator as a matrix diagonalization. The general result of Floquet theory states that the solution of a differential equation $\dot{x}(t) = \mathrm{A}(t)x(t)$, where $\mathrm{A}(t)$ is a $n \times n$ matrix periodic in time $\mathrm{A}(t) = \mathrm{A}(t+\mathscr{T})$ and $x(t)$ is a column vector, does not need to be periodic, however it must be of the form

$$\mathrm{X}(t) = \mathrm{P}(t)e^{\mathscr{M}t}, \quad \mathrm{P}(t) = \mathrm{P}(t+\mathscr{T}) \tag{C.1}$$

where $\mathrm{X}(t)$ is the fundamental-matrix solution and $\mathscr{M}$ is a complex diagonal matrix. In the case of the Schrödinger equation, $\mathrm{A}(t)$ is the Hamiltonian, which is an hermitian matrix; hence, $\mathscr{M}$ is purely imaginary and is defined as $\mathscr{M} \equiv -i\mathrm{Q}$ where Q is a real diagonal matrix. The eigenvectors for the Schrödinger equation $\hat{\mathrm{H}}(t)|\psi_\alpha(t)\rangle = i\hbar\partial_t|\psi_\alpha(t)\rangle$ are the set $\{|\psi_\alpha(t)\rangle\}_\alpha$. The formal solution for the Schrödinger equation is $|\psi_\alpha(t)\rangle = \mathrm{U}(t,t_0)|\psi_\alpha(t_0)\rangle$ where

$$\mathrm{U}(t,t_0) = \mathfrak{T}\exp\left[-\frac{i}{\hbar}\int_{t_0}^{t}\hat{\mathrm{H}}(t')dt'\right] \Rightarrow \begin{matrix}\text{Jacobi's}\\ \text{formula}\end{matrix} \Rightarrow \det\mathrm{U}(t,t_0) = \mathfrak{T}\exp\left[-\frac{i}{\hbar}\int_{t_0}^{t}\mathrm{Tr}\hat{\mathrm{H}}(t')dt'\right] \tag{C.2}$$

$\mathfrak{T}$ is the time ordering operator. Being $\Psi(t)$ the *fundamental matrix* of the Schrödinger equation, the Floquet theorem states that it can be written as

$$\Psi(t) = \Phi(t)e^{-iQt}, \quad \Phi(t) = \Phi(t+\mathscr{T}), \tag{C.3}$$

$$|\psi_\alpha(t)\rangle = |\phi_\alpha(t)\rangle\, e^{-iq_\alpha t}, \quad |\phi_\alpha(t)\rangle = |\phi_\alpha(t+\mathscr{T})\rangle\,, \tag{C.4}$$

where q_α, which are the eigenvalues of Q, are named quasi-energies. Using the notation $\psi_{\beta\alpha}(t) \equiv \langle\beta|\psi_\alpha(t)\rangle$ that refers to the weight of the β on-site state in the α eigenstate (same for $\phi_{\beta\alpha} \equiv \langle\beta|\phi_\alpha(t)\rangle$), and substituting Eq. (C.4) in the Schrödinger equation:

$$\psi_{\beta\alpha}(t) = \phi_{\beta\alpha}(t)e^{-iq_\alpha t} \Rightarrow \quad \sum_\beta \hat{\mathrm{H}}_{\gamma\beta}(t)\phi_{\beta\alpha}(t)e^{-iq_\alpha t} = i\frac{\partial}{\partial t}\left[\phi_{\gamma\alpha}(t)e^{-iq_\alpha t}\right], \tag{C.5}$$

with $\hat{\mathrm{H}}_{\gamma\beta}(t) = \langle\gamma|\hat{\mathrm{H}}(t)|\beta\rangle$. Expanding $\hat{\mathrm{H}}(t)$ and $\phi(t)$, as they are periodic functions, in Fourier series:

$$\hat{\mathrm{H}}(t) = \sum_{k=-\infty}^{\infty} \hat{\mathrm{H}}^k \mathrm{e}^{ik\omega t}, \quad |\phi_\alpha(t)\rangle = \sum_{l=-\infty}^{\infty} |\phi_\alpha^l\rangle \mathrm{e}^{il\omega t} \tag{C.6}$$

where $|\phi_\alpha^l\rangle$ is named Floquet mode. With Eq. (C.6) the Eq. (C.5) reads:

$$\sum_{\beta kl} \hat{\mathrm{H}}^k_{\gamma\beta} e^{ik\omega t} \phi^l_{\beta\alpha} e^{il\omega t} e^{-iq_\alpha t} = i\frac{\partial}{\partial t}\left[\sum_n \phi^n_{\gamma\alpha} e^{in\omega t} e^{-iq_\alpha t}\right]$$

$$\sum_{\beta kl} \hat{\mathrm{H}}^k_{\gamma\beta} e^{ik\omega t} \phi^l_{\beta\alpha} e^{il\omega t} e^{-iq_\alpha t} = \sum_n \phi^n_{\gamma\alpha}[q_\alpha - n\omega] e^{in\omega t} e^{-iq_\alpha t} \tag{C.7}$$

$$\sum_{\beta kl} \hat{\mathrm{H}}^k_{\gamma\beta} e^{ik\omega t} \phi^l_{\beta\alpha} e^{il\omega t} = \sum_n \phi^n_{\gamma\alpha}[q_\alpha - n\omega] e^{in\omega t} \tag{C.8}$$

$$\sum_k \left\{\sum_{\beta l} \hat{\mathrm{H}}^k_{\gamma\beta} e^{ik\omega t} \phi^l_{\beta\alpha} e^{il\omega t}\right\} = \sum_n \left\{\phi^n_{\gamma\alpha}[q_\alpha - n\omega] e^{in\omega t}\right\} \tag{C.9}$$

Doing the transformation $k = n - l$ Eq. C.9 reads

$$\sum_{\beta l}\left(\hat{\mathrm{H}}^{n-l}_{\gamma\beta} + n\omega\delta_{nl}\delta_{\gamma\beta}\right)\phi^l_{\beta\alpha} = q_\alpha \phi^n_{\gamma\alpha} \tag{C.10}$$

This set of equations are solved with a matrix diagonalization, where q_α are the eigenvalues and $|\phi_\alpha^l\rangle$ the eigenvectors of the matrix. For $\Psi(t)$ being unitary the evolution operator can be written as $\mathrm{U}(t,t_0) = \Psi(t)\Psi^{-1}(t_0)$, hence:

$$\mathrm{U}(t,t_0) = \sum_\alpha \mathrm{e}^{-iq_\alpha(t-t_0)} |\phi_\alpha(t)\rangle\langle\phi_\alpha(t_0)| \Rightarrow \mathrm{U}(t,t_0) = \sum_{\alpha,\beta,\gamma} \mathrm{e}^{-iq_\alpha(t-t_0)} |\beta\rangle\langle\beta|\phi_i(t)\rangle\langle\phi_i(t_0)|\gamma\rangle\langle\gamma| \tag{C.11}$$

with Eq. (C.4, C.11) it is stated that $\mathrm{U}(t_0+\mathscr{T},t_0)$ has the same eigenvalues as $\exp[-iQ\mathscr{T}]$. Therefore Eq. (C.2) is rewritten as,

$$\sum_\alpha q_\alpha = \frac{1}{\mathscr{T}}\int_0^{\mathscr{T}} \mathrm{Tr}\hat{\mathrm{H}}(t')dt'. \tag{C.12}$$

The energy $\mathrm{E}_\alpha(t)$ of the quantum sate $|\psi_\alpha(t)\rangle$ is

$$\begin{aligned}
\mathrm{E}_\alpha(t) &= \langle\psi_\alpha(t)|\, i\frac{\partial}{\partial t}|\psi_\alpha(t)\rangle = \mathrm{e}^{iq_\alpha t}\langle\phi_\alpha(t)|\, i\frac{\partial}{\partial t}\mathrm{e}^{-iq_\alpha t}|\phi_\alpha(t)\rangle \\
&= q_\alpha\langle\phi_\alpha(t)|\phi_\alpha(t)\rangle + \langle\phi_\alpha(t)|\, i\frac{\partial}{\partial t}|\phi_\alpha(t)\rangle \\
&= q_\alpha + \sum_{kl}\mathrm{e}^{-i\omega kt}\langle\phi^k_\alpha|\, i\frac{\partial}{\partial t}\mathrm{e}^{i\omega lt}|\phi^l_\alpha\rangle = q_\alpha - \sum_{kl} l\hbar\omega\langle\phi^k_\alpha|\phi^l_\alpha\rangle\mathrm{e}^{i\omega(l-k)t} \\
&= \sum_{kl}(q_\alpha - l\hbar\omega)\langle\phi^k_\alpha|\phi^l_\alpha\rangle\mathrm{e}^{i\omega(l-k)t}
\end{aligned} \tag{C.13}$$

The energy average in one period is

$$\begin{aligned}
\bar{\mathrm{E}}_\alpha &= q_\alpha - \frac{1}{\mathscr{T}}\sum_{kl} l\hbar\omega\langle\phi^k_\alpha|\phi^l_\alpha\rangle\int_t^{t+\mathscr{T}}\mathrm{e}^{i\omega(l-k)t} = q_\alpha - \frac{1}{\mathscr{T}}\sum_{kl} l\hbar\omega\langle\phi^k_\alpha|\phi^l_\alpha\rangle\mathscr{T}\delta_{l,k} \\
&= \sum_k(q_\alpha - k\omega\hbar)\langle\phi^k_\alpha|\phi^k_\alpha\rangle
\end{aligned} \tag{C.14}$$

List of publications

1. Rafael Sánchez, Fernando Gallego-Marcos and Gloria Platero,*Superexchange blockade in triple quantum dots*, Phys. Rev. B **89**, 161402(R) (2014)

2. Fernando Gallego-Marcos, Christian Nietner, Gernot Schaller, Gloria Platero and Tobias Brandes, *Non-equilibrium relaxation transport of ultracold atoms*, Phys. Rev. A **90**, 033614 (2014)

3. Fernando Gallego-Marcos, Rafael Sánchez and Gloria Platero, *Photon assisted long-range tunneling*. J. Appl. Phys. **117**, 112808 (2015)

4. Fernando Gallego-Marcos, Rafael Sánchez and Gloria Platero, *Coupled Landau-Zener-Stuckelberg quantum dot interferometers*. Phys. Rev. B **93**, 075424 (2016)

5. Monika Kotzian, Fernando Gallego-Marcos, Gloria Platero and Rolf J. Haug, *Channel Blockade in a Two-Path Triple-Quantum-Dot System*. Phys. Rev. B **94**, 035442 (2016)

6. Fernando Gallego-Marcos and Gloria Platero, *Coherent Long-Range Thermoelectrics in Nonadiabatic Driven Quantum Systems*. arXiv

Acronyms

2DEG Two Dimensional Electron Gas. 1, 11, 12

CB Coulomb Blockade. 3, 4, 8, 47

CDT Coherent Destruction of Tunneling. 9, 59

CTAP Coherent Transfer by Adiabatic Passage. 9, 10

DQD Double Quantum Dot. 2, 4–9, 96

DS Dark State. 10, 49, 51

LR Long Range. 10, 11, 14, 15, 45, 46, 51, 71–73

LZS Landau-Zener-Stückelberg. 8, 59, 61

LZT Landau-Zener Transitions. 8, 59

MOD MOdulation Doping. 11

MODFET MOdulation Doped Field Effect Transistor. 11

MOSFET Metal Oxide Semiconductor Field Effect Transistor. 11

PAT Photo Assisted Transition. 8, 9, 59, 71

QD Quantum Dot. 1–8, 10–12, 45, 47, 110

QP Quadruple Point. 10

QPC Quantum Point Contact. 5, 6, 46, 49

RWA Rotating Wave Approximation. 21

SB Spin Blockade. 7

TLS Two Level System. 7, 8

TP Triple Point. 6, 7, 9

TQD Triple Quantum Dot. 9–12, 14, 19, 46, 47, 60, 71, 83, 96

BIBLIOGRAPHY

[1] L. P. Kouwenhoven, D. G. Austing, and S. Tarucha, Reports on Progress in Physics **64**, 701 (2001).

[2] R. Hanson, L. P. Kouwenhoven, J. R. Petta, S. Tarucha, and L. M. K. Vandersypen, Reviews of Modern Physics **79**, 1217 (2007), cond-mat/0610433 .

[3] A. P. Alivisatos, Science **271**, 933 (1996).

[4] M. A. Kastner, Physics Today **46**, 24 (1993).

[5] R. C. Ashoori, Nature (London) **379**, 413 (1996).

[6] J. M. Elzerman, R. Hanson, J. S. Greidanus, L. H. Willems van Beveren, S. de Franceschi, L. M. Vandersypen, S. Tarucha, and L. P. Kouwenhoven, Phys. Rev. B **67**, 161308 (2003), cond-mat/0212489 .

[7] M. Ciorga, A. Sachrajda, P. Hawrylak, C. Gould, P. Zawadzki, Y. Feng, and Z. Wasilewski, Physica E: Low-dimensional Systems and Nanostructures **11**, 35 (2001).

[8] H.-A. Engel, L. P. Kouwenhoven, D. Loss, and C. M. Marcus, Quantum Information Processing **3**, 115132 (2004).

[9] Y. Meir, N. S. Wingreen, and P. A. Lee, Physical Review Letters **66**, 3048 (1991).

[10] L. L. Sohn, L. P. Kouwenhoven, and G. Schön, eds., *Mesoscopic Electron Transport*, 1st ed., Nato Science Series E:, Vol. 345 (Springer Netherlands, 1997).

[11] W. G. van der Wiel, S. de Franceschi, J. M. Elzerman, T. Fujisawa, S. Tarucha, and L. P. Kouwenhoven, Reviews of Modern Physics **75**, 1 (2002), cond-mat/0205350 .

[12] L. Zhuang, L. Guo, and S. Y. Chou, Applied Physics Letters **72**, 1205 (1998).

[13] J. Fernández-Rossier and R. Aguado, Physical Review Letters **98**, 106805 (2007), cond-mat/0604437 .

[14] L. A. Ponomarenko, F. Schedin, M. I. Katsnelson, R. Yang, E. W. Hill, K. S. Novoselov, and A. K. Geim, Science **320**, 356 (2008), arXiv:0801.0160 .

[15] S. de Franceschi, L. Kouwenhoven, C. Schönenberger, and W. Wernsdorfer, Nature Nanotechnology **5**, 703 (2010).

[16] D. Loss and D. P. Divincenzo, Phys. Rev. A **57**, 120 (1998), cond-mat/9701055 .

[17] G. Burkard, D. Loss, and D. P. Divincenzo, Phys. Rev. B **59**, 2070 (1999), cond-mat/9808026 .

[18] C. Kloeffel and D. Loss, Annual Review of Condensed Matter Physics **4**, 51 (2013), arXiv:1204.5917 [cond-mat.mes-hall] .

[19] P. W. Shor, in *Proc. 35nd Annual Symposium on Foundations of Computer Science*, edited by S. Goldwasser (IEEE Computer Society Press, 1994) pp. 124–134.

[20] L. P. Kouwenhoven, T. H. Oosterkamp, M. W. S. Danoesastro, M. Eto, D. G. Austing, T. Honda, and S. Tarucha, Science **278**, 1788 (1997), cond-mat/9708229 .

[21] U. Meirav, M. A. Kastner, and S. J. Wind, Physical Review Letters **65**, 771 (1990).

[22] H. Grabert and M. H. Devoret, *Single charge tunneling: Coulomb blockade phenomena in nanostructures*, Vol. 294 (Plenum Press, New York, 1992).

[23] D. Goldhaber-Gordon, J. Göres, M. A. Kastner, H. Shtrikman, D. Mahalu, and U. Meirav, Physical Review Letters **81**, 5225 (1998), cond-mat/9807233 .

[24] F. Simmel, R. H. Blick, J. P. Kotthaus, W. Wegscheider, and M. Bichler, Physical Review Letters **83**, 804 (1999), cond-mat/9812153 .

[25] S. M. Cronenwett, T. H. Oosterkamp, and L. P. Kouwenhoven, Science **281**, 540 (1998), cond-mat/9804211 .

[26] C. W. J. Beenakker, Phys. Rev. B **44**, 1646 (1991).

[27] C. L. Kane and M. P. A. Fisher, Phys. Rev. B **46**, 15233 (1992).

[28] M. Field, C. G. Smith, M. Pepper, D. A. Ritchie, J. E. F. Frost, G. A. C. Jones, and D. G. Hasko, Physical Review Letters **70**, 1311 (1993).

[29] T. Hayashi, T. Fujisawa, H. D. Cheong, Y. H. Jeong, and Y. Hirayama, Physical Review Letters **91**, 226804 (2003), cond-mat/0308362 .

[30] K. Ono, D. G. Austing, Y. Tokura, and S. Tarucha, Science **297**, 1313 (2002).

[31] R. H. Blick, R. J. Haug, J. Weis, D. Pfannkuche, K. V. Klitzing, and K. Eberl, Phys. Rev. B **53**, 7899 (1996).

[32] M. Pioro-Ladrière, M. Ciorga, J. Lapointe, P. Zawadzki, M. Korkusiński, P. Hawrylak, and A. S. Sachrajda, Physical Review Letters **91**, 026803 (2003), cond-mat/0301360 .

[33] J. R. Petta, A. C. Johnson, J. M. Taylor, E. A. Laird, A. Yacoby, M. D. Lukin, C. M. Marcus, M. P. Hanson, and A. C. Gossard, Science **309**, 2180 (2005).

[34] N. C. van der Vaart, S. F. Godijn, Y. V. Nazarov, C. J. P. M. Harmans, J. E. Mooij, L. W. Molenkamp, and C. T. Foxon, Physical Review Letters **74**, 4702 (1995).

[35] T. Hatano, M. Stopa, and S. Tarucha, Science **309**, 268 (2005).

[36] M. Pioro-Ladrière, M. R. Abolfath, P. Zawadzki, J. Lapointe, S. A. Studenikin, A. S. Sachrajda, and P. Hawrylak, Phys. Rev. B **72**, 125307 (2005).

[37] D. P. DiVincenzo, D. Bacon, J. Kempe, G. Burkard, and K. B. Whaley, Nature (London) **408**, 339 (2000), quant-ph/0005116 .

[38] T. Tanamoto, Phys. Rev. A **61**, 022305 (2000).

[39] B. J. van Wees, L. P. Kouwenhoven, D. van der Marel, H. von Houten, and C. W. J. Beenakker, Physical Review Letters **60**, 848 (1988).

[40] M. C. Rogge, B. Harke, C. Fricke, F. Hohls, M. Reinwald, W. Wegscheider, and R. J. Haug, Phys. Rev. B **72**, 233402 (2005), cond-mat/0508130 .

[41] T. H. Stievater, X. Li, D. G. Steel, D. Gammon, D. S. Katzer, D. Park, C. Piermarocchi, and L. J. Sham, Physical Review Letters **87**, 133603 (2001).

[42] D. V. Bulaev and D. Loss, Physical Review Letters **95**, 076805 (2005), cond-mat/0503181 .

[43] S. Laurent, B. Eble, O. Krebs, A. Lemaître, B. Urbaszek, X. Marie, T. Amand, and P. Voisin, Physical Review Letters **94**, 147401 (2005).

[44] D. Heiss, S. Schaeck, H. Huebl, M. Bichler, G. Abstreiter, J. J. Finley, D. V. Bulaev, and D. Loss, Phys. Rev. B **76**, 241306 (2007), arXiv:0705.1466 [cond-mat.mes-hall] .

[45] J. Fischer, W. A. Coish, D. V. Bulaev, and D. Loss, Phys. Rev. B **78**, 155329 (2008), arXiv:0807.0386 .

[46] B. D. Gerardot, D. Brunner, P. A. Dalgarno, P. Öhberg, S. Seidl, M. Kroner, K. Karrai, N. G. Stoltz, P. M. Petroff, and R. J. Warburton, Nature (London) **451**, 441 (2008).

[47] O. Klochan, J. C. H. Chen, A. P. Micolich, A. R. Hamilton, K. Muraki, and Y. Hirayama, Applied Physics Letters **96**, 092103 (2010).

[48] K. de Greve, P. L. McMahon, D. Press, T. D. Ladd, D. Bisping, C. Schneider, M. Kamp, L. Worschech, S. Höfling, A. Forchel, and Y. Yamamoto, Nature Physics **7**, 872 (2011), arXiv:1106.5676 [quant-ph] .

[49] D. Q. Wang, A. R. Hamilton, I. Farrer, D. A. Ritchie, and O. Klochan, Nanotechnology **27**, 334001 (2016).

[50] R. Li, F. E. Hudson, A. S. Dzurak, and A. R. Hamilton, Nano Letters **15**, 7314 (2015), arXiv:1509.00553 [cond-mat.mes-hall] .

[51] R. Maurand, X. Jehl, D. Kotekar-Patil, A. Corna, H. Bohuslavskyi, R. Laviéville, L. Hutin, S. Barraud, M. Vinet, M. Sanquer, and S. D. Franceschi, Nature Communications **7** (2016), 10.1038/ncomms13575.

[52] D. Weinmann, W. Häusler, and B. Kramer, Physical Review Letters **74**, 984 (1995).

[53] T. Fujisawa, D. G. Austing, Y. Tokura, Y. Hirayama, and S. Tarucha, Physical Review Letters **88**, 236802 (2002), cond-mat/0204314 .

[54] T. H. Oosterkamp, T. Fujisawa, W. G. van der Wiel, K. Ishibashi, R. V. Hijman, S. Tarucha, and L. P. Kouwenhoven, Nature (London) **395**, 873 (1998).

[55] J. R. Petta, A. C. Johnson, C. M. Marcus, M. P. Hanson, and A. C. Gossard, Physical Review Letters **93**, 186802 (2004), cond-mat/0408139 .

[56] T. Fujisawa and S. Tarucha, Superlattices and Microstructures **21**, 247 (1997).

[57] T. Fujisawa and S. Tarucha, Japanese Journal of Applied Physics **36**, 4000 (1997).

[58] T. H. Oosterkamp, L. P. Kouwenhoven, A. E. A. Koolen, N. C. van der Vaart, and C. J. P. M. Harmans, Physical Review Letters **78**, 1536 (1997).

[59] M. Pioro-Ladrière, T. Obata, Y. Tokura, Y.-S. Shin, T. Kubo, K. Yoshida, T. Taniyama, and S. Tarucha, Nature Physics **4**, 776 (2008), arXiv:0805.1083 [cond-mat.mtrl-sci] .

[60] K. C. Nowack, F. H. L. Koppens, Y. V. Nazarov, and L. M. K. Vandersypen, Science **318**, 1430 (2007), arXiv:0707.3080 .

[61] F. H. L. Koppens, C. Buizert, K. J. Tielrooij, I. T. Vink, K. C. Nowack, T. Meunier, L. P. Kouwenhoven, and L. M. K. Vandersypen, Nature (London) **442**, 766 (2006), cond-mat/0608459 .

[62] L. D. Landau, Physikalische Zeitschrift der Sowjetunion **2**, 46 (1932).

[63] C. Zener, Proceedings of the Royal Society of London Series A **137**, 696 (1932).

[64] E. Stückelberg, Helvetica Physica Acta **5**, 369 (1932).

[65] S. N. Shevchenko, S. Ashhab, and F. Nori, Phys. Rep. **492**, 1 (2010), arXiv:0911.1917 [cond-mat.supr-con] .

[66] F. Großmann, P. Jung, T. Dittrich, and P. Hänggi, Zeitschrift fur Physik B Condensed Matter **84**, 315 (1991).

[67] R. Bavli and H. Metiu, Phys. Rev. A **47**, 3299 (1993).

[68] L. Gaudreau, S. A. Studenikin, A. S. Sachrajda, P. Zawadzki, A. Kam, J. Lapointe, M. Korkusinski, and P. Hawrylak, Physical Review Letters **97**, 036807 (2006), cond-mat/0601597 .

[69] D. Schröer, A. D. Greentree, L. Gaudreau, K. Eberl, L. C. L. Hollenberg, J. P. Kotthaus, and S. Ludwig, Phys. Rev. B **76**, 075306 (2007), cond-mat/0703450 .

[70] G. Granger, L. Gaudreau, A. Kam, M. Pioro-Ladrière, S. A. Studenikin, Z. R. Wasilewski, P. Zawadzki, and A. S. Sachrajda, Phys. Rev. B **82**, 075304 (2010), arXiv:1006.2331 [cond-mat.mes-hall] .

[71] F. Meier, J. Levy, and D. Loss, Physical Review Letters **90**, 047901 (2003), cond-mat/0206310 .

[72] L. Gaudreau, G. Granger, A. Kam, G. C. Aers, S. A. Studenikin, P. Zawadzki, M. Pioro-Ladrière, Z. R. Wasilewski, and A. S. Sachrajda, Nature Physics **8**, 54 (2012).

[73] M. C. Rogge and R. J. Haug, New Journal of Physics **11**, 113037 (2009), arXiv:0908.0282 [cond-mat.mes-hall] .

[74] E. A. Laird, J. M. Taylor, D. P. Divincenzo, C. M. Marcus, M. P. Hanson, and A. C. Gossard, Phys. Rev. B **82**, 075403 (2010), arXiv:1005.0273 [cond-mat.mes-hall] .

[75] J. Medford, J. Beil, J. M. Taylor, S. D. Bartlett, A. C. Doherty, E. I. Rashba, D. P. DiVincenzo, H. Lu, A. C. Gossard, and C. M. Marcus, Nature Nanotechnology **8**, 654 (2013).

[76] T. Takakura, M. Pioro-Ladrière, T. Obata, Y.-S. Shin, R. Brunner, K. Yoshida, T. Taniyama, and S. Tarucha, Applied Physics Letters **97**, 212104 (2010).

[77] C. Hsieh, Y. Shim, M. Korkusinski, and P. Hawrylak, Rep. Prog. Phys. **75**, 114501 (2012).

[78] M. Stopa, Physical Review Letters **88**, 146802 (2002).

[79] A. Vidan, R. M. Westervelt, M. Stopa, M. Hanson, and A. C. Gossard, Applied Physics Letters **85**, 3602 (2004).

[80] D. S. Saraga and D. Loss, Physical Review Letters **90**, 166803 (2003), cond-mat/0205553 .

[81] D. Bacon, J. Kempe, D. A. Lidar, and K. B. Whaley, Physical Review Letters **85**, 1758 (2000), quant-ph/9909058 .

[82] C. S. Lent, P. D. Tougaw, W. Porod, and G. H. Bernstein, Nanotechnology **4**, 49 (1993).

[83] A. D. Greentree, J. H. Cole, A. R. Hamilton, and L. C. L. Hollenberg, Phys. Rev. B **70**, 235317 (2004), cond-mat/0407008 .

[84] A. D. Greentree, J. H. Cole, A. R. Hamilton, and L. C. L. Hollenberg, in *Micro- and Nanotechnology: Materials, Processes, Packaging, and Systems II*, Proceedings of SPIE, Vol. 5650, edited by J.-C. Chiao, D. N. Jamieson, L. Faraone, and A. S. Dzurak (2005) pp. 72–80.

[85] M. C. Rogge and R. J. Haug, Phys. Rev. B **77**, 193306 (2008), arXiv:0707.2058 .

[86] C. Pöltl, C. Emary, and T. Brandes, Phys. Rev. B **80**, 115313 (2009), arXiv:0905.2087 [cond-mat.mes-hall] .

[87] M. Kotzian, F. Gallego-Marcos, G. Platero, and R. J. Haug, Phys. Rev. B **94**, 035442 (2016), arXiv:1507.03595 [cond-mat.mes-hall] .

[88] T. Kuzmenko, K. Kikoin, and Y. Avishai, Physical Review Letters **96**, 046601 (2006), cond-mat/0507488 .

[89] C. Emary, Phys. Rev. B **76**, 245319 (2007), arXiv:0705.2934 [cond-mat.mes-hall] .

[90] M. Busl, R. Sánchez, and G. Platero, Phys. Rev. B **81**, 121306 (2010), arXiv:0907.0182 [cond-mat.mes-hall] .

[91] M. Seo, H. K. Choi, S.-Y. Lee, N. Kim, Y. Chung, H.-S. Sim, V. Umansky, and D. Mahalu, Physical Review Letters **110**, 046803 (2013), arXiv:1402.6451 [cond-mat.mes-hall] .

[92] H. B. Gray and J. R. Winkler, Proceedings of the National Academy of Science **102**, 3534 (2005).

[93] M. A. Ratner, J. Phys. Chem. **94** (1990), 10.1021/j100375a024.

[94] Y. Hu and S. Mukamel, Chemical Physics Letters **160**, 410 (1989).

[95] J. Jortner, M. Bixon, T. Langenbacher, and M. E. Michel-Beyerle, Proceedings of the National Academy of Science **95**, 12759 (1998).

[96] B. Giese, J. Amaudrut, A.-K. Köhler, M. Spormann, and S. Wessely, Nature (London) **412**, 318 (2001).

[97] C. Zener, Physical Review **82**, 403 (1951).

[98] P. W. Anderson, Physical Review **115**, 2 (1959).

[99] P. W. Anderson, Physical Review **124**, 41 (1961).

[100] J. Kondo, Progress of Theoretical Physics **32**, 37 (1964).

[101] M. Busl, G. Granger, L. Gaudreau, R. Sánchez, A. Kam, M. Pioro-Ladrière, S. A. Studenikin, P. Zawadzki, Z. R. Wasilewski, A. S. Sachrajda, and G. Platero, Nature Nanotechnology **8**, 261 (2013), arXiv:1310.5269 [cond-mat.mes-hall] .

[102] R. Sánchez, G. Granger, L. Gaudreau, A. Kam, M. Pioro-Ladrière, S. A. Studenikin, P. Zawadzki, A. S. Sachrajda, and G. Platero, Physical Review Letters **112**, 176803 (2014), arXiv:1312.5060 [cond-mat.mes-hall] .

[103] F. R. Braakman, P. Barthelemy, C. Reichl, W. Wegscheider, and L. M. K. Vandersypen, Nature Nanotechnology **8**, 432 (2013), arXiv:1303.1034 [cond-mat.mes-hall] .

[104] D. J. Reilly, Nature Nanotechnology **8**, 395 (2013).

[105] T. Hatano, S. Amaha, T. Kubo, S. Teraoka, Y. Tokura, J. A. Gupta, D. G. Austing, and S. Tarucha, Applied Physics Letters **97**, 062108 (2010), arXiv:1008.0071 [cond-mat.mes-hall] .

[106] P. Hawrylak, C. Gould, A. Sachrajda, Y. Feng, and Z. Wasilewski, Phys. Rev. B **59**, 2801 (1999).

[107] M. Ciorga, A. S. Sachrajda, P. Hawrylak, C. Gould, P. Zawadzki, S. Jullian, Y. Feng, and Z. Wasilewski, Phys. Rev. B **61**, R16315 (2000), cond-mat/9912446 .

[108] F. Stern and S. Das Sarma, Phys. Rev. B **30**, 840 (1984).

[109] R. Dingle, H. Störmer, A. Gossard, and W. Wiegmann, Surface Science **98**, 90 (1980).

[110] A. Khondker and A. Anwar, Solid-State Electronics **30**, 847 (1987).

[111] F. Stern and W. E. Howard, Phys. Rev. **163**, 816 (1967).

[112] R. Dingle, H. L. Störmer, A. C. Gossard, and W. Wiegmann, Applied Physics Letters **33**, 665 (1978).

[113] K. Ismail, W. Chu, A. Yen, D. A. Antoniadis, and H. I. Smith, Applied Physics Letters **54**, 460 (1989).

[114] H. Ehrenreich, Phys. Rev. **120**, 1951 (1960).

[115] "Physical properties of semiconductors," Data from Ioffe Physico-Thechnical Institute.

[116] M. Ishii and K. Matsumoto, Japanese Journal of Applied Physics **34** (1995), 10.1143/JJAP.34.1329/meta.

[117] U. Keyser, H. W. Schumacher, U. Zeitler, R. J. Haug, and K. Eberl, Applied Physics Letters **76**, 457 (2000).

[118] J. Bayer, *Herstellung und Charakterisierung von Mehrfachquantenpunkten*, Master's thesis, Intitut für Festkörperphysik, Liebniz Universität, Hannover (2014).

[119] R. K. Wangsness and F. Bloch, Physical Review **89**, 728 (1953).

[120] F. Bloch, Physical Review **102**, 104 (1956).

[121] U. Fano, Physical Review **96**, 869 (1954).

[122] A. G. Redfield, IBM Journal of Research and Development **1**, 19 (1957).

[123] G. Lindblad, Communications in Mathematical Physics **48**, 119 (1976).

[124] C. Lindblad, *Non-Equilibrium Entropy and Irreversibility*, Mathematical Physics Studies, Vol. 5 (Springer Netherlands, Dordrecht, Holland, 1983).

[125] M. Esposito and C. van den Broeck, Phys. Rev. E **82**, 011143 (2010), arXiv:1005.1683 [cond-mat.stat-mech] .

[126] M. Grifoni and P. Hänggi, Phys. Rep. **304**, 229 (1998).

[127] G. Platero and R. Aguado, Phys. Rep. **395**, 1 (2004), cond-mat/0311001 .

[128] S. Kohler, J. Lehmann, and P. Hänggi, Phys. Rep. **406**, 379 (2005), cond-mat/0409251 .

[129] S. Goldstein, J. L. Lebowitz, R. Tumulka, and N. Zanghì, Physical Review Letters **96**, 050403 (2006), cond-mat/0511091 .

[130] N. Linden, S. Popescu, A. J. Short, and A. Winter, Phys. Rev. E **79**, 061103 (2009), arXiv:0812.2385 [quant-ph] .

[131] V. I. Yukalov, Laser Physics Letters **8**, 507 (2011).

[132] P. Reimann and M. Kastner, New Journal of Physics **14**, 043020 (2012), arXiv:1202.2768 [cond-mat.stat-mech] .

[133] A. Riera, C. Gogolin, and J. Eisert, Physical Review Letters **108**, 080402 (2012), arXiv:1102.2389 [quant-ph] .

[134] A. Ivanov, G. Kordas, A. Komnik, and S. Wimberger, European Physical Journal B **86**, 345 (2013), arXiv:1304.5503 [cond-mat.mes-hall] .

[135] A. Recati, P. O. Fedichev, W. Zwerger, J. von Delft, and P. Zoller, Physical Review Letters **94**, 040404 (2005), cond-mat/0404533 .

[136] C. Nietner, G. Schaller, and T. Brandes, Phys. Rev. A **89**, 013605 (2014), arXiv:1309.3488 [cond-mat.quant-gas] .

[137] A. V. Ponomarev, S. Denisov, and P. Hänggi, Physical Review Letters **106**, 010405 (2011), arXiv:1004.2232 [cond-mat.stat-mech] .

[138] M. Bruderer and W. Belzig, Phys. Rev. A **85**, 013623 (2012), arXiv:1107.4792 [cond-mat.quant-gas] .

[139] D. B. Gutman, Y. Gefen, and A. D. Mirlin, Phys. Rev. B **85**, 125102 (2012), arXiv:1111.4925 [cond-mat.quant-gas] .

[140] J.-P. Brantut, J. Meineke, D. Stadler, S. Krinner, and T. Esslinger, Science **337**, 1069 (2012), arXiv:1203.1927 [cond-mat.quant-gas] .

[141] S. Krinner, D. Stadler, J. Meineke, J.-P. Brantut, and T. Esslinger, Physical Review Letters **110**, 100601 (2013).

[142] J.-P. Brantut, C. Grenier, J. Meineke, D. Stadler, S. Krinner, C. Kollath, T. Esslinger, and A. Georges, Science **342**, 713 (2013), arXiv:1306.5754 [cond-mat.quant-gas] .

[143] C.-C. Chien, S. Peotta, and M. di Ventra, Nature Physics **11**, 998 (2015), arXiv:1504.02907 [cond-mat.quant-gas] .

[144] S. Krinner, D. Stadler, D. Husmann, J.-P. Brantut, and T. Esslinger, Nature (London) **517**, 64 (2015), arXiv:1404.6400 [cond-mat.quant-gas] .

[145] G. Bulnes Cuetara, A. Engel, and M. Esposito, New Journal of Physics **17**, 055002 (2015), arXiv:1412.0283 [cond-mat.stat-mech] .

[146] G. Schaller, C. Nietner, and T. Brandes, New Journal of Physics **16**, 125011 (2014), arXiv:1409.5311 [cond-mat.mes-hall] .

[147] S. Eckel, J. G. Lee, F. Jendrzejewski, C. J. Lobb, G. K. Campbell, and W. T. Hill, Phys. Rev. A **93**, 063619 (2016), arXiv:1506.08413 [cond-mat.quant-gas] .

[148] A. J. Groszek, T. P. Simula, D. M. Paganin, and K. Helmerson, Phys. Rev. A **93**, 043614 (2016), arXiv:1511.06552 [cond-mat.quant-gas] .

[149] J. Cerrillo, M. Buser, and T. Brandes, ArXiv e-prints (2016), arXiv:1606.05074 [quant-ph] .

[150] Y. Nishida, Phys. Rev. A **93**, 011606 (2016), arXiv:1508.07098 [cond-mat.quant-gas] .

[151] D. V. Averin and Y. V. Nazarov, "Single charge tunneling," (Springer US, 1992) Chap. Macroscopic Quantum Tunneling of Charge and Co-Tunneling.

[152] T. Brandes and F. Renzoni, Physical Review Letters **85**, 4148 (2000), cond-mat/0009229 .

[153] B. Michaelis, C. Emary, and C. W. J. Beenakker, EPL (Europhysics Letters) **73**, 677 (2006), cond-mat/0506005 .

[154] R. Sánchez and G. Platero, Phys. Rev. B **87**, 081305 (2013), arXiv:1210.1595 [cond-mat.mes-hall] .

[155] R. M. Whitley and C. R. Stroud, Jr., Phys. Rev. A **14**, 1498 (1976).

[156] H. R. Gray, R. M. Whitley, and C. R. Stroud, Jr., Optics Letters **3**, 218 (1978).

[157] E. Arimondo and G. Orriols, Lettere al Nuovo Cimento **17**, 333 (1976).

[158] T. Ito, T. Otsuka, S. Amaha, M. R. Delbecq, T. Nakajima, J. Yoneda, K. Takeda, G. Allison, A. Noiri, K. Kawasaki, and S. Tarucha, ArXiv e-prints (2016), arXiv:1604.04426 [cond-mat.mes-hall] .

[159] P. Stano, J. Klinovaja, F. R. Braakman, L. M. K. Vandersypen, and D. Loss, Phys. Rev. B **92**, 075302 (2015), arXiv:1409.4852 [cond-mat.mes-hall] .

[160] T. A. Baart, T. Fujita, C. Reichl, W. Wegscheider, and L. M. K. Vandersypen, Nature Nanotechnology **188** (2016), 10.1038/nnano.2016.188.

[161] F. Gallego-Marcos, R. Sánchez, and G. Platero, Phys. Rev. B **93**, 075424 (2016), arXiv:1508.05943 [cond-mat.mes-hall] .

[162] J. Stehlik, M. D. Schroer, M. Z. Maialle, M. H. Degani, and J. R. Petta, Physical Review Letters **112**, 227601 (2014), arXiv:1312.3875 [cond-mat.mes-hall] .

[163] F. R. Braakman, P. Barthelemy, C. Reichl, W. Wegscheider, and L. M. K. Vandersypen, Applied Physics Letters **102**, 112110 (2013), arXiv:1303.2533 [cond-mat.mes-hall] .

[164] C. W. J. Beenakker and A. A. M. Staring, Phys. Rev. B **46**, 9667 (1992).

[165] A. A. M. Staring, L. W. Molenkamp, B. W. Alphenaar, H. van Houten, O. J. A. Buyk, M. A. A. Mabesoone, C. W. J. Beenakker, and C. T. Foxon, EPL (Europhysics Letters) **22**, 57 (1993).

[166] M. Rey, M. Strass, S. Kohler, P. Hänggi, and F. Sols, Phys. Rev. B **76**, 085337 (2007), cond-mat/0610155 .

[167] T. Ruokola and T. Ojanen, Phys. Rev. B **83**, 241404 (2011).

[168] R. S. Whitney, Phys. Rev. B **87**, 115404 (2013), arXiv:1211.4737 [cond-mat.mes-hall] .

[169] D. Sánchez and R. López, Physical Review Letters **110**, 026804 (2013), arXiv:1209.1264 [cond-mat.mes-hall] .

[170] H. Thierschmann, R. Sánchez, B. Sothmann, F. Arnold, C. Heyn, W. Hansen, H. Buhmann, and L. W. Molenkamp, Nature Nanotechnology **10**, 854 (2015), arXiv:1603.08570 [cond-mat.mes-hall] .

[171] K. Schwab, E. A. Henriksen, J. M. Worlock, and M. L. Roukes, Nature (London) **404**, 974 (2000).

[172] M. Meschke, W. Guichard, and J. P. Pekola, Nature **444**, 187 (2006).

[173] O.-P. Saira, M. Meschke, F. Giazotto, A. M. Savin, M. Möttönen, and J. P. Pekola, Phys. Rev. Lett. **99**, 027203 (2007).

[174] L. Arrachea, M. Moskalets, and L. Martin-Moreno, Phys. Rev. B **75**, 245420 (2007), cond-mat/0612059 .

[175] S. Juergens, F. Haupt, M. Moskalets, and J. Splettstoesser, Phys. Rev. B **87**, 245423 (2013), arXiv:1303.5225 [cond-mat.mes-hall] .

[176] M. F. Ludovico, F. Battista, F. von Oppen, and L. Arrachea, Phys. Rev. B **93**, 075136 (2016), arXiv:1506.08617 [cond-mat.mes-hall] .

[177] M. F. Ludovico, J. S. Lim, M. Moskalets, L. Arrachea, and D. Sánchez, Phys. Rev. B **89**, 161306 (2014).

[178] M. F. Ludovico, M. Moskalets, D. Sánchez, and L. Arrachea, Phys. Rev. B **94**, 035436 (2016).

[179] F. Barra and M. Esposito, Phys. Rev. E **93**, 062118 (2016), arXiv:1602.01905 [cond-mat.stat-mech] .

[180] T. Takakura, A. Noiri, T. Obata, T. Otsuka, J. Yoneda, K. Yoshida, and S. Tarucha, Applied Physics Letters **104**, 113109 (2014), arXiv:1401.2212 [cond-mat.mes-hall] .

[181] M. R. Delbecq, T. Nakajima, T. Otsuka, S. Amaha, J. D. Watson, M. J. Manfra, and S. Tarucha, Applied Physics Letters **104**, 183111 (2014), arXiv:1404.6047 [cond-mat.mes-hall] .

[182] R. Sánchez, F. Gallego-Marcos, and G. Platero, Phys. Rev. B **89**, 161402 (2014), arXiv:1312.2512 [cond-mat.mes-hall] .

[183] A. Cottet, W. Belzig, and C. Bruder, Physical Review Letters **92**, 206801 (2004), cond-mat/0308564 .

[184] A. Cottet, W. Belzig, and C. Bruder, Phys. Rev. B **70**, 115315 (2004), cond-mat/0403507 .

[185] W. Belzig, Phys. Rev. B **71**, 161301 (2005), cond-mat/0501141 .

[186] R. Sánchez, G. Platero, and T. Brandes, Physical Review Letters **98**, 146805 (2007).

[187] R. Sánchez, G. Platero, and T. Brandes, Phys. Rev. B **78**, 125308 (2008), arXiv:0807.4641 .

[188] R. Sánchez, B. Sothmann, A. N. Jordan, and M. Büttiker, New Journal of Physics **15**, 125001 (2013), arXiv:1307.0598 [cond-mat.mes-hall] .

[189] R. Sánchez, R. López, D. Sánchez, and M. Büttiker, Physical Review Letters **104**, 076801 (2010), arXiv:0910.3300 [cond-mat.mes-hall] .

[190] R. Sánchez, S. Kohler, P. Hänggi, and G. Platero, Phys. Rev. B **77**, 035409 (2008), arXiv:0706.2950 .

[191] R. Sánchez, S. Kohler, and G. Platero, New Journal of Physics **10**, 115013 (2008), arXiv:0809.1368 .

[192] P. Barthold, F. Hohls, N. Maire, K. Pierz, and R. J. Haug, Physical Review Letters **96**, 246804 (2006), cond-mat/0603512 .